Stability Investigation of Car-trailer Combinations based on Time-Frequency Analysis

Vom Fachbereich Maschinenbau an der
Technischen Universität Darmstadt
zur Erlangung des Grades eines
Doktor-Ingenieurs (Dr.-Ing.)
genehmigte

Dissertation

vorgelegt von

Ning Zhang, M.Sc.
aus Xuzhou, Jiangsu, China

Erstreferent:	Prof. Dr. rer. nat. Hermann Winner
Korreferent:	Prof. Dr.-Ing. Stephan Rinderknecht

Tag der Einreichung:	15.04.2015
Tag der mündlichen Prüfung:	07.07.2015

Darmstadt, 2015
D 17

Preface

This research work is conducted during the nearly five years time, when I was a research assistant (Wissenschftlicher Mitarbeiter) in the Institute of Automotive Engineering (Fachgebiet Fahrzeugtechnik, FZD) of Technische Universität Darmstadt, under the supervision of Prof. Dr. rer. nat. Hermann Winner. My research and living in Darmstadt are mainly supported by the China Scholarship Council (CSC) under the State Scholarship Fund. Therefore, I would like to express my acknowledgment to the CSC here.

First and foremost, I want to express my heartfelt thanks to my supervisor "Doktorvater" Prof. Winner, not only for his supervision in the past five years but also for his patience, understanding, tolerance, consistent guide and support. I really have learnt a lot from him during this exciting time. Moreover, I think the research methodology, persistent efforts to solve endless problems and high sense of responsibility from his personality charm are the most precious treasures that I learnt from him. They inspired and will still inspire me in the future.

I would also like to express my grateful thanks to Prof. Dr.-Ing. Stephan Rinderknecht, a co-supervisor for my dissertation. I enjoy and benefit a lot from our pleasant communication and exchange of research interest and activities.

Then I would like to express my grateful thanks to Adam Opel AG at Ruesselsheim. Without their consistent support in the cooperation project including the road test and exchange of R&D experience, the success of this research work might be impossible. Here I would like to express my special thanks to Dr. Marcus Reul for his coordination and cooperation in this research project.

Furthermore, I would like to express my grateful thanks to my colleagues in FZD, the alumni, current colleagues, our secretaries and our workshop staff. All of them gave me consistent support and friendly help in the past five years. Here, I would like to give my special thanks to Dr. Sebastian Geyer for his contribution to the organization of FZD international PhD program, special thanks to my general mentor Dr. Kai Schröter for his thoughtful help to my life in every aspect, special thanks to my professional mentor Dipl.-Ing. Sebastian Claus for his cooperation and support in my project, special thanks to our senior engineer Dr.-Ing. Norbert Fecher for his help and support in the financial affairs related to the project.

I would like to give my kind thanks to my friends in Germany and China, who gave me understanding, encouragement and support in any aspect in the past five years. Thanks to your continuous accompany in the happy time or difficult time. I feel I am not alone in either the academic society or the foreign country. We go further together.

Last but not the least, I would like to express many thanks to my family, my parents in my hometown and my wife, Ma Hui, in my new house in Nanjing. They are always

standing at my back with consistent support, understanding and love. This dissertation is also in memory of my grandmother in heaven and all what I lost at my homeland in the past five years including my youth.

“路漫漫其修远兮，

吾将上下而求索。”

—— 屈原 •《离骚》

“The journey is long,

I’ll search up and down.”

—— Qu, Yuan • “Li Sao”

Ning Zhang Darmstadt, February 2015

Contents

List of Abbreviations

Abbreviation	Description
ABS	Antilock braking system
CDC	Continuous damping control
COG	Center of gravity
CTC	Car-trailer combination
CTCs	Car-trailer combinations
DC	Direct current
DOF	Degree of freedom
DOFs	Degrees of freedom
DSP	Digital signal processing
DTM	Double-track model
ECU	Electronic control unit
ESC	Electronic stability control
FFT	Fast Fourier transform
FT	Fourier transform
FZD	Fachgebiet Fahrzeugtechnik der Technischen Universität Darmstadt
GUI	Graphical user interface
HT	Hilbert transform
IIR	Infinite impulse response
IMU	Inertial measurement unit
ISO	International standards organization
MTWFFT	Moving-time-windowed fast Fourier transform
OP	Operating point
OPs	Operating points
PIM	Parameter identification method
PIMs	Parameter identification methods
R&D	Research and development
STFT	Short-time Fourier transform
STM	Single-track model
TFA	Time-frequency analysis
TFD	Time-frequency distribution
TFR	Time-frequency representation
TSA	Trailer stability assist
TUD	Technische Universität Darmstadt
WT	Wavelet transform

List of Symbols and Indices

Symbol	Unit	Description
a	m/s²	Acceleration
c	-	Regression coefficient or polynomial coefficient
f	Hz	Frequency, eigenfrequency
g	m/s^2	Gravitational acceleration
i	-	Ratio, any wheel or axle, arbitrary
j	-	Imaginary unit
l	m	Distance
m	kg	Mass
q	mm	Rack position
r	rad/s, -	Damping factor, ratio
s	-	Laplace operator
t	s	Time
v	m/s	Velocity
A	misc.	Amplitude
Arg	rad, °	Phase or argument
C	kN/rad	Cornering stiffness
F	N	Force
I	kgm^2	Moment of inertia
Im	-	Imaginary part
K	-	Gain factor, influencing factor
K_u	-	Understeer gradient
O	-	Original point
Re	-	Real part
T	s, Nm	Period, torque
W	N	Static axle load
X	-	X direction in coordinate system
Y	-	Y direction in coordinate system
α	rad, °	Side-slip angle
β	rad, °	Body side-slip angle at COG
δ	rad, °	Steering angle
ζ	rad^{-1}	Normalized cornering stiffness
θ	rad, °	Hitch angle
$\dot{\theta}$	rad/s, °/s	Hitch angle rate or hitch angle velocity
μ	-	Friction coefficient
ξ	-	Damping ratio
π	-	Pi
φ	rad, °	Initial phase or argument
ψ	rad, °	Yaw angle

Symbol	Unit	Description
$\dot{\psi}$	rad/s, °/s	Yaw rate or yaw angle velocity
$\ddot{\psi}$	rad/s^2, °/s^2	Yaw angle acceleration
ω	rad/s	Angular frequency, yaw angular frequency
Δ	-	Difference
∂	-	Partial differential operator

Index	Description
0	Static value or DC value
1	Towing car
2	Trailer
a	Additional
c	Car
crit	Critical
d	Damper or shock absorber, damped, dominant
dot	Differential
e	Earth
eff	Effective
engine	Engine
exp	Experiment
f	Front axle
h	Hitch point
n	Natural, integer
r	Rear axle
s	Steering
sim	Simulation
td	True dominant
test	Experiment or road test
tire	Tire
u	Understeer
w	Wheel
x	in x direction (e.g. vehicle longitudinal direction)
y	in y direction (e.g. vehicle lateral direction)
z	in z direction (e.g. vehicle vertical direction)
H	Handling, by hand
L	Left wheel
OP	Operating point
R	Right wheel
α	Side-slip

List of Figures

List of Tables

Abstract

Stability investigation of car-trailer combinations (CTCs) based on time-frequency analysis (TFA) is the focus of this thesis. A state-of-the-art survey shows that very few research activities were performed to study the influence of the coupling between the vertical dynamics and horizontal dynamics, particularly for the system stability analysis. Even for the normal passenger car, stability analysis is mainly focused in the horizontal plane. However, this dynamic coupling deserves more attention for CTCs due to their dynamically natural characteristics. Besides the static stability, the dynamic stability is of more concern for CTCs.

Based on the theoretical foundation of the stability analysis for CTCs, a time-frequency analysis based parameter identification method (TFA-based PIM) is proposed, in which a linear single-track model (STM), a Moving-Time-Windowed-Fast Fourier transform (MTWFFT) analysis method and an evaluation algorithm for the instantaneous cornering stiffness and the instantaneous effective axle load are integrated. It aims to study the time varying vehicle dynamics characteristics under harmonic conditions. Only common lateral and yaw measurements are necessary for the purpose of indispensible inputs. With this PIM, vehicle dynamics parameters can be estimated continuously in time domain with a high accuracy in case a suitable model representing the system (here is a linear STM) is available. Other vehicle dynamics parameters, like normalized axle cornering stiffness and instantaneous friction coefficient, are also available with such a method. Besides, the coupling between the vertical dynamics and horizontal dynamics is also discussed with the derivation of an effective axle load, by which the influence of a harmonic dynamic axle load on the axle cornering stiffness is described. Also, they can be cross-checked by the phases of the obtained complex values of the general parameters involved here. In principle, the TFA-based PIM can be applied for any time varying vehicle system, if its linear STM is available. This adaptability is a prominent advantage.

For the analysis of the impact of the nonlinearity-induced harmonic dynamic axle load on the dynamic stability of CTCs, a complex driving dynamics simulation model of a CTC validated in the horizontal plane is utilized. With the PIM, the system characteristics of the simulation model are adjusted aiming for those delivered from the CTC applied in the road tests. This original work introduces the analysis of nonlinear dynamics to this thesis as an intermediate step to the ultimate intention, investigation of the influence from vertical dynamics on the system dynamic stability in the horizontal plane (e.g. influence from the damper characteristics in the suspension). Although impact study of harmonic dynamic axle load induced by undesired nonlinearity or failure of

some suspension component is the ultimate objective, interaction from harmonic dynamic axle load induced by original existing expected nonlinearity cannot be excluded because of many possible sources like the practical damper characteristics in the system. A theoretical analysis of the system dynamic stability and the influence of harmonic dynamic axle load on the axle cornering stiffness lay a solid foundation for a study of the harmonic influence on the system dynamic stability. Based on the TFA-based PIM including the effective axle load evaluation algorithm, the time varying harmonic effect found in the axle load in the experimental study is quantified. To simulate the influence of the harmonic wheel load oscillations, a synthetic force generator is applied, which is synchronized to the phase of the yaw rate with a defined phase shift. Hence, the sensitivity analysis of the influence of the harmonic amplitude or phase of this force on the system dynamic stability is performed with a simulation model validated in the horizontal plane. The relative phase shift of the harmonic force can induce a change of ca. 10 km/h in v_{crit} while the amplitude change of the harmonic force can induce a change of ca. 10 km/h in v_{crit} as well (amplitude of the harmonic force is within 0.2-1.2 kN).

The application scope of this novel TFA-based PIM is mainly identification of systems with time varying properties, which aims for the model identification to build up simulation models. An application case, parameter identification of a car-caravan combination under its dynamically critical stable state, is performed for the purpose of a complex simulation model validation within the range of linear lateral dynamics. The results show that the TFA-based PIM is effective and has great application potential in vehicle system dynamics. Moreover, based on the impact study of nonlinearity-induced harmonic dynamic axle load, the change of the system dynamic critical speed is actually determined and so is the reason why the temporal changes of the system dynamic stability can be explained by the fluctuations in the amplitude and/or the phase of the superimposed harmonic dynamic axle load.

1 Introduction

1.1 Motivation and objectives

1.1.1 Motivation

Different from a single passenger car, every car-trailer combination (CTC) has a specific dynamic critical speed by which the system dynamic stability boundary is defined. From some physical models and experimental data, it is found that the dynamic critical speed has a close relationship with a parameter defined in the horizontal plane, yaw damping ratio. A CTC will exhibit actual dynamic unstable behavior when its dynamic critical speed is exceeded. At this speed, the yaw damping ratio of the system converges to zero and even becomes negative if the longitudinal velocity increases further. As a result, the yaw rate of the system increases steadily, which is normally expected to be avoided since it can cause a traffic accident[1].

Since car-trailer combinations (CTCs) have many types of variations particularly for the trailer, car-caravan combinations are in the research focus of this thesis. Although an articulated vehicle can also be represented by a similar mathematical model, there are mainly two big differences between a car-caravan combination and an articulated vehicle. Firstly, the mass ratio of the trailer to the towing vehicle is different. It is normally below one for a car-caravan combination[2], but can be bigger than 10 for an extremely huge articulated vehicle[3]. Secondly, they have a different coupling at the hitch point. As a result, a car-caravan combination can have a relatively bigger hitch angle in the yaw plane regardless of the structural form. Considering the two differences above, the CTC hereinafter is referred to a car-caravan combination. Besides, only one trailer is towed in such a system.

Even the towing car can be equipped with active braking systems, like Trailer Stability Assist[4] (TSA, based on ESC, Electronic Stability Control[5]) in order to assure trailer stability under critical situations, which is available in production passenger cars or

[1] Zomotor: Fahrwerktechnik: Fahrverhalten, 2. Auflage, Vogel, 1991, p. 206.

[2] Caravan Buyers Guide – virtual, 2015.

[3] Hoepke et al. Nutzfahrzeugtechnik, 6. Auflage, Vieweg, 2010.

[4] Autoevolution – virtual, 2015.

[5] Rajamani: Vehicle Dynamics and Control, Springer, 2011, p. 221.

trailers today, the handling and stability performance is still not essentially improved. If an increasing yaw rate with a specific dominant yaw oscillation frequency is detected, TSA stabilizes yaw oscillations and decelerates the system below its dynamic critical speed[6]. But although TSA ensures system stability, the system dynamic critical speed has not been increased essentially. And it is expected to be as high as possible anyway in order to reduce annoying TSA interactions to a minimum.

From the view of kinematics, it is also worth mentioning that normally the stability of CTCs is just studied in the horizontal plane[7], in which the longitudinal and lateral motions are concerned. But in a cooperation project with an industrial company, the influence of damper's properties on the system dynamic stability is particularly concerned. Damper, also called shock absorber, is a suspension component of a vehicle and is used to reduce vibration of the vehicle body caused by road disturbances for the purpose of good ride quality and comfort. And it also has significant influence on the system roll behavior, handling and stability performance as well. So, it is clear that the damper properties may influence both the vertical dynamics and lateral dynamics of the system. Therefore, vertical motion has to be considered as well. And the dynamic coupling between the horizontal plane and vertical plane deserves a comprehensive understanding.

The system dynamic critical speed is not a fixed quantity but depends on the system parameters and external forces acting on the system (aerodynamics, acceleration force, etc.). Apart from the system inertial and geometric parameters, chassis properties incl. tire characteristics determine the dynamic critical speed as well. Especially the influence of the car's vertical chassis properties on the system yaw damping ratio or dynamic critical speed does currently not seem to be well investigated and thus not well understood. Some results in the horizontal plane are discussed by Mitschke *et al.*[8]. If it is known that which chassis parameters and physical effects change the dynamic critical speed primarily, these chassis parameters might be adapted more deterministically. In that content, damper properties (stationary damper characteristics, hysteresis, elasticity, transient behavior, etc.) are of special interest. Several damper parameters are changed dynamically when semi-active dampers change their characteristics due to the control strategy. Therefore, it seems to be possible to change the dynamic critical speed by changing damper characteristics. However, responsible damper properties for significant changes of the system stability are currently still unknown.

[6] Hac et al.: Stability and Control Considerations of Vehicle-Trailer Combination, 2008.

[7] Sagan: Fahreigenschaften von Pkw-Wohnanhängerzügen, 1983.

[8] Mitschke et al.: Fahrdynamik von Pkw-Wohnanhängerzügen, 1988.

However, this research topic is relatively difficult due to the reasons at least in three aspects. Firstly, because the dynamic critical speed determines the system stability margin which is known as critical stability, such system is very sensitive to any small disturbances, like dynamic wheel load, nonlinear steering/tire characteristics or aerodynamics at this stability boundary. Hence, it makes the experimental research more difficult because other unexpected disturbances cannot be excluded completely. Secondly, the vertical dynamics and horizontal dynamics are coupled by the tire behavior. If a simulation research is necessary for the problem, whether the normal tire model, e.g. Magic Formula tire model, can represent the real tire behavior under the critical situation even within the tire linear range in the road test is still not completely confirmed. Finally, the real damper behavior is very complicated compared with the design curve from the bench test data. On the one hand, the internal fluid dynamics incl. compressibility, cavitations and aeration can make the damper characteristics irregular. On the other hand, real damper behavior is a superposition of damper responses in different frequency range due to the excitations from the road irregularities. Besides, there is a great potential that the real damper behavior is time varying and consequently both time-domain and frequency-domain digital signal processing (DSP) methods might be necessary in the analysis. Hence, it puts forward a challenge that system parameter identification method (PIM) might be difficult for the purpose of high resolution. This challenge might become extremely difficult when the useful system response under the critical situation is very short in order to avoid any potential accident in the road test.

The three points proposed above are all considered in the whole process of the project and research. The first point is solved by a systematic design of a series of driving tests and specific small research packages in a teamwork. The second problem about the tire model is still focused on now and the influence of damper's properties cannot be revealed unless it is completely solved. The final problem considering the PIM especially for time varying vehicle dynamics serves as the focus of this thesis.

The motivation of this thesis is a PIM that is helpful in the stability investigation of CTCs, especially in which potential time varying vehicle dynamics resulting from real damper behavior is concerned. With its assistance, the potential time varying vehicle dynamics variables can be identified and quantified. Therefore, stability investigation of CTCs in either experimental study or simulation study can be achieved on this basis.

1.1.2 Objectives

This thesis deals with the stability investigation of CTCs. The system dynamic stability described by the dynamic critical speed or the corresponding yaw damping ratio is focused on. For this purpose, an appropriate time-frequency analysis based parameter identification method (TFA-based PIM) is expected to identify and quantify the potential time varying parameters for vehicle dynamics due to the real damper behavior in the

road test. Moreover, a harmonic dynamic axle load oscillation is found in the experimental data and quantification of an effective axle load incl. this harmonic phenomenon is also expected because it is related to the dynamic coupling. Finally, from the perspective of application, the validation of a complex simulation model built in commercial software can be performed with the assistance of this TFA-based PIM as an application case.

The objectives described above can be summarized as the following points:

- A linear single-track model (STM) for CTCs and description of system dynamic stability
- Sensitivity analysis of system parameters in the STM to system dynamic critical speed
- A TFA-based PIM derived for time varying vehicle dynamics, which aims for the system identification to build up simulation models
- Quantification of an effective axle load in which the harmonic dynamic axle load oscillation is considered
- Study of the nonlinearity-induced harmonic dynamic axle load and its impact on the dynamic stability of CTCs
- Validation of a complex simulation model built in commercial software with the assistance of this TFA-based PIM

In one word, the stability investigation of CTCs in this thesis is based on the TFA for the purpose of potential time varying vehicle dynamics resulting from the real damper behavior in the road test. Another constructive original work is the study of nonlinearity-induced harmonic dynamic axle load and its impact on the dynamic stability of CTCs. The TFA-based PIM proposed can also serve as a powerful tool in the validation of simulation models. This work lays a foundation for the further research about the influence of damper's properties on the system dynamic stability.

1.2 System description and phenomenon of instability

1.2.1 System description

The researched system in this thesis is a CTC. To be more in detail, it is a car-caravan combination. The towing car here is a normal passenger car, and the trailer is a tandem-axle caravan. The two separate vehicles are connected by a standard hitch coupling

device. Under an empty load condition, the mass ratio of the trailer to the towing car is ca. 1.0. The system is shown in a schematic view in Figure 1-1 below.

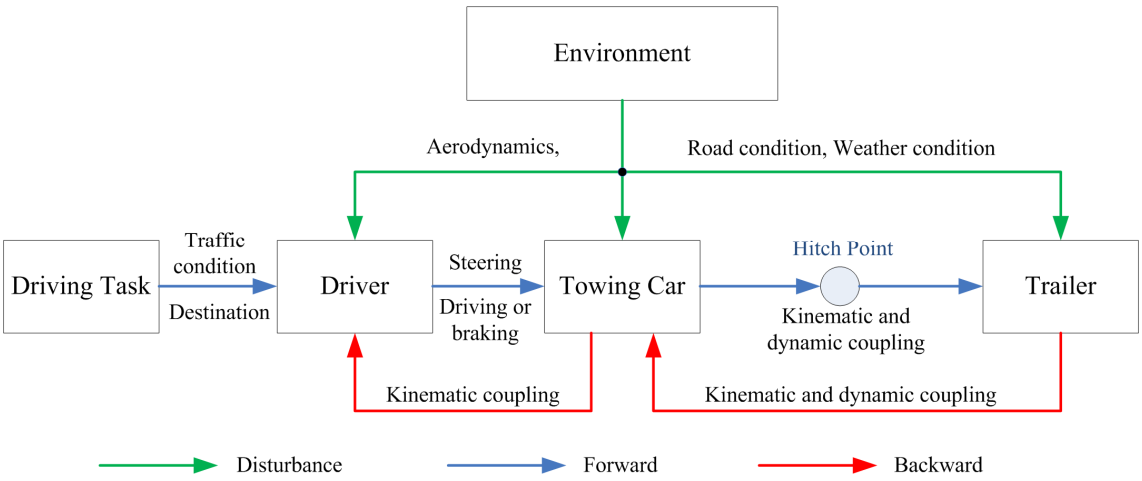

Figure 1-1: Schematic diagram of a car-trailer combination

The system has some differences from a single passenger car. Due to the existence of a trailer, the kinematics and dynamics of the towing car and trailer are coupled with each other. While a single passenger car has no dynamic critical speed even at very high longitudinal velocity, a CTC has a dynamic critical speed by which the system dynamic stability boundary is determined. If the parameter setting of the towing car or trailer is not proper, the dynamic critical speed can decrease significantly. Then the system handling and stability performance at high speed decreases as well. Since a CTC is a very popular transport means on the highways all over the world, especially in Europe, the research topic of this thesis is meaningful.

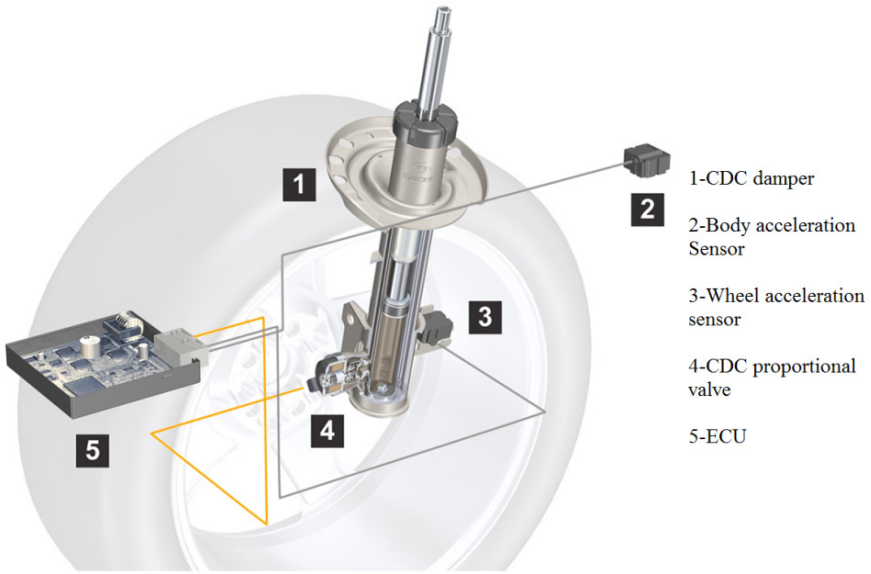

Figure 1-2: Semi-active CDC damper system by ZF Sachs[9]

Another important part in the project is the semi-active damper installed in the suspension of the towing car. It is called continuous-damping-control (CDC) damper system (see Figure 1-2) designed by ZF Sachs Company in Germany, in which an electromagnetic proportional valve that could continuously adjust the damping coefficient is included. Depending on the valve setting, the damper's function varies in the range from soft to middle, up to hard. CDC is an electronic damping system that could noticeably increase driving dynamics, comfort and safety by adjusting damping force optimally for each individual wheel on a continuous basis[9].

In order to simplify the damper behavior and its influence on system, the control strategy of CDC is disabled. It only works under two different conditions, extremely hard or soft mode, which is selected by the input control current for the electromagnetic valve (0mA for the hard mode, 1600mA for the soft mode). Besides, the dampers installed in the trailer suspension are passive dampers and their influence on the system dynamic stability is not concerned in this research.

1.2.2 Phenomenon of instability

To investigate the dynamic stability of car-trailer combinations, a series of road tests are designed and performed according to the lateral stability test standard ISO 9815[10]. A car-caravan combination is applied in the road test. The system works at its critical

[9] ZF Sachs: Suspension Technology, 2011.

[10] ISO 9815: Road vehicles - Passenger-car and trailer combinations - Lateral stability test, 2003.

stable state under which the longitudinal speed is set to the previously determined dynamic critical speed v_{crit}.

Two variations of a semi-active damper are applied in the road test, series dampers and prototype dampers. Both variations have same damper characteristics under the bench test. But due to internal small structural differences, their real behaviors are different in the road test. The difference between the prototype dampers and series dampers mainly lies in the structural design, especially in the bottom valve and bypass washers. To simplify the research, only extreme damper mode, hard or soft, works in the road test.

The original intention of this project is the optimization of the damper design considering the occurrence of yaw instability of a car-caravan combination at its dynamic critical speed with prototype dampers installed in the towing car. And the same system with another series dampers installed in the towing car behaves only steady state yaw oscillation at the critical stable condition without obvious yaw instability.

Yaw instability here is directly indicated by a sudden and progressive change of yaw damping ratio. A CTC under its dynamic critical speed or dynamic critical stable state behaves a free natural yaw oscillation with constant amplitude in either the towing car or trailer. However, if the amplitude of yaw rate is progressively increasing over time, the system will be out of control after a moment and hence a catastrophe occurs. This dangerous phenomenon in the horizontal plane is defined as the yaw instability here.

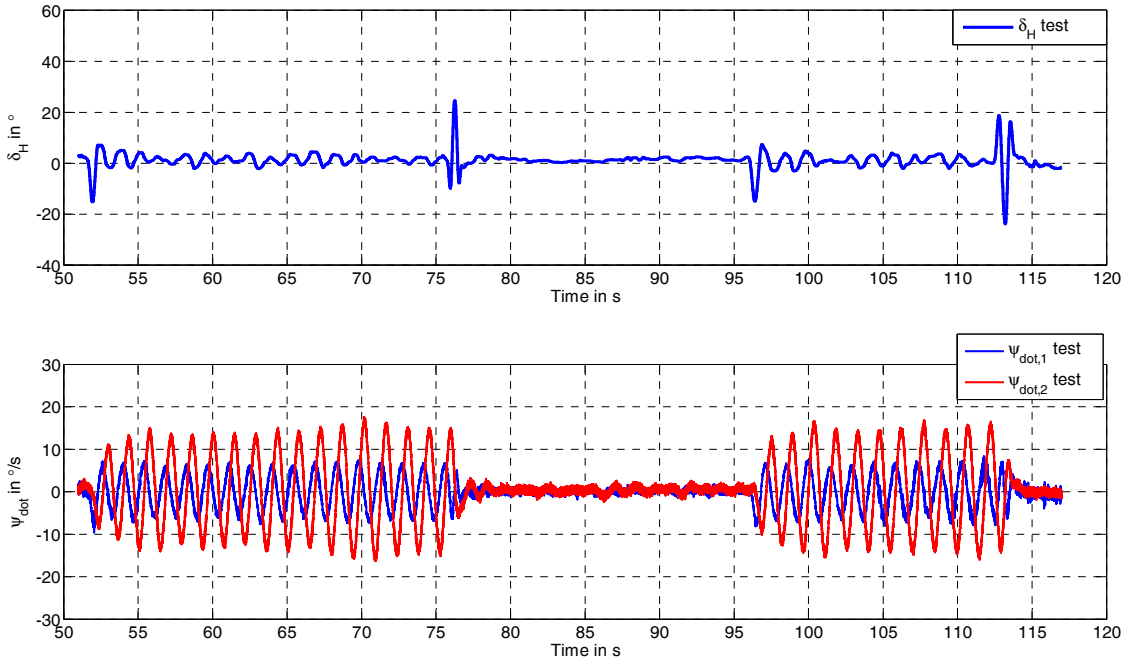

Figure 1-3: System yaw rates under steering impulse excitation and series damper setup

In the road test, a steering impulse serves as the system input to excite the harmonic oscillations. Furthermore, two sequential impulse input signals are adopted to excite

system dynamic behavior for the purpose of searching potential time varying properties induced by the damper characteristics.

For the system with series damper setup, it has not such an unstable behavior in both impulse responses (see Figure 1-3). Although the steering input signal after the impulse still shows a noteworthy oscillation, the system response performs a steady state oscillation in the yaw rate of the towing car and that of the trailer as well. The responses under both impulse excitations are nearly the same. The amplitude of the yaw rate of trailer is almost twice of that of the towing car.

For the system with prototype damper setup, it clearly shows that the system has such an unstable behavior and it cannot be kept stable without the correction signal from the driver (see Figure 1-4). Under the first impulse excitation, the system behaves a steady state oscillation at the beginning of the first impulse response. After several oscillations, the amplitude of the yaw rates increase dramatically along with a negative degressive yaw damping ratio. When the driver feels a loss of control, a green trigger signal is marked and then the driver should give a high frequency correction signal to the system input for the purpose of getting it back to controllable condition. But the system response under the second impulse excitation does not show such steady state oscillation at the beginning. Instead a suddenly immediate instability occurs after the impulse excitation and the duration of the impulse response is comparatively rather short. That reveals the system has more critical behavior under the second impulse excitation and system stability margin also decreases due to a reduced dynamic critical speed or yaw damping ratio.

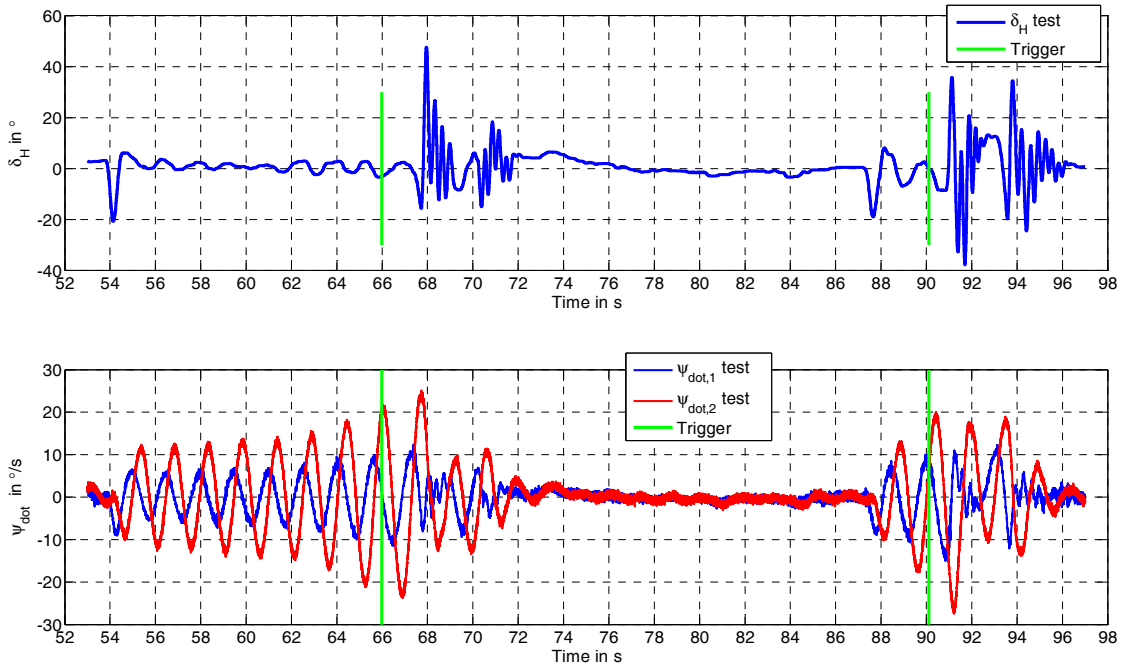

Figure 1-4: System yaw rates under steering impulse excitation and prototype damper setup

By comparing the two figures above, the research focus of this project is clear. Not just the yaw rate but also lateral acceleration and some other dynamic characteristic variables have this progressively increasing oscillation phenomenon along with a negative degressive yaw damping ratio. Since the only difference in system setting is the different dampers installed in the suspension of the towing car, the root cause for this unstable behavior should relate to the modified properties of the prototype dampers.

From the view of control theory, assuming that the transfer function of yaw rate to steering wheel angle is available, various root locations of the transfer function in s-plane and the corresponding impulse response can be got either analytically or numerically (see Figure 1-5). For the response to be stable - that is, bounded for an impulse input - the real part of all the roots must be in the left-hand portion of the s-plane[11]. A trailer introduces another pair of system conjugate characteristic roots by which the system dynamic stability is dominated, while the normal pair of system conjugate characteristic roots, same as that of a normal passenger car, is not related to system dynamic stability. For the CTC with series dampers, the real part of the dominant characteristic roots is nearly zero. But it shifts gradually and significantly from nearly zero to the positive portion of the s-plane for the CTC with prototype dampers. The problem is that it is not easy to obtain this transfer function due to the nonlinearity when the complicated coupling between the lateral dynamics and vertical dynamics has to be concerned.

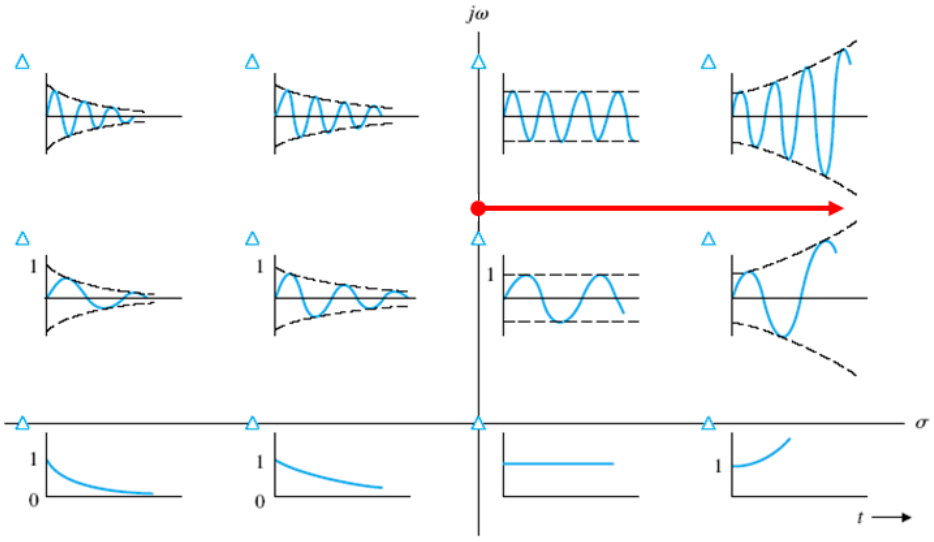

Figure 1-5: Impulse responses for various root locations in s-plane (the conjugate root is not shown)[11]

From another point of view, the stability reserve of the system with series dampers is sufficient enough to avoid such yaw instability. But for the system with prototype dampers, the stability reserve is very critical to keep the system stable all the time.

[11] Dorf et al.: Modern Control Systems, twelfth edition, 2011.

1.3 Methodology

1.3.1 Top-down analysis method

In order to find the root cause for the system instability, a systematic derivation of system effect chain is pursued. Since this unstable behavior is obviously characterized by the system yaw oscillations and it is induced by the dynamic behavior of prototype dampers, a top-down analysis method is introduced for the purpose of this effect chain. A schematic diagram describing the methodology detailedly is shown in Figure 1-6 below.

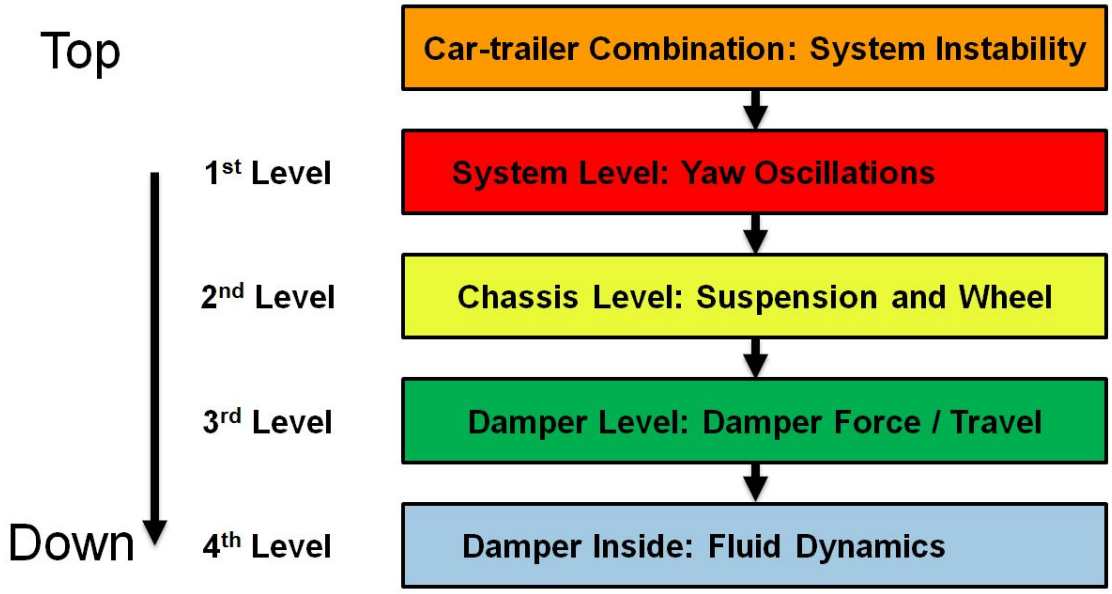

Figure 1-6: Top-down analysis method for the search of the system effect chain

As is shown from the top level, the system instability is observed in the yaw oscillations of the system level. This yaw oscillation is the output of a dynamically unstable system under an impulse excitation. The focus in the system level is the system motion, i.e. body motion of the towing car or the trailer including all the six degrees of freedom (DOFs).

The chassis level, in which the suspension and wheel forces are investigated, is the connection between the system level and damper level. Suspension, wheel and tire characteristics which can affect the system handling and stability are studied. Since the wheel load is the direct connection with the damper force in the damper level, it deserves special attention considering the different frequency ranges. Besides, the tire characteristics are of interest particularly as well.

Further deep research about the damper behavior is taken in two aspects, outside and inside the damper. As the direct damper's outputs, damper force, displacement and

velocity are focused on to search the potential change which causes significant differences in the chassis level. And fluid dynamics inside the damper also deserves attention to explain the potential change of damper force or displacement in the damper level. This is the bottom level in the system effect chain, since the root cause of system instability lies in the damper behavior.

The top-down analysis method serves as the methodology in this research. Once the prototype dampers installed in the towing car differ from the series dampers by some degree of time varying properties, the time varying phenomenon might happen in each level and hence a PIM with which the time varying vehicle dynamics can be identified and quantified is necessary for the analysis in each level. It is clear that such PIM plays an important role in the search of the system effect chain as well as the understanding of the influence of damper properties on the system dynamic stability.

1.3.2 Systematic investigation with different models

Three different models are applied for the purpose of a systematic investigation in this research. They consist of a real experimental system, a complex vehicle dynamics simulation model and a simplified analytical model.

The real experimental system is the car-caravan combination applied in the road test. The system instability is observed with special attention in the road test as well. It is a real system with a large number of nonlinearities and more detailed sensitivity analysis with such a model is nearly impossible. Under the system critical stable state, it is very sensitive to any disturbance including side wind or damper internal failure. Therefore, a system that is dynamically critically stable but highly oscillatory is really difficult to be controlled by inexperienced drivers for safety reasons. This real system is applied in the road test and the measurement data are collected for further data analysis. Measuring technology has to be concerned in this model, especially considering measurement error correction.

The simulation model is a complex and complete model built in a commercial software IPG CarMaker®[12] (Version 4.0.5). A complete validation with sufficient accuracy is a big challenge for this model. It has a significant advantage that the sensitivity analysis for some system parameters, e.g. suspension parameter, can only be performed with this model. The reason is that building a complete analytical model including large number of nonlinearities is infeasible. Even if such a complex analytical model is available, an analytical solution is impossible as well. Instead, implementation or modification of some specific module is convenient and makes the sensitivity analysis or instability study easier and faster.

[12] IPG CarMaker – virtual: www.ipg.de, last access: February 26th 2015.

The simplified analytical model is a linear single-track model (STM) of car-trailer combinations (CTCs). It is a general representation for all such systems including a car-caravan combination or an articulated vehicle. It has an important role in two aspects. Firstly, it serves as a simple model to understand the stability of a CTC. All the system parameters which are related to the system stability under a constant longitudinal velocity in the horizontal plane are included in this model and their sensitivities are available on different operating points (OPs or OP) of system parameters. Secondly, it also lays a foundation for the Time-Frequency analysis based parameter identification method (TFA-based PIM), which is derived to identify the time varying vehicle dynamics, the focus in this thesis.

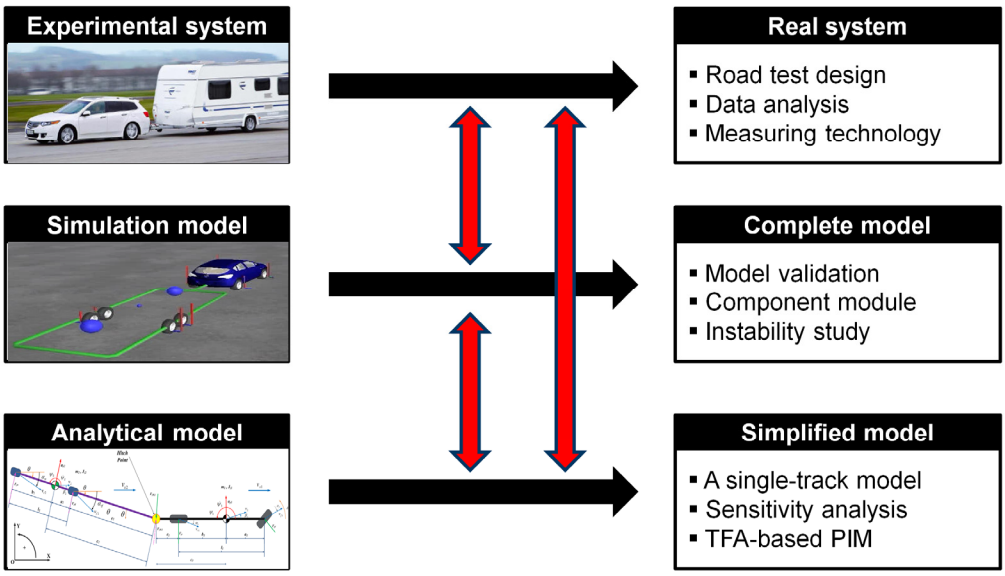

Figure 1-7: Three different models used in a systematic investigation

The three different models used in a systematic investigation with their functions are illustrated in Figure 1-7 above. Data analysis result with a specific method can be obtained in either model. Through their comparison, many applications including a simulation model validation or influence investigation of a specific module can be accomplished. This part is discussed in Chapter 6 after the state of the art, stability of CTCs, TFA-based PIM and its integration in vehicle dynamics are sequentially introduced in the following chapters.

2 State of the Art

The research topic of this thesis includes two branches, one is the system stability of CTCs and the other is the PIMs, which are capable of evaluate the potential time varying vehicle dynamics, especially the axle or tire cornering stiffness, deserve special concern. The state of the art in the two aspects above is summarized separately in this chapter.

2.1 System stability of car-trailer combinations

Considering the research topic on system stability of CTCs, it is much more helpful and meaningful if the topic is extended to the stability of articulated vehicles. Because these vehicles play an important role in logistics, there have been serious concerns about their handling and stability on highways.

For the system instability, the research on this topic can be traced back to 1960s. Eshleman[13] has performed a literature survey on handling safety problems of trucks and articulated vehicles. Furthermore, Kurtz and Anderson[14] have presented a state-of-the-art survey on the handling characteristics of car-trailer systems. Cars towing trailers or caravans can exhibit three kinds of instabilities as presented in this survey. The first one, known as jackknifing, is an aperiodic instability in which the towing car yaws continuously in one direction along with the trailer yawing only slightly. The second kind of instability, called as trailer swing, sway or snaking, is in fact the opposite of the first one, mainly an aperiodic instability where the trailer yaws continuously in one direction along with the towing car yawing only slightly. These two types of aperiodic instabilities are also defined as divergent instabilities. The last instability is a natural oscillation in which both the towing car and trailer yaw more or less sinusoidally with increasing amplitudes over time, until either a limit cycle or a catastrophe occurs. This very dangerous type of instability is known as flutter. From the phenomenon of instability in Section 1.2.2, it is clear that the researched instability in this project belongs to type 3, flutter. Historically, attention was first focused on the flutter of CTCs when the longitudinal velocity of the towing car exceeds a so-called dynamic critical speed for every

[13] Eshleman: Particular Handling Safety Problems of Trucks and Articulated Vehicles, 1973.

[14] Kurtz et al.: Handling Characteristics of Car-Trailer Systems; A State-of-the-Art Survey, 1977.

such system. Later attention is still being devoted to flutter, but the research emphasis has shifted to jackknifing, probably due to the attitude of government agencies that jackknifing of commercial trailer vehicles is a more serious safety problem than flutter. The literature by Dugoff and Murphy[15] describes this very well.

Actually flutter demonstrates a so-called dynamic instability which is characterized by the oscillatory yawing and rolling motions of CTCs at the system dynamic critical speed. This kind of oscillation happens to the towing car and trailer and interacts with each other. A typical yaw oscillation frequency of such system is around 0.6 Hz. Not only the theoretical analysis but also the simulation and experimental investigation have been contributed to this problem.

A number of analytical models and analysis have been developed to understand the instability of CTCs better. Deng and Kang[16] and Bevan *et al*.[17] developed mathematical models with 3-DOFs in their research. These models have 3 degrees of freedom including yaw of towing car, yaw of trailer, body side-slip angle or lateral acceleration of towing car along with a constant longitudinal velocity. Anderson and Kurtz[18] developed both a 4-DOFs model and 6-DOFs model in which the longitudinal dynamics with acceleration/deceleration is considered as well. The 6-DOFs model also takes into account the roll dynamics of the towing car and trailer. A more complicated analytical model derived from Lagrange equations with 24-DOFs, which include the towing car and trailer's yaw, pitch and roll motions, was built by Fratila and Darling[19]. This model also contains the vertical and roll motions of the unsprung mass. Recently with the help of commercial software AutoSim®, Sharp and Fernandez developed a highly sophisticated system model[20] with 32-DOFs for CTCs. Besides, because the roll over is another serious problem for such a system, Wu D. H. pointed out roll steer influenced by roll motion could change the yaw response through the tire lateral forces simultaneously. His results from his analytical model show that a parameter called roll steer coefficient influences the system dynamic critical speed significantly[21]. The doctoral dissertation of Fratila D. gave a summary of various parameters' influences on the system dynamic critical speed[22] or lateral stability. The most important factors that affect the system

[15] Dugoff et al: The Dynamic Performance of Articulated Highway Vehicles…, 1971.

[16] Deng et al.: Parametric study on vehicle-trailer dynamics for stability control, 2003.

[17] Bevan et al.: Some factors influencing the stability of car/caravan combinations, 1983.

[18] Anderson et al.: Handling characteristics simulations of car-trailer systems, 1980.

[19] Fratila et al.: Simulation of coupled car and caravan handling behavior, 1996.

[20] Sharp et al.: Car-caravan snaking. Part 1: the influence of pintle pin friction, 2002.

[21] Wu: A theoretical study of the yaw/roll motions of a multiple steering articulated vehicle, 2001.

[22] Fratila: Lateral stability of passenger car/caravan combinations, 1994.

lateral stability include the longitudinal velocity, trailer mass, trailer yaw moment of inertia, hitch load, axle position, wheel track and tires. Secondary suspension damping, trailer roll moment of inertia and the height of COG, which make the trailer more prone to roll over, have a small influence on system stability. These researches show that, besides the influences from the geometric parameters, inertial parameters and cornering stiffness, roll motion and roll stiffness also play an important role for the instability problem because of the coupling of yaw sway and roll over.

Meanwhile, Weir *et al*.[23] analyzed the influence of aerodynamic forces and moments on the system stability and then concluded that they have little influence on the system stability of CTCs. Sharp and Fernandez[20] also studied the influence of pintle pin friction on the system stability and then suggested improving the stability with an active braking method in trailer[24].

There are also another two interesting research activities which were conducted in this field. Compared with so many model-based theoretical research works, contribution to experimental investigation of the system stability of CTCs are limited. Although a small quantity of publications presented some measurement results for the purpose of validating their simulation work[18,19], few work has been conducted to investigate the parameter's influence on the system stability with a sensitivity analysis through the road test. One research team led by Darling[25] has made some effort on it. Extensive experimental investigations on the high speed stability (at nearly the system dynamic critical speed) of CTCs are also performed[26]. Here an adjustable trailer is used to examine the influence of each individual parameter on the system stability. In addition, performances of devices intended to enhance the system stability, e.g. trailer stabilizers and ESC, were also investigated. Besides this, Williams[27] created a mathematical theory of the snaking of two wheeled trailers. The most important point in his analysis is a mathematical proof that snaking is impossible unless the dynamics at hitch point are included, i.e. lateral deflection of the rear tires of towing car is hence a factor. This theory is backed up by the fact that snaking does not occur when the trailer is light and the towing car is heavy.

Sagan[28] performed a comprehensive study on the handling characteristics of car-caravan combinations in his doctoral dissertation and the sensitivity of system parameters to

[23] Weir et al.: Crosswind response and stability of car plus utility trailer combinations, 1982.

[24] Sharp et al.: Car-caravan snaking. Part 2: Active caravan braking, 2002.

[25] Darling et al.: An experimental investigation into car & caravan stability, 2002.

[26] Darling et al.: An experimental investigation of car-trailer high-speed stability, 2009.

[27] Williams: The mathematical theory of the snaking of two-wheeled trailers, 1951.

[28] Sagan: Fahreigenschaften von Pkw-Wohnanhängerzügen, 1983.

dynamic stability were achieved by simulation as well. However, they were obtained with a simple model in the horizontal plane and influence from the vertical dynamics was not concerned. Recently abundant research works can be found in the area of improving the handling and stability of CTCs with Driver Assistance Systems (DAS)[29,30,31], which are not instructive to our problem.

Because of the complexity and less practical demand, few contributions are found on the topic of dynamic coupling between the horizontal dynamics and vertical dynamics, especially for CTCs. Most works are performed only in the horizontal plane and normally the horizontal dynamics and vertical dynamics are modeled and studied separately[28]. Recently Bedük *et al*.[32] publish a research on "Effect of damper failure on vehicle stability" and point out that damper failure might lead to system instability in some critical driving situations without ESP control and this criticality of vehicle cornering is different from one maneuver to another. But no contribution is conducted on the effect of vertical dynamics on the dynamic stability of CTCs. It is a research topic for a specific vehicle system with a specific maneuver under a critical situation.

2.2 Parameter identification methods

Parameter identification plays an important role in the system identification, a broad research field. Isermann *et al*.[33] cover nearly all the methods in their academic works, especially for the dynamic systems. Hence to concentrate on our instability problem, the state of the art about the PIMs focuses on the following application scope:

1) For dynamic systems;
2) For time varying system parameters;
3) For driving dynamics in automotive engineering, in which evaluation of axle/wheel cornering stiffness is particularly concerned.

[29] Kageyama et al.: Stabilization of passenger car-caravan combination…, 1995.

[30] Deng et al.: An integrated chassis control for vehicle-trailer stability and handling performance, 2004.

[31] Fernandez et al.: Caravan active braking system, 2001.

[32] Bedük et al.: Effects of damper failure on vehicle stability, 2013, p. 1024-1039.

[33] Isermann et al.: Identification of Dynamic Systems, 2011.

In the study of vehicle dynamics, the STM is frequently used to investigate the system handling and stability[34,35,36,37,38,39]. Because of its simplicity and validity, the characteristics of steady state cornering, also called as static stability, are represented well by this model, although the coupling from vertical dynamics is not concerned. At such condition, system parameters can be treated as constants. But if the vertical dynamics has to be concerned at critical maneuvers, linearized system parameters become time varying. For instance, a dynamic wheel load can result in a time varying tire cornering stiffness. Furthermore, time varying system parameters determine time varying system characteristics. Therefore, such time varying parameters can be a linkage to investigate the coupling between the vertical dynamics and horizontal dynamics. Meanwhile, the application scope of the linear STM can be extended to study time varying vehicle dynamics. Consequently, how to identify these time varying system parameters is a constructive topic in vehicle dynamics.

System parameters in the linear STM can be divided into three categories. The first category contains the inertias, i.e. mass and yaw moment of inertia. The geometric parameters are sorted into the second category, i.e. wheel base and COG. The last category contains the rest, including axle cornering stiffness and longitudinal velocity. Normally, only the system parameters in the last category can be time varying and deserve special attention.

The longitudinal velocity is available by a wheel speed sensor or an optical sensor like Correvit®[40]. The axle cornering stiffness is considered as the most important one in the lateral dynamics. Although the tire cornering stiffness contributes the main component, other contributions from anti-roll bar and suspension linkage cannot be neglected even in the linear lateral dynamics. Hence the axle cornering stiffness is of concern on the basis of a linear STM.

At steady state conditions, the axle cornering stiffness can be treated as a constant in the linear lateral dynamics while both axles including the suspensions and tires function as a time-invariant system respectively. In this case, if the steering wheel angle, yaw rate, lateral acceleration and lateral wheel force are already available with the normal vehicle

[34] Dixon: Linear and non-linear steady state vehicle handling, 1988.

[35] Her et al.: Integrated control of the differential braking…, 2014.

[36] Zhu et al.: Handling transient response of a vehicle with a planar suspension system, 2011.

[37] Obermüller: Modellbasierte Fahrzustandsschätzung zur Ansteuerung…, 2012.

[38] Lundquist et al.: Recursive Identification of Cornering Stiffness Parameters…, 2009.

[39] Florissen: Autonomes anhängerbasiertes elektronisches Bremskonzept…, 2007.

[40] Kistler Automotive: User Manuals of Correvit S-350 Aqua Sensor…, 2012.

experiment, parameter identification can be performed in both the time and frequency domains. Both time-domain- and frequency-domain-based estimation methods are proposed by several researchers.

PIMs for dynamic systems have been introduced by Isermann *et al*.[33] in detail, especially in frequency domain. With the least squares parameter estimation[41] or dynamic equations directly[42], time-domain identification methods are also possible based on the linear STM. Furthermore, the transfer function representation of dynamic system performs satisfactorily for a time-invariant system with linear tire characteristics[43]. Besides, estimation method for cornering stiffness from basic tire information is also available with a ±30% error of the measured value[44]. Moreover, side-slip, tire force and wheel cornering stiffness can also be estimated with the state observer or normal/extended Kalman filter[45].

Most of the PIMs above are only capable of estimating time-invariant cornering stiffness on the basis of a linear STM. Hence they are not helpful to identify time varying cornering stiffness. In the current state of the art, only the time-domain identification methods based on dynamic equations[42] and methods based on the state observer or normal/extended Kalman filter[45] can estimate a time varying cornering stiffness. The first method cannot deliver time varying cornering stiffness with sufficient accuracy due to two main drawbacks. One is the inevitable singularity condition with zero side-slip angle or very low longitudinal speed (ca. zero). The other is the difficulty of an underdeterminate problem[42]. The advantage of the second option is the real time online performance, which can provide a simultaneous estimation in the road test. But they are much more complicated and a high robustness is required to estimate an accurate side-slip angle[45]. And they mainly aim for online model identification in the vehicle dynamics control if unknown components are used by customer, which is different from our goal – the system identification to build up simulation models. Besides, although the change of the dynamic wheel/axle load or road friction can also be indicated by a time varying cornering stiffness estimated, the coupling between the vertical dynamics and horizontal dynamics is not discussed.

The axle cornering stiffness in the STM can be time varying at critical maneuvers. The real tire cornering characteristics is neither a linear system nor constant concerning the cornering stiffness. Instead, it changes due to several reasons, including the well-known

[41] Wesemeier et al.: Identification of vehicle parameters using stationary driving maneuvers, 2009.

[42] Sierra et al.: Cornering stiffness estimation based on vehicle lateral dynamics, 2006.

[43] Börner et al.: Adaptive one-track model for critical lateral driving situations, 2004.

[44] Hewson: Method for estimating tyre cornering stiffness from basic tyre information, 2005.

[45] Baffet et al.: Estimation of vehicle sideslip, tire force and wheel cornering stiffness, 2009.

degressive capability, dynamic wheel load, etc. In principle, such effects can be sorted into two categories: one is nonlinear effect and the other is time varying property. For instance, the degressive tire capability is a nonlinear effect which is neglected in the STM. The dynamic wheel load is a time varying property which introduces a time varying cornering stiffness even within the tire linear range.

The identification of a time varying axle cornering stiffness is investigated as the main focus in this thesis. A time varying cornering stiffness has significant influence on vehicle dynamics under some critical maneuvers, e.g. for a car-trailer combination with harmonic behavior at its dynamic critical speed. Under such circumstance, identification of a time varying axle cornering stiffness is very beneficial to study system instability. Besides, if the cornering stiffness can be simplified by the slope of a line between the OP of the tire behavior and the origin even within the nonlinear lateral dynamics, change of the cornering stiffness due to the change of the OP of the tire behavior is also of great concern. Because of the limitations of the available PIMs proposed above, a time varying axle cornering stiffness cannot be described in both the time and frequency domains simultaneously. Therefore, new PIMs have to be considered.

Rather than a one-dimensional representation of a signal from one domain to another domain by Fourier transform, the time-frequency analysis is a two-dimensional representation of a signal in both the time and frequency domains simultaneously. It is a refinement of the Fourier transform for the cases when signal characteristics are generally time varying but exhibit small changes within a short time interval. The basic form of time-frequency analysis is the short-time Fourier transform[46] (STFT) and the alternative is multi-resolution based Wavelet transform[47] (WT). There are two main differences between them. Firstly, STFT still uses the Fourier basic functions, i.e. sines and cosines, but the basic functions of WT are various wavelets. Secondly, STFT has a fixed resolution in both the time and frequency domains[46] while WT can give good temporal resolution for high-frequency components and good frequency resolution for low-frequency components, a combination best suited for many real signals[47]. But in the application of this thesis, the research is focused on the vehicle dynamics at the dominant yaw oscillation frequency and its harmonics, WT is not necessary and STFT can satisfy all the requirements.

[46] Quatieri: Discrete-Time Speech Signal Processing: Principles and Practice, 2001.

[47] Gao et al.: Wavelets: Theory and applications for manufacturing, 2010.

STFT has a wide application scope in the automotive engineering, especially in the parameter identification[48,49,50], fault detection and diagnosis[51,52]. Based on the STFT, a new method, moving-time-windowed-fast Fourier transform (MTWFFT)[53], is introduced to optimize the accuracy with additional spectrum-line-interpolation correction algorithms[53,54,55,56]. The MTWFFT method is very flexible in that the resolutions in the time and frequency domains can be easily changed. With MTWFFT, analysis of various time varying parameters related to vehicle dynamics becomes possible.

[48] Vulli et al.: Time-frequency analysis of single-point engine-block vibration measurements…, 2009.

[49] Stanković et al.: Time–frequency analysis of multiple resonances in combustion engine signals, 1999.

[50] Wagner et al.: Time variant system identification for car engine signal analysis, 1994.

[51] Payri et al.: Injection diagnosis through common-rail pressure measurement, 2006.

[52] Leontopoulos et al.: Vibration analysis for the design of a high-speed generator…, 1998.

[53] Zhang et al.: Analysis Methods for Time-Variant Harmonic Vehicle Dynamics Experiments, 2013.

[54] Ming et al.: Corrections for Frequency, Amplitude and Phase in A Fast Fourier Transform…, 1996.

[55] Kang et al.: Phase difference correction method for phase and frequency…, 2000.

[56] Niu et al.: An Algorithm for … Triple-spectrum-line Interpolation FFT, 2012.

3 Stability of Car-trailer Combinations

The proposed TFA-based PIM is derived for the purpose of vehicle dynamics study focusing on CTCs. Since the handling and stability behavior of such systems is more complex than that of normal passenger cars, this PIM is more meaningful and helpful for such systems, especially at critical maneuvers. However, this method can also be easily applied for normal passenger cars. Hence, only the linear STM of car-trailer combinations is introduced here.

3.1 Single-track model

The detailed derivation of this model has been presented in the past publications[16,57], only some important descriptions and assumptions are given here. Different from a relatively simple model with a single-axle trailer in the publications above, a STM with a tandem-axle trailer is built to be closer to the real experimental system. The reference coordinate system of the model is body-fixed coordinate system of the towing car X_cOY_c. The aerodynamics and its effect on lateral dynamics are ignored. The tire cornering behavior is assumed to be linear and all the angles, e.g. wheel steering angle δ_w, side-slip angle α_i and hitch angle θ_h, are assumed to be small (no more than 5°). Under such condition accompanied by the small angle approximation ($\sin x \approx x$, $\cos x \approx 1$) and a constant longitudinal velocity ($v_{x,1}=v_{x,2}=v_x$), the STM of a car-trailer combination is accomplished with 3 degrees of freedom (DOFs). A schematic diagram of the model is shown in Figure 3-1 below.

[57] Hac et al.: Stability and Control Considerations of Vehicle-Trailer Combination, 2008.

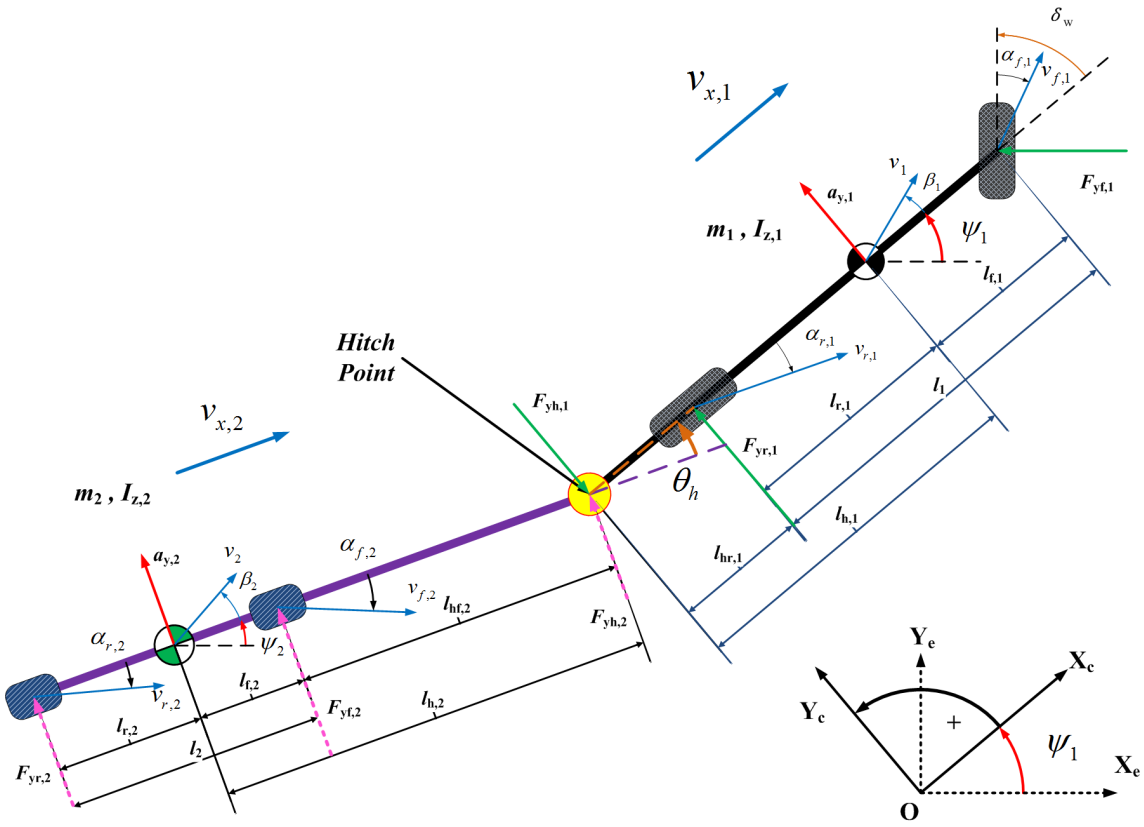

Figure 3-1: Linear single-track model with a tandem-axle trailer for car-trailer combinations

In the model, m_1 and m_2 denote the masses of the towing car and the trailer while $I_{z,1}$ and $I_{z,2}$ denote their yaw moments of inertia respectively. The front wheel steering angle is δ_w, $\alpha_{f,1}$ and $\alpha_{r,1}$ are the front and rear axle side-slip angles of the towing car, respectively. $C_{\alpha f,1}$ and $C_{\alpha r,1}$ denote the front and rear axle cornering stiffnesses of the towing car. $F_{yf,1}$ and $F_{yr,1}$ denote the front and rear axle lateral forces of the towing car. ψ_1, $\dot{\psi}_1$ denote the yaw angle and yaw rate of the towing car. $v_{y,1}$, $a_{y,1}$ denote the lateral velocity and acceleration at COG of the towing car. l_1, $l_{f,1}$ and $l_{r,1}$ denote the wheel base, the distance from front axle to COG and the distance from rear axle to COG of the towing car. $l_{h,1}$ and $l_{hr,1}$denote the distance from hitch point to COG and the distance from hitch point to rear axle of the towing car. Moreover, other parameters with subscript "2" instead of "1" denote the relevant parameters for the trailer.

Considering the lateral and yaw motions of the towing car, these equations are got with the Newton's law. Here $F_{yh,1}$ denotes the lateral force acting on the hitch point of the towing car.

$$m_1 a_{y,1} = F_{yf,1} + F_{yr,1} - F_{yh,1} \tag{3.1}$$

$$I_{z,1}\ddot{\psi}_1 = F_{yf,1} l_{f,1} - F_{yr,1} l_{r,1} + F_{yh,1} l_{h,1} \tag{3.2}$$

The lateral force at the front or rear axle of the towing car can be expressed as follows,

$$\begin{cases} \alpha_{f,1} = \delta_w - \frac{v_{y,1}}{v_x} - \frac{\dot{\psi}_1 l_{f,1}}{v_x} \\ F_{yf,1} = C_{\alpha f,1}\alpha_{f,1} = C_{\alpha f,1}\left(\delta_w - \frac{v_{y,1}}{v_x} - \frac{\dot{\psi}_1 l_{f,1}}{v_x}\right) \end{cases} \tag{3.3}$$

$$\begin{cases} \alpha_{r,1} = -\frac{v_{y,1}}{v_x} + \frac{\dot{\psi}_1 l_{r,1}}{v_x} \\ F_{yr,1} = C_{\alpha r,1}\alpha_{r,1} = C_{\alpha r,1}\left(-\frac{v_{y,1}}{v_x} + \frac{\dot{\psi}_1 l_{r,1}}{v_x}\right) \end{cases} \tag{3.4}$$

Also for the trailer, lateral and yaw motions are represented in the same way. Here $F_{yh,2}$ denotes the lateral force acting on the hitch point of the trailer.

$$m_2 a_{y,2} = F_{yf,2} + F_{yr,2} + F_{yh,2} \tag{3.5}$$

$$I_{z,2}\ddot{\psi}_2 = F_{yf,2} l_{f,2} - F_{yr,2} l_{r,2} + F_{yh,2} l_{h,2} \tag{3.6}$$

The lateral force at the front or rear axle of the trailer can be expressed as follows. Here the reference baseline for the definition of the hitch angle θ_h is the centreline of the trailer body.

$$\begin{cases} \alpha_{f,2} = -\theta_h - \frac{v_{y,2}}{v_x} - \frac{\dot{\psi}_2 l_{f,2}}{v_x} \\ F_{yf,2} = C_{\alpha f,2}\alpha_{f,2} = C_{\alpha f,2}\left(-\theta_h - \frac{v_{y,2}}{v_x} - \frac{\dot{\psi}_2 l_{f,2}}{v_x}\right) \end{cases} \tag{3.7}$$

$$\begin{cases} \alpha_{r,2} = -\theta_h - \frac{v_{y,2}}{v_x} + \frac{\dot{\psi}_2 l_{r,2}}{v_x} \\ F_{yr,2} = C_{\alpha r,2}\alpha_{r,2} = C_{\alpha r,2}\left(-\theta_h - \frac{v_{y,2}}{v_x} + \frac{\dot{\psi}_2 l_{r,2}}{v_x}\right) \end{cases} \tag{3.8}$$

The steering system is assumed to be rigid with a steering ratio i_s. δ_H is the steering wheel angle by hand.

$$\delta_w = \frac{\delta_H}{i_s} \tag{3.9}$$

To build the kinematic and dynamic relationships between the towing car and the trailer, yaw rates, velocities, forces and accelerations are connected considering the coupling at the hitch point with the following equations. Here $v_{y,h}$ denotes the lateral velocity at the hitch point of the system.

$$\dot{\psi}_1 - \dot{\psi}_2 = \dot{\theta}_h \tag{3.10}$$

$$v_{y,h} = v_{y,1} - \dot{\psi}_1 l_{h,1} = v_{y,2} + \dot{\psi}_2 l_{h,2} \tag{3.11}$$

$$F_{yh,1} = F_{yh,2} \tag{3.12}$$

$$\begin{cases} a_{y,1} = \dot{v}_{y,1} + v_x\dot{\psi}_1 \\ a_{y,2} = \dot{v}_{y,2} + v_x\dot{\psi}_1 \end{cases} \tag{3.13}$$

Combining the 13 equations above, a linear system written in state space form is obtained:

$$\mathbf{M}\dot{x} = \mathbf{D}(v_x)\boldsymbol{x} + \mathbf{E}u \tag{3.14}$$

M, **D** and **E** are the system matrices which are also given in Appendix A.2. While the matrices **M** and **E** only contain the constant system parameters, matrix **D** also contains the system longitudinal velocity v_x. The system state vector $\boldsymbol{x}$ and system input u are given by

$$\begin{cases} \boldsymbol{x} = \left[v_{y,1}, \dot{\psi}_1, \dot{\theta}_h, \theta_h\right]^T \\ u = \delta_H \end{cases} \tag{3.15}$$

Further, the system state-space equation is obtained as

$$\dot{\boldsymbol{x}} = \mathbf{A}(v_x)\boldsymbol{x} + \mathbf{B}u \tag{3.16}$$

Where

$$\mathbf{A}(v_x) = \mathbf{M}^{-1}\mathbf{D}(v_x), \mathbf{B} = \mathbf{M}^{-1}\mathbf{E} \tag{3.17}$$

Matrix **A** is a function of system longitudinal velocity v_x while matrix **B** is a constant.

So the CTCs can be represented by the analytical STM which is described by Eq. (3.16) in the horizontal plane. And it has a same form as a linear STM of a passenger car without a trailer.

3.2 System stability

System stability is an important requirement in the system design and control in engineering, especially in aeronautical or automotive engineering. In general, it is closely related to the system handling and safety. A simple physical interpretation of the stability concept is based on the vibration theory for a single-degree-of-freedom (1-DOF) system, which consists of an inertial lumped mass *m*, a spring stiffness *k* and a damping coefficient *d*. If the mass tends to return to its original equilibrium position after a displacement disturbance, the system is called to be statically stable. Otherwise, the system is called to be statically unstable. This kind of stability is named as static stability, which is opposite to static instability.

If the damping force opposes the motion of the mass then it will dissipate energy from any motion of the mass. Under this condition, the system is dynamically stable. But once the damping force acts in the same direction as the motion of the mass, then it will add energy to the system. In this case, the system is dynamically unstable. This kind of stability is named as dynamic stability, which is opposite to dynamic instability.

The motion of the mass after a displacement disturbance x_0 from its original equilibrium position is determined by the type of stability (see Figure 3-2 below). Regardless of the dynamic stability firstly, a system with static instability behaves a continuous divergence from its original equilibrium position (see Figure 3-2 (a)). That is the reason why the system instability is called divergent instability as well. An additional dynamic instability under this condition can enhance this divergence more rapidly. A system, which possesses static stability and dynamic instability simultaneously, will have an oscillatory motion with a progressively increasing amplitude (see Figure 3-2 (b)). Under this condition, the system's damping ratio is negative ($\xi < 0$). In contrast, a system with static stability coupled with dynamic stability has a decreasing amplitude in its response. In this case, the system response might be oscillatory or not, which is depending on the damping coefficient. If the system's damping ratio is smaller than one ($0 < \xi < 1$), the response still has oscillation (see Figure 3-2 (d)). Once the system's damping ratio reaches one or even bigger ($\xi \geq 1$), the oscillation is suppressed and the response is a smooth return to the original equilibrium position (see Figure 3-2 (e)). When the system's damping ratio is one ($\xi = 1$), its damping coefficient is called as critical damping coefficient.

However, there is still an intermediate stability state for such a system, which is called dynamic critical stability coupled with static stability (see Figure 3-2 (c)). Under such condition, the system's damping ratio is zero ($\xi = 0$). It matches with the critical stable state of a system, which is characterized by one pair of conjugate roots with zero real part (see Figure 1-5). This dynamic critical stability is very sensitive to any external disturbance or change of system parameter.

One point has to be mentioned for the static instability or dynamic instability. Normally the instability problem is not very concerned in the vibration theory for linear systems. If the spring force and damping force can be simplified by the linear expressions, there is no instability problem under a fixed OP. However, the real spring/damping force is more complex, either nonlinearity or a phase shift between the force and displacement/velocity can make the system unstable. Then the system's damping ratio might be around zero or negative ($\xi \leq 0$). However, for a practical system with a distributed mass, influence of different parameters on the damping ratio is more complex.

In principle, any type of instability should be avoided in the system design for safety reasons. Moreover, from an engineering point of view, to guarantee the system stability is only a prerequisite. Meanwhile, a certain degree of stability, called as stability margin, is also necessary in the practical application, because a system with highly oscillatory response ($\xi \approx 0$) might be difficult to control in practice. Therefore, an optimal system design should provide the stability margin as much as possible.

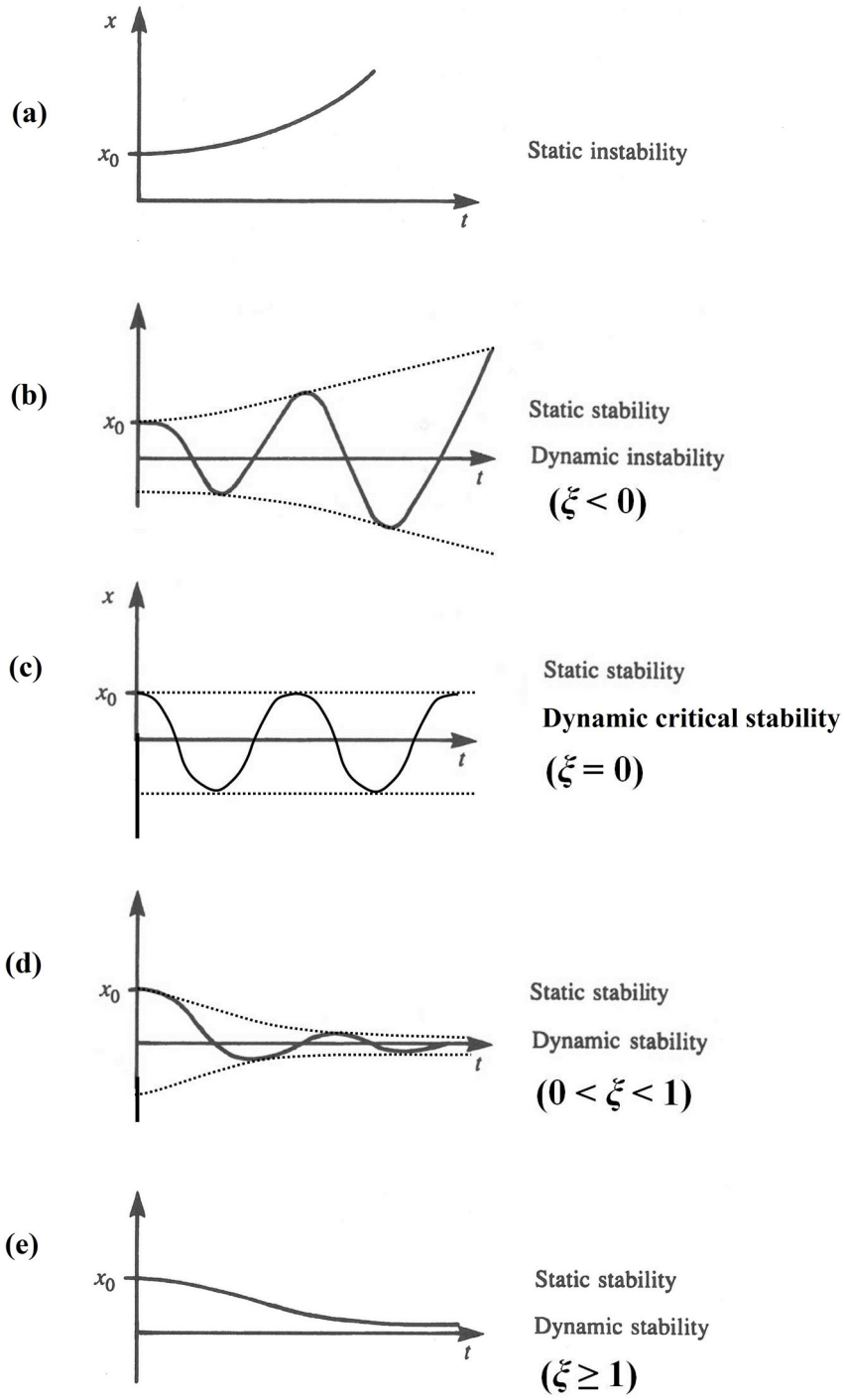

Figure 3-2: Static stability and dynamic stability described by possible motions of a mass after a displacement disturbance [58]

[58] Dixon: Tires, Suspension and Handling, second edition, 1996, p. 433.

Considering the stability of vehicle systems, there are two different types of instability problems in the horizontal plane: static instability and dynamic instability[57]. Once static instability occurs, the typical system state variables, like yaw rate, increase without experiencing oscillations. In order to avoid this static instability, passenger cars are normally designed with a positive understeer gradient. However, for special vehicle systems like CTCs, system understeer gradient might become negative at a particular OP due to trailer design or improper load distribution even when the towing car is understeering. This type of static instability is well known as jackknifing, especially for articulated vehicles.

Besides the demand of static stability, it is necessary to investigate system dynamic stability. A statically stable system with a big oscillatory response is also difficult to control for an inexperienced driver, like a CTC under its critical stable state. This nature is named as dynamic instability. The dynamic instability in the horizontal plane is known as snaking, swing or flutter[14]. The phenomenon of instability observed in the project is the dynamic instability. Moreover, this dynamic critical stability is the OP for the CTC and potential influence resulting from time varying vertical dynamics on the dynamic critical stability is the research focus in this thesis.

3.2.1 Static stability

System static stability is also called divergent stability, in which "the variables describing the system response increase exponentially in magnitude without oscillations"[57]. Research[59,60] has shown that the static stability of the CTCs depends only on the parameters of the towing car and the vertical hitch load. The trailer mass and the location of the trailer COG in the longitudinal direction affect the vertical hitch load. It shows that reducing the vertical hitch load can improves the static stability of the CTCs.

Static stability is more concerned for the design of the normal passenger cars. It is indicated by the understeer gradient, a measure of performance under steady state conditions. Therefore, a vehicle system described by Eq. (3.16) without the steering input is considered in a steady state cornering condition.

$$\dot{\boldsymbol{x}} = \mathbf{A}(v_x)\boldsymbol{x} = 0 \tag{3.18}$$

The system yaw rate gain can be obtained once the Eq. (3.18) is solved. Its relationship with the longitudinal velocity for normal passenger cars is shown in Figure 3-3 below. While a car designed with understeering behavior has a characteristic velocity, a car

[59] Kurtz et al.: Handling Characteristics of Car-Trailer Systems; A State-of-the-Art Survey, 1977.

[60] Bevan et al.: Some factors influencing the stability of car/caravan combinations, 1983.

designed with oversteering behavior has a static critical velocity with an infinite yaw rate gain, which characterizes a static instability. However, the self-steering characteristic can be changed by adjusting the COG and cornering stiffness. Both of them are drastically influenced by the payload distribution, which depends mainly on the engine mounting position. "High-performance cars like sports cars are intended to be very maneuverable and strive for a neutral steering characteristic, but most passenger cars are designed to be understeer for safety reasons."[61] For an oversteering car, its static critical speed is often designed significantly higher than the car's top speed to avoid practical instability problem.

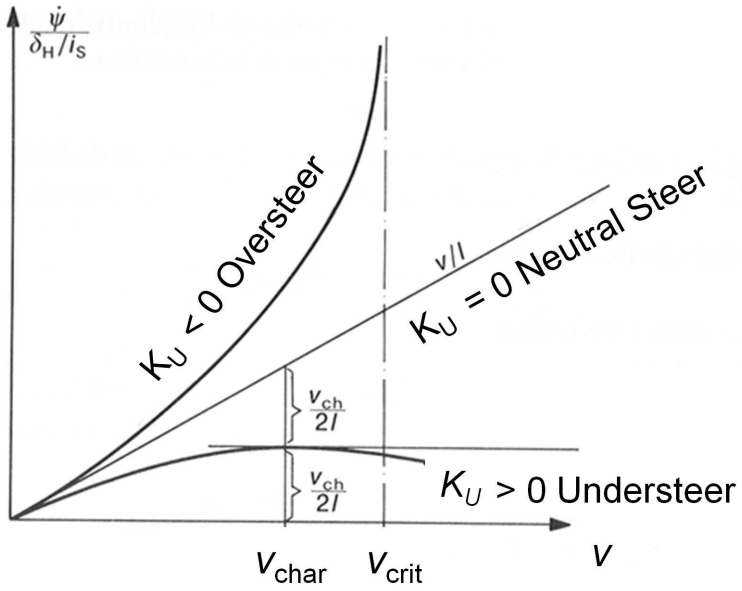

Figure 3-3: System yaw rate gain in dependence on longitudinal velocity v for passenger cars[62]

However, for the CTCs, the load distribution is rather more complex from an empty condition to full load condition. It is not possible to absolutely characterize the system self-steering characteristic as optimal. Instead, one must consider the type of car involved and the normal operating speeds. In general, to avoid undriveable situation at moderate speeds and instability at high speeds, the towing car should be designed to have relatively more understeer margin than would be desirable from a handling point of view.

Here, a comparison of the towing car understeer gradient between a normal passenger car, a CTC with a single-axle trailer and a CTC with a tandem-axle trailer is performed based on the expression of the system yaw rate gain. Another comparison of the equiva-

[61] Karnopp: Vehicle Stability, 2004, p. 130.

[62] Winner: Skriptum zur Vorlesung "Fahrdynamik und Fahrkomfort" (Ride and Handling), 2014.

lent trailer understeer gradient between a CTC with a single-axle trailer and a CTC with a tandem-axle trailer is performed based on the expression of the system hitch angle gain.

Towing car understeer gradient

For **a normal passenger car**, the yaw rate gain of the towing car is given by Eq. (3.19) [63] below.

$$\frac{\dot{\psi}_1}{\delta_w} = \frac{v_x}{l_1 + K_u \cdot \frac{v_x^2}{g}} \tag{3.19}$$

A corresponding towing car understeer gradient $K_{u,1}$ is given by Eq. (3.20)[63] below.

$$K_{u,1} = \frac{W_{f,1}}{C_{\alpha f,1}} - \frac{W_{r,1}}{C_{\alpha r,1}} = \frac{m_1 g}{l_1}\left(\frac{l_{r,1}}{C_{\alpha f,1}} - \frac{l_{f,1}}{C_{\alpha r,1}}\right) \tag{3.20}$$

Here, $W_{f/r,1}$ denotes the front/rear static axle load of the towing car expressed by Eq. (3.21) and g is the gravitational acceleration.

$$\begin{cases} W_{f,1} = m_1 g \cdot \frac{l_{r,1}}{l_1} \\ W_{r,1} = m_1 g \cdot \frac{l_{f,1}}{l_1} \end{cases} \tag{3.21}$$

For **a CTC with a single-axle trailer**, the yaw rate gain of the towing car is given by Eq. (3.22) [64] below. Under such condition, the trailer front axle is absent and so are the relevant system parameters in Figure 3-1.

$$\frac{\dot{\psi}_1}{\delta_w} = \frac{v_x}{l_1 + K'_{u,1} \cdot \frac{v_x^2}{g}} = \frac{v_x}{l_1 + (K_{u,1} - \Delta K_{u,1}) \cdot \frac{v_x^2}{g}} \tag{3.22}$$

A corresponding towing car understeer gradient $K'_{u,1}$ is given by Eq. (3.23)[64] below.

$$K'_{u,1} = K_{u,1} - \Delta K'_{u,1} = \frac{W_{f,1} + \Delta W_{f,1}}{C_{\alpha f,1}} - \frac{W_{r,1} + \Delta W_{r,1}}{C_{\alpha r,1}} = \left(\frac{W_{f,1}}{C_{\alpha f,1}} - \frac{W_{r,1}}{C_{\alpha r,1}}\right) - \left(\frac{\Delta W_{r,1}}{C_{\alpha r,1}} - \frac{\Delta W_{f,1}}{C_{\alpha f,1}}\right) \tag{3.23}$$

$$\Delta K'_{u,1} = \frac{\Delta W_{r,1}}{C_{\alpha r,1}} - \frac{\Delta W_{f,1}}{C_{\alpha f,1}} = \frac{m_2 g}{(l_{r,2} + l_{h,2})} \cdot \frac{l_{r,2}}{l_1}\left(\frac{l_{hr,1}}{C_{\alpha f,1}} + \frac{l_1 + l_{hr,1}}{C_{\alpha r,1}}\right) \tag{3.24}$$

$\Delta K'_{u,1}$ in Eq. (3.24) is the change of the towing car understeer gradient due to the existence of a single-axle trailer, i.e. the change in the front/rear static axle load of the towing car due to an additional vertical hitch load, $\Delta W_{f/r,1}$ expressed in Eq. (3.25) below.

---

[63] Gillespie: Fundamentals of Vehicle Dynamics, 1992, p. 206.

[64] Hac et al.: Stability and Control Considerations of Vehicle-Trailer Combination, 2008.

$$\begin{cases} \Delta W_{f,1} = -m_2 g \cdot \frac{l_{r,2} l_{hr,1}}{l_1 (l_{r,2} + l_{h,2})} < 0 \\ \Delta W_{r,1} = m_2 g \cdot \frac{l_{r,2} (l_1 + l_{hr,1})}{l_1 (l_{r,2} + l_{h,2})} > 0 \end{cases} \tag{3.25}$$

It is clear from Eq. (3.25) that the front static axle load of the towing car decreases while the rear static axle load of the towing car increases in any case. It matches with the result of a negative vertical hitch load (a down force at the hitch point) when a single-axle trailer is towed.

For **a CTC with a tandem-axle trailer**, the yaw rate gain of the towing car is given by Eq. (3.26) below.

$$\frac{\dot{\psi}_1}{\delta_w} = \frac{v_x}{L + K''_{u,1} \cdot \frac{v_x^2}{g}} \tag{3.26}$$

While the parameter L and the corresponding towing car understeer gradient $K''_{u,1}$ are given by Eq. (3.27) and Eq. (3.28) below. Their expressions are relatively complex.

$$L = l_1 - \frac{C_{\alpha f,2} \cdot C_{\alpha r,2} \cdot l_2^2 [C_{\alpha f,1} (l_1 + l_{hr,1}) + C_{\alpha r,1} \cdot l_{hr,1}]}{C_{\alpha f,1} \cdot C_{\alpha r,1} \cdot l_1 [C_{\alpha f,2} \cdot l_{hf,2} + C_{\alpha r,2} (l_2 + l_{hf,2})]} \tag{3.27}$$

$$K''_{u,1} = K_{u,1} - \Delta K''_{u,1} \tag{3.28}$$

$$\Delta K''_{u,1} = \frac{m_2 g (C_{\alpha r,2} \cdot l_{r,2} - C_{\alpha f,2} \cdot l_{f,2}) [C_{\alpha f,1} (l_1 + l_{hr,1}) + C_{\alpha r,1} \cdot l_{hr,1}]}{C_{\alpha f,1} \cdot C_{\alpha r,1} \cdot l_1 [C_{\alpha f,2} \cdot l_{hf,2} + C_{\alpha r,2} (l_2 + l_{hf,2})]} \tag{3.29}$$

Under this condition, the towing car understeer gradient has two components as well, similar as that of a CTC with a single-axle trailer. One component is related to the towing car mass and the other is related to the trailer mass.

Besides, the yaw rate gain of the trailer is the same as the yaw rate gain of the towing car in a steady state cornering condition, because the yaw rate of the trailer is the same as the yaw rate of the towing car under such condition. It can be derived based on Eq. (3.30).

$$\dot{\theta}_h = \dot{\psi}_1 - \dot{\psi}_2 = 0 \tag{3.30}$$

Equivalent trailer understeer gradient

While the static stability is mainly determined by the understeer gradient for a normal passenger car only, an equivalent understeer gradient related to the trailer can affect the system stability as well. It can be derived based on the system hitch angle gain.

For **a CTC with a single-axle trailer**, the system hitch angle gain is given by Eq. (3.31)[65] below. Under such condition, the trailer front axle is absent and so are the relevant system parameters in Figure 3-1.

$$\frac{\theta_h}{\delta_w} = \frac{l_2 + K'_{u,2} \cdot \frac{v_x^2}{g}}{l_1 + K'_{u,1} \cdot \frac{v_x^2}{g}} \tag{3.31}$$

$K'_{u,2}$ is defined as the equivalent trailer understeer gradient. It is expressed by Eq. (3.32) below.

$$\begin{aligned} K'_{u,2} &= \frac{W_{r,1}}{C_{\alpha r,1}} + \frac{m_2 g}{(l_{r,2} + l_{h,2})} \cdot \left(\frac{l_{r,2}}{l_1} \cdot \frac{l_1 + l_{hr,1}}{C_{\alpha r,1}} - \frac{l_{h,2}}{C_{\alpha r,2}}\right) \\ &= \frac{m_1 g}{l_1} \cdot \frac{l_{f,1}}{C_{\alpha r,1}} + \frac{m_2 g}{(l_{r,2} + l_{h,2})} \cdot \left(\frac{l_{r,2}}{l_1} \cdot \frac{l_1 + l_{hr,1}}{C_{\alpha r,1}} - \frac{l_{h,2}}{C_{\alpha r,2}}\right) \end{aligned} \tag{3.32}$$

For **a CTC with a tandem-axle trailer**, the system hitch angle gain is given by Eq. (3.33) below.

$$\frac{\theta_h}{\delta_w} = \frac{L_\theta + K''_{u,2} \cdot \frac{v_x^2}{g}}{L + K''_{u,1} \cdot \frac{v_x^2}{g}} \tag{3.33}$$

While the parameter L_θ and the corresponding equivalent trailer understeer gradient $K''_{u,2}$ are given by Eq. (3.34) and Eq. (3.35) below. Their expressions are relatively complex.

$$L_\theta = -\frac{C_{\alpha r,1}\left[C_{\alpha f,2}(l_{hr,1} + l_{hf,2}) l_{hf,2} + C_{\alpha r,2}(l_2 + l_{hf,2})(l_2 + l_{hf,2} + l_{hr,1})\right] + C_{\alpha f,2} \cdot C_{\alpha r,2} \cdot l_2^2}{C_{\alpha r,1}\left[C_{\alpha f,2} \cdot l_{hf,2} + C_{\alpha r,2}(l_2 + l_{hf,2})\right]} \tag{3.34}$$

$$K''_{u,2} = -\frac{m_1 g}{l_1} \cdot \frac{l_{f,1}}{C_{\alpha r,1}} + \frac{m_2 g}{l_1} \cdot \frac{(C_{\alpha f,2} \cdot l_{f,2} - C_{\alpha r,2} \cdot l_{r,2})(l_1 + l_{hr,1}) + C_{\alpha r,1} \cdot l_1 \cdot (l_{f,2} + l_{hf,2})}{C_{\alpha r,1}\left[C_{\alpha f,2} \cdot l_{hf,2} + C_{\alpha r,2}(l_2 + l_{hf,2})\right]} \tag{3.35}$$

While the yaw rate gain is totally determined by the towing car understeer gradient, the hitch angle gain is determined by both understeer gradients. Although the towing car understeer gradient still has the dominant influence, the equivalent trailer understeer gradient can also amplify its magnitude when it is positive. Therefore, both understeer gradients should be considered in the design related to system static stability of the CTCs.

[65] Wei: Study on Handling Stability of Caravan, 2008.

3.2.2 Dynamic stability

The system dynamic stability is of particular concern in this thesis. A free system described by Eq. (3.16) without the steering input can be described by the equation below,

$$\dot{\boldsymbol{x}} = \mathbf{A}\boldsymbol{x} \tag{3.36}$$

The system eigenvalues are the roots of the corresponding characteristic equation

$$det(s\mathbf{I} - \mathbf{A}) = 0 \tag{3.37}$$

Here, $\mathbf{I}$ is an identity matrix and s is the Laplace operator. The complex characteristic roots are

$$s_{1,2} = -r \pm j\omega_d \tag{3.38}$$

Where r is called the damping factor, ω_d is the damped natural frequency and j is the imaginary unit.

The state-space equation of a single passenger car or of a single trailer is a 2nd order system, which has only one pair conjugate roots and one yaw damping ratio. However, a CTC is a 4th order system, which has two pairs of complex conjugate roots with one yaw damping ratio for each pair. They are either real or complex occurring in conjugate pairs. For an asymptotical stable system, all the roots must have negative real parts. Once any pair of the roots has a positive real part, the system becomes dynamically unstable. Because the system matrix $\mathbf{A}$ is a function of the longitudinal velocity v_x, the system characteristic roots also depend on the longitudinal velocity v_x.

The system root locus plot in dependence on the longitudinal velocity v_x (80-140 km/h) in s-plane is illustrated in Figure 3-4 below. System eigenvalues of three related systems (a CTC, a single passenger car and a single trailer) are compared in the root locus plot. They share one set of parameters delivered from the real experimental system. The OPs of system parameters are listed in Table A and Table B in Appendix A.1. It is clear that when v_x exceeds 123.3 km/h corresponding to one pair of eigenvalues with zero real part, the CTC becomes dynamically unstable. This longitudinal velocity is defined as the system dynamic critical speed v_{crit}, which indicates the boundary of system dynamic stability. In contrary to a CTC, a single passenger car or a single trailer does not have such v_{crit} even at very high v_x.

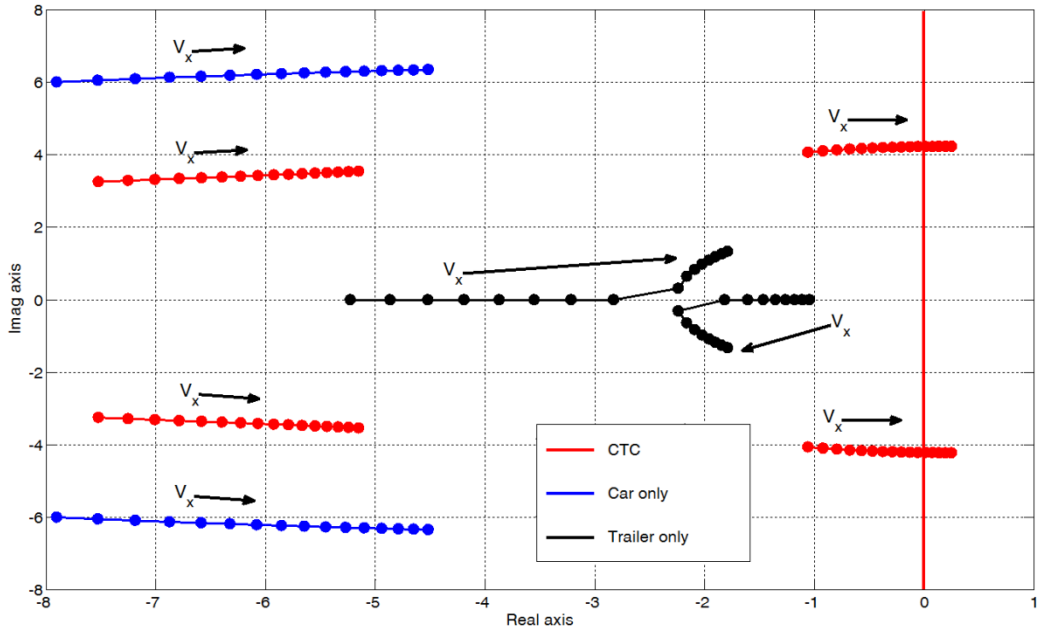

Figure 3-4: System root locus in dependence on the longitudinal velocity v_x (80-140 km/h) in *s*-plane

Because the real part of the eigenvalues delivers the information of damping factor or damping ratio, a dynamic critical stable system can also be characterized by its yaw damping ratio and natural frequency. In fact, the system dynamic critical speed is related to a zero yaw damping ratio[66]. The damping ratio ξ and the undamped natural frequency ω_n are determined by the equations below.

$$\xi = \frac{r}{\sqrt{r^2+\omega_d^2}} \tag{3.39}$$

$$\omega_n = \sqrt{r^2 + \omega_d^2} \tag{3.40}$$

The system yaw damping ratio is also a good indicator of system dynamic stability. It is a function of the longitudinal velocity v_x as well. For a passenger car or a single trailer, its unique yaw damping ratio is given by the equation[67] below.

$$\xi(v_x) = \frac{\xi_0}{\sqrt{1+v_x^2.\frac{K_u}{l_1}}} \tag{3.41}$$

Here, ξ_0 represents the yaw damping ratio at zero longitudinal velocity ($v_x = 0$). It is a function of the geometric parameters and cornering stiffness. In a practical way, it has a limit by the Eq. (3.42) derived from the physical solutions[68]. Generally, it is ca. 1.0.

[66] ISO 9815: Road vehicles - Passenger-car and trailer combinations - Lateral stability test, 2003.

[67] Dixon: Tires, Suspension and Handling, second edition, 1996, p. 455.

[68] Dixon: Tires, Suspension and Handling, second edition, 1996, p. 457.

From a practical point of view, it is recommended that $\xi > 0.45$ at the maximum velocity of a vehicle[68].

$$\xi_0 \geq 1.0 \tag{3.42}$$

A significant difference between the static stability and dynamic stability can be stated based on the Eq. (3.41) here. At high longitudinal velocity, the system yaw damping ratio becomes rather small if the system has a large understeer gradient[68]. High-speed yaw oscillation is difficult to control and dangerous. Hence, it should be avoided in system design. It is clear that an increasing understeer gradient can improve the static stability but reduce the dynamic stability at high speeds at the same time[69]. It is a conflict and a trade-off for the system understeer gradient is necessary in the system design considering stability. Because most system parameters affect the understeer gradient, an optimal range of K_u or significant parameter, e.g. corresponding hitch load, is recommended.

For a CTC, the derivation of system yaw damping ratio is relatively complex due to a 4th order system. However, it can be obtained in the numerical way. In practical road test, the relationship between the yaw damping ratio and dynamic critical speed can be linearized in a small speed range around the v_{crit}. A straight line representing the best fit to the experimental data is determined by regression of the data to the following form:

$$\xi(v_x) = c_0 + c_1 \cdot v_x \tag{3.43}$$

Here, c_0 and c_1 are the regression coefficients. It is also a convenient way to determine the system v_{crit} by a zero yaw damping ratio in a graphical way.

Through numerical calculation, yaw damping ratios of three related systems above (a normal passenger car, a single trailer and a CTC) in dependence on the longitudinal velocity v_x (30-140 km/h) are compared in Figure 3-5 below. The result is consistent with that in the root locus plot in Figure 3-4. A zero yaw damping ratio which only exists in one of the two damping ratios for a CTC determines the system critical stable state and its dynamic critical speed v_{crit} at 123.3 km/h as well.

The difference in the unique damping ratio between the passenger car and the single trailer deserves special attention. The trailer has a nearly constant yaw damping ratio of 1.0, which can be explained by its neutral steering characteristic due to the nearly same quantities of the both trailer axles. But for the passenger car, a significant difference in the front and rear axle cornering stiffnesses determines an understeering characteristic and hence its yaw damping ratio decreases along an increasing longitudinal velocity v_x.

[69] Hac et al.: Stability and Control Considerations of Vehicle-Trailer Combination, 2008.

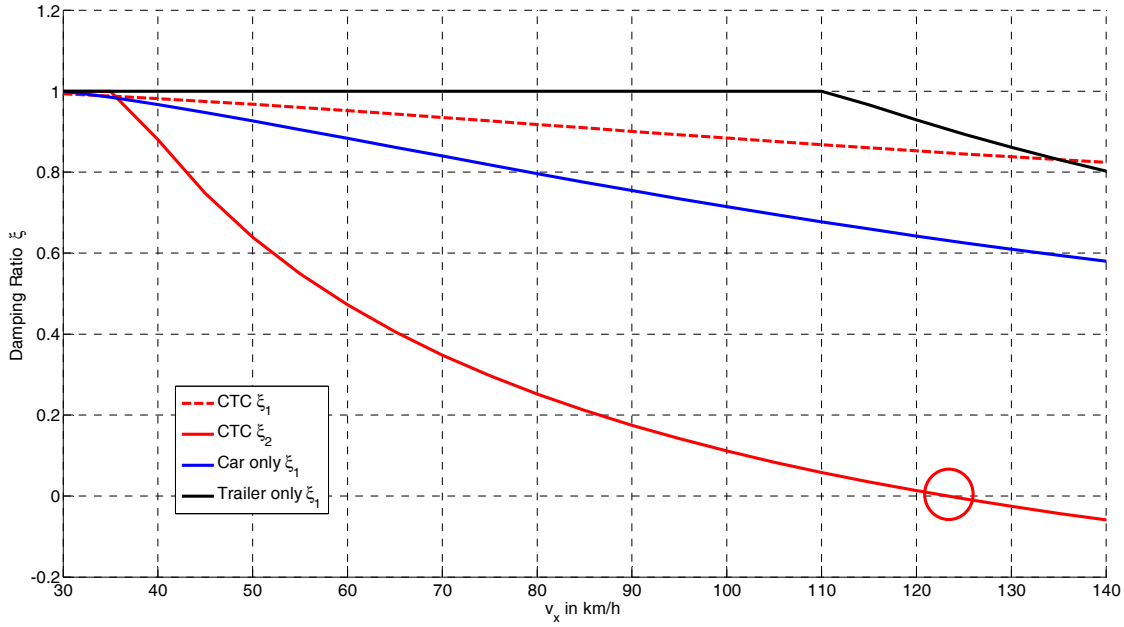

Figure 3-5: Comparison of system yaw damping ratios depending on the longitudinal speed v_x

The system dynamic critical speed or yaw damping ratio is determined by the OP of system parameters. Therefore, each system parameter in the STM has influence on system dynamic stability. Based on the STM, sensitivity analysis of these system parameters can be achieved. To quantify its influence with the problem that each parameter has different physical meaning and unit, system parameter's influence is defined by the following formula, where x represents each system parameter.

$$\Delta v_{crit} = \frac{\partial v_{crit}}{\partial x} \times x_{OP} \cdot 1\% \tag{3.44}$$

Under the OP defined in Table A and Table B in Appendix A.1, sensitivity analysis is achieved and the result is shown in Figure 3-6 below. For the quantification and comparison, the result contains the corresponding change of system dynamic critical speed v_{crit} when each parameter increases by 1% on the basis of OP delivered from the real experimental system. They are sorted into 3 categories, incl. inertial parameters (in blue), geometric parameters (in black) and axle cornering stiffnesses (in red).

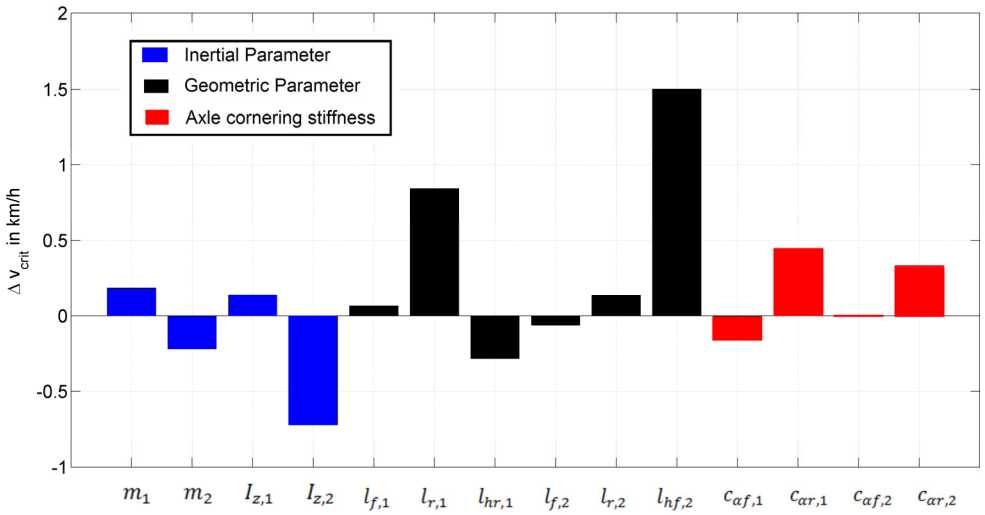

Figure 3-6: Sensitivity analysis of system parameters existing in the linear STM

However, the inertial and geometric parameters are usually constant over time in practice. Their influences are rarely considered once the system OP is already available. Instead, the axle cornering stiffness depends on various conditions and their influences on the v_{crit} are of more concern.

Since the axle cornering stiffnesses serve as a connection between the vertical dynamics and horizontal dynamics, they are of special concern in the linear STM. Therefore, their sensitivity to the v_{crit} of a CTC is particularly considered and illustrated in Figure 3-7 below. A short conclusion is that, an increasing rear axle cornering stiffness of the towing car or trailer has a positive impact on the system dynamic stability, while an increasing front axle cornering stiffness of the towing car makes the stability worse. Change of the front axle cornering stiffness of the trailer has nearly no influence on the stability. Besides, the rear axle cornering stiffness of the towing car $C_{\alpha\mathrm{r},1}$ has biggest influence on the stability among them and hence it deserves special and more attention in system stability analysis.

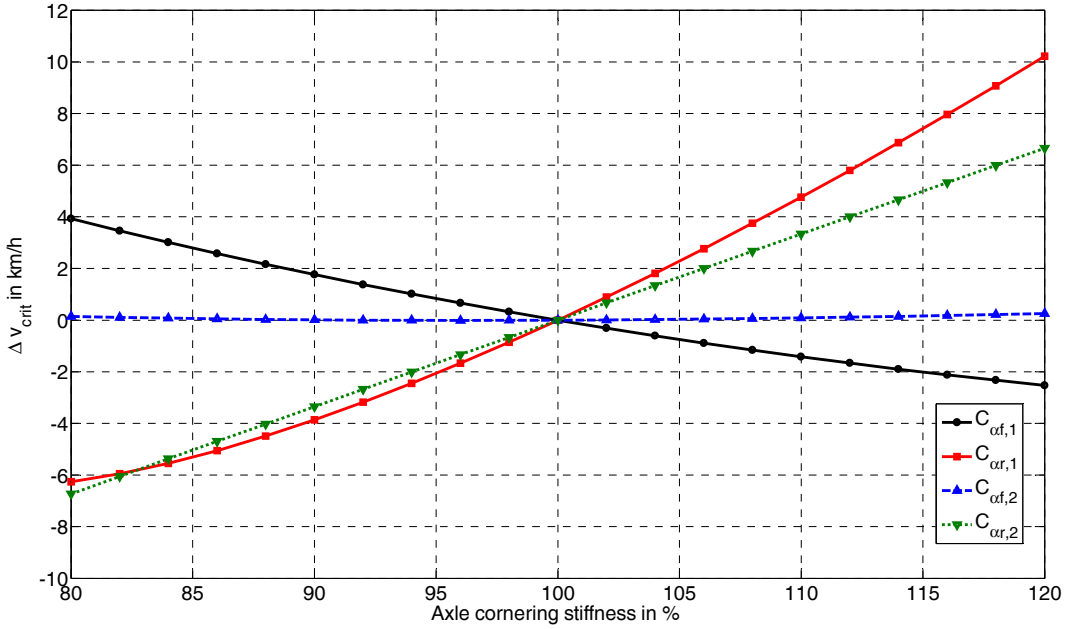

Figure 3-7: System dynamic critical speed in dependence on the axle cornering stiffness

3.3 Conclusions

A state-of-the-art survey shows that very few research activities were performed to study the coupling between the vertical dynamics and horizontal dynamics, particularly for the system stability analysis. Even for the normal passenger car, stability analysis is mainly focused in the horizontal plane. This is mainly due to two reasons. On the one hand, influence on system stability from vertical dynamics is small. On the other hand, dynamic stability is not a severe problem for the normal passenger car even at high longitudinal velocity. However, the driving dynamics and stability analysis of CTCs are obviously different from that of a normal passenger car. Dynamic stability is of more concern for CTCs, because the system dynamic critical speed, which is only ca. 100 km/h, can be easily exceeded at highways. Moreover, dynamic critical stability is very sensitive to any external disturbance or change of system parameter. In such a situation, even small influence from the vertical dynamics might make a dynamic critical stable system unstable. Therefore, the coupling between the vertical dynamics and horizontal dynamics is a constructive topic for the dynamic stability of CTCs.

This chapter lays a theoretical foundation for the stability investigation of CTCs. Because the driving dynamics and stability analysis of CTCs are obviously different from that of a normal passenger car, a short overview from the stability perspective becomes necessary before further stability investigation.

Firstly, a linear STM for a CTC with a tandem-axle trailer is derived and its system state space expression is achieved. Although a STM for a CTC with a single-axle trailer is

popularly used in the publications, the contribution with a tandem-axle trailer is relatively novel. It has a similar form as that of a normal passenger car but is a 4^{th} order system with 3 DOFs.

General system stability is defined based on a single-DOF mass-spring-damper system. Both static stability and dynamic stability are described with their corresponding behavior under a displacement disturbance. Then the instability of vehicle systems are introduced and special attention is paid on the static stability and dynamic stability of the CTCs.

For the static stability, system understeer gradient derived from the yaw rate gain serves as a measure to quantify the system static stability. For the CTCs, towing car understeer gradient and an equivalent trailer understeer gradient are defined and derived based on the yaw rate gain and hitch angle gain. Although the towing car understeer gradient still dominates the static stability, the equivalent trailer understeer gradient also has extra influence. Therefore, both understeer gradients should be considered in the design related to system static stability of the CTCs.

The dynamic stability is of more concern for the CTCs. The system dynamic critical speed v_{crit}, which indicates the boundary of system dynamic stability, is defined based on the system root locus plot with variant longitudinal velocity. It is closely related to a zero yaw damping ratio. Both of them are utilized to characterize the dynamic stability of a CTC. It reveals that an increasing understeer gradient can improve the static stability but reduce the dynamic stability at the same time. It is a conflict and a trade-off for the system understeer gradient is necessary in the system design considering stability. And so are the system parameters.

Sensitivity analysis of system parameters to the dynamic critical speed is obtained on the basis of the linear STM. A short conclusion is that, an increasing rear axle cornering stiffness of the towing car or trailer has a positive impact on the system dynamic stability, while an increasing front axle cornering stiffness of the towing car makes the stability worse. Change of the front axle cornering stiffness of the trailer has nearly no influence on the stability. Besides, the rear axle cornering stiffness of the towing car $C_{\alpha r,1}$ has biggest influence on the stability among them and hence it deserves special and more attention in system stability analysis.

4 Time-Frequency Analysis based Parameter Identification Method (TFA-based PIM)

Because the instability problem studied in this thesis is the dynamic instability of a CTC, it generally starts from a steady state oscillation, i.e. system dynamic critical stable state. A CTC behaves a steady state yaw oscillation in this situation. However, once the characteristic of some component changes over time, a dynamically stable CTC becomes unstable. That is to say, the system state shifts from dynamic critical stable to dynamic unstable. Hence, the root cause of this instability problem is a time varying phenomenon existing in some specific component.

Another three aspects make the investigation of the problem more challengeable. Firstly, a dynamically stable system is very sensitive to any small disturbances, like dynamic wheel load, nonlinear steering/tire characteristics or aerodynamics at this stability boundary. It makes the experimental research more difficult because other unexpected disturbances cannot be completely excluded. Secondly, the experience from stability analysis of passenger cars reveals that, influence from vertical dynamics like damper characteristic is very small. It indicates the difference between different damper setups, which makes a dynamically stable system unstable, might be very small as well. Finally, for safety reasons, useful system response is relatively short in time domain in the road test (see Figure 1-4). It is often less than 10 seconds under the first steering impulse excitation and extremely shorter, mostly less than 3 seconds, under the second steering impulse excitation. All these three aspects put forward high demands on the performance of DSP for the purpose of high resolution.

On this basis, two main requirements have to be satisfied in the process of system identification, identification of time varying property and improvement of resolution. In order to identify the potential time varying property, TFA-based PIM has to be considered. For the purpose of high resolution, further measures like the spectrum-line-interpolation correction algorithms might be helpful.

The PIM proposed in this thesis is a combination of a linear STM and the MTWFFT. It is a TFA-based PIM, which can be used to estimate time-invariant and time varying system parameters. The PIM aims for the system model identification to build up simulation models. A complete block diagram of the TFA-based PIM for the application of a CTC or normal passenger car with necessary sensors is shown in Figure 4-1. The TFA-based PIM contains three components, mainly MTWFFT, a STM and an effective axle load evaluation algorithm. The former two are indispensable while the last part takes a phenomenon of nonlinearity-induced harmonic dynamic axle load into account. All the

three parts are described in this chapter. Besides, the inputs and outputs for the PIM are also illustrated in the diagram and their definitions can be found in the equations in this chapter. Standard (in green blocks) and necessary (but non-standard, in blue blocks) measurement sensors in the road test are shown as well. Inertial and geometric parameters including steering ratio (in yellow blocks) are necessary and assumed to be available in advance. The diacritic "^" is used to label the complex amplitudes in frequency domain (similarly hereinafter).

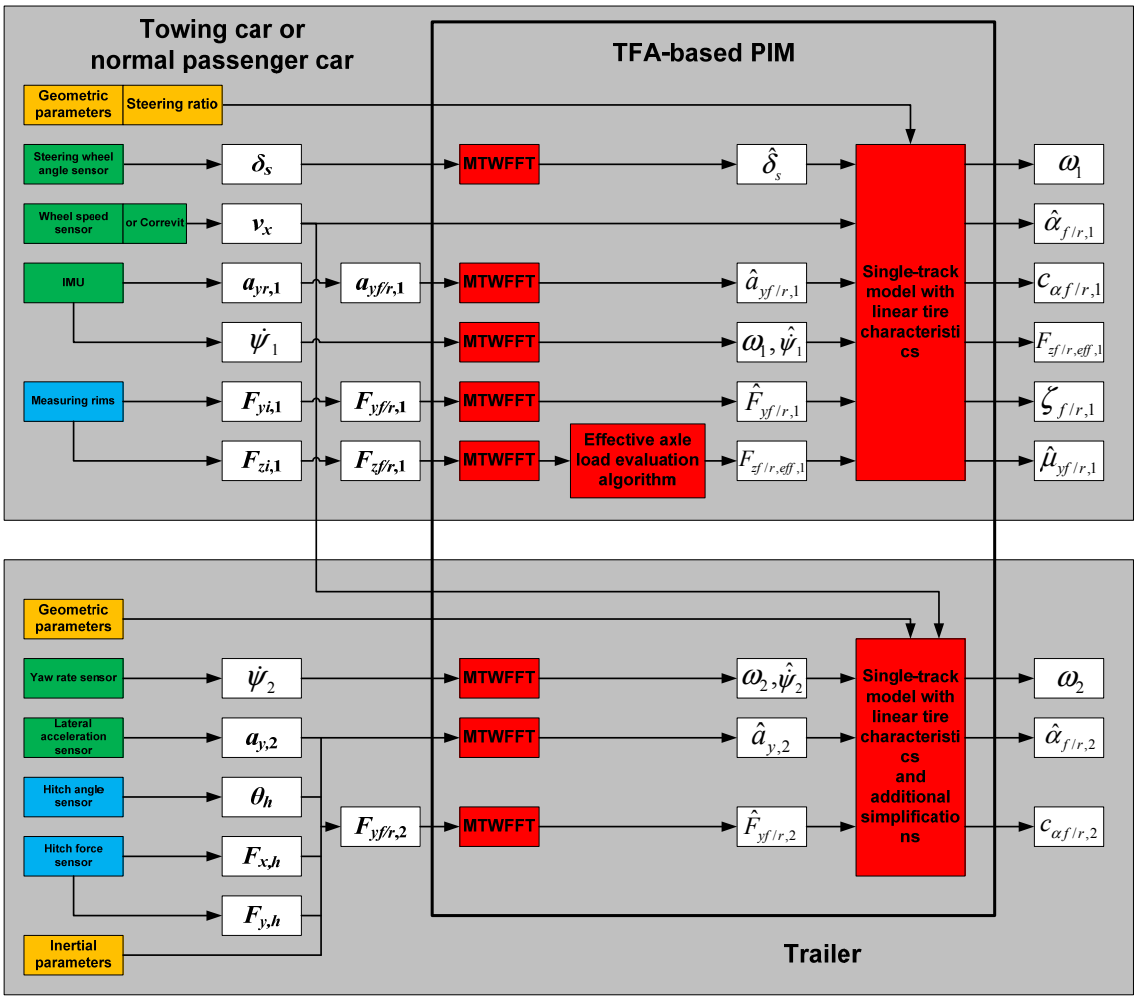

Figure 4-1: A complete block diagram of the TFA-based PIM for the application of a car-trailer combination or normal passenger car with necessary sensors

4.1 Time-frequency analysis

"In signal processing, TFA comprises those techniques that study a signal in both the time and frequency domains simultaneously, using various time-frequency representations (TFRs)"[70]. A TFR is a view of a signal represented over both time and frequency domains. TFA is analysis into the time-frequency domain provided by a TFR. This is achieved with a formulation called as time-frequency distribution (TFD)[71].

In the state of the art, several well-known TFDs are generated by the following ways, such as:

- Short-time Fourier transform incl. the Gabor transform
- Wavelet transform
- Bilinear time-frequency distribution function (Wigner distribution function)
- Modified Wigner distribution function, Gabor-Wigner distribution function, etc (see Gabor-Wigner transform).

Since the STFT is the most basic form of TFA and such a linear TFR can satisfy all the requirements in the research of instability problem in this thesis, the MTWFFT is introduced based on the STFT for the purpose of identifying time varying vehicle dynamics under harmonic conditions. Although other TFDs have their own advantages in the TFA, they are more complex and unnecessary in the application here.

4.1.1 MTWFFT

In principle, MTWFFT has the same essence as the STFT. The principle of the MTWFFT method is illustrated in Figure 4-2. Normally, the dynamic signals are directly obtained by the measurements in time domain. The standard Discrete/Fast Fourier transform (DFT/FFT) can be used to get the complete frequency domain information. With a pre-defined moving time window, the instantaneous characteristics (incl. frequency, amplitude and phase) are available. A MTWFFT, similar as STFT, can then be performed. Both the temporal and frequency resolutions are dependent on the length of the moving time window.

---

[70] Wikipedia – virtual: http://en.wikipedia.org/wiki/Time-frequency_analysis, last access: February 23rd 2015.

[71] Wikipedia – virtual: http://en.wikipedia.org/wiki/Time-frequency_representation, last access: February 23rd 2015.

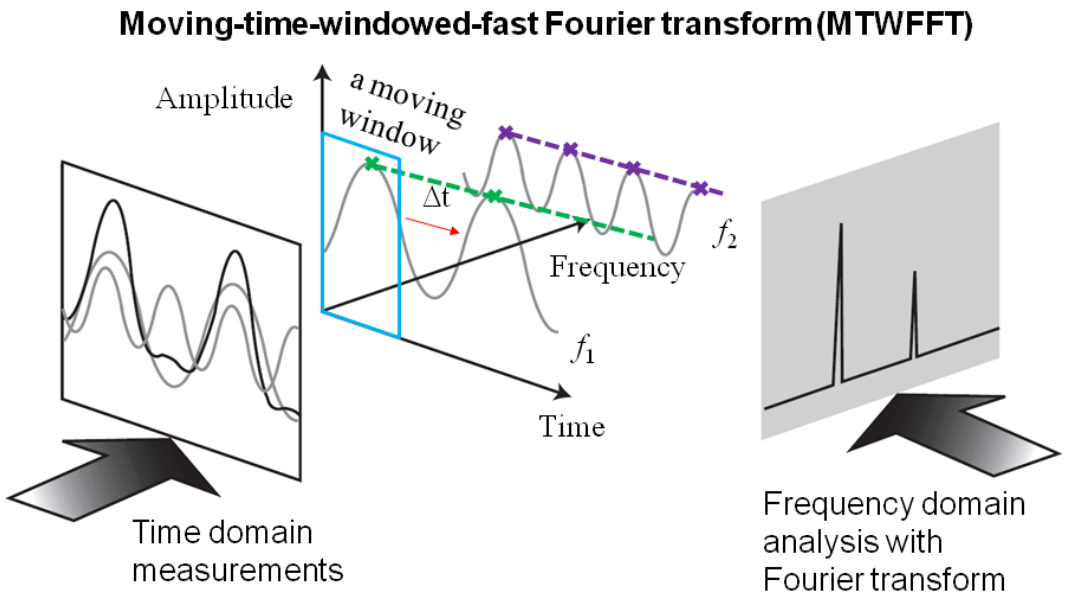

Figure 4-2: Principle of the time-frequency analysis MTWFFT[72]

This MTWFFT is a powerful tool to identify even a small change of the dynamic signal in the time domain. To be more precise, FFT is adopted to obtain the signal's dynamic amplitude at discrete frequencies. A selective weighting time window can be employed in the transform. For example, a Hanning window can be utilized in the transform to eliminate the leakage effect and "Picket Fence" effect in the standard FFT. For a system with harmonic response, the parameter identification is performed at the dominant frequency f_d. For a compromise between the temporal and frequency resolutions, the length of the moving time window can be determined as roughly two dominant oscillations (T=2/f_d). The overlap is also helpful to avoid loss of data and can be fixed by the moving step Δt (e.g. T/16). Then a standard FFT is performed in every small time window as it moves forward along the time axis. And the signal's dynamic amplitude at the dominant frequency f_d can be described nearly continuously in time domain. The system parameter's instantaneous amplitude, phase, and frequency are the direct analysis results. The system's instantaneous transfer functions can also be calculated using the quotient of complex amplitudes. Another advantage of the MTWFFT method is that, the signal's dynamic amplitude at other frequency of interest (e.g. harmonics, $n{\cdot}f_d$, where n is an integer) is also available. Hence it provides a convenient way for harmonic analysis. But restricted by the Fourier uncertainty principle[73], the frequency resolution is possibly not sufficient due to a limited moving-window length, which results from a trade-off between the temporal and frequency resolutions. This problem is particularly severe when any system parameter changes rapidly over time. Under such condition,

[72] Agilent Technologies: Spectrum Analysis Basics, Application Note 150, 2004, p. 5.

[73] Hogan et al.: Time–Frequency and Time–Scale Methods, 2004.

further measures like the spectrum-line-interpolation correction algorithms[74,75] have to be considered. It is a universal analysis method for the parameter identification of any time varying system, no matter whether it is linear or not.

4.1.2 Pros and cons

The MTWFFT method is very flexible in that the resolutions in the time and frequency domains can be easily changed. With the MTWFFT, analysis of various time varying vehicle dynamics becomes possible.

Besides, a time-domain Hilbert transform[76] (HT) method is also possible to estimate time varying system parameters. Unlike the STFT, it conducts transform only in the same time domain and a resulting analytic signal is constructed. With this analytic signal, system instantaneous amplitude, phase and frequency can be estimated. However, HT is limited by only one dominant frequency in the signal analyzed. If the signal has more than one interesting frequency, special digital filter has to be considered. Moreover, if the interesting frequencies are very close with each other, e.g. fundamental and harmonics, HT cannot distinguish and extract them accurately.

A comparison of the pros and cons between the FFT, HT and MTWFFT is summarized in Table 4-1 below. It serves as a basic guideline for the analysis of various signals.

Table 4-1: A comparison of the pros and cons between the FFT, HT and MTWFFT

Analysis method	Pros (+)	Cons (-)
FT/DFT/FFT	Time-invariant systems, Harmonic response with constant characteristics	Useless for time varying systems
HT	Time varying systems, Harmonic response with changed characteristics	Limited by one dominant frequency
STFT/MTWFFT	Time varying systems, Harmonic response with changed characteristics, Time-frequency analysis	Temporal and frequency resolutions are limited by the Fourier uncertainty principle

[74] Zhang et al.: Analysis Methods for Time-Variant Harmonic Vehicle Dynamics Experiments, 2013.

[75] Ming et al.: Corrections for Frequency, Amplitude and Phase in A Fast Fourier Transform…, 1996.

[76] Feldman: Hilbert Transform Applications in Mechanical Vibration, 2011.

4.2 Correction with spectrum-line-interpolation algorithm

As mentioned above, useful system response is relatively short in the time domain in the road tests. This results in a poor temporal and frequency resolutions in the TFA-based PIM. In this condition, further measures should be considered to improve frequency resolution without a significant reduction in the temporal resolution.

One solution could be a moving-time window with an adaptive length, which is determined by the instantaneous dominant frequency. In such a case, obtaining the instantaneous dominant frequency is a prerequisite. It can be solved with a combination of other analysis methods, e.g. HT.

Another solution is the introduction of an additional correction algorithm, which can refine the instantaneous dominant frequency within the spectrum of the moving-time window. Under such condition, a special spectrum-line-interpolation algorithm with the information near the dominant frequency can be helpful. Such a correction algorithm (see Eq. (4.1)) for identification of the true instantaneous dominant frequency, f_{td}, is designed to avoid a frequency shift error due to low frequency resolution in the MTWFF. The relationship between the true dominant frequency f_{td} and the detected dominant frequency f_i including its adjacent frequencies $f_{i\pm1}$ is illustrated in Figure 4-3 below.

$$\begin{cases} x = \frac{f_{td}-f_i}{\Delta f} \\ sinc(x) = \frac{sinx}{x} \\ r_A = \frac{A_{i+1}-A_{i-1}}{A_i} = \frac{\left(sinc(x+1)-sinc(x-1)\right)-0.5(sinc(x+2)-sinc(x-2))}{sinc(x)-0.5(sinc(x+1)+sinc(x-1))} \end{cases} \tag{4.1}$$

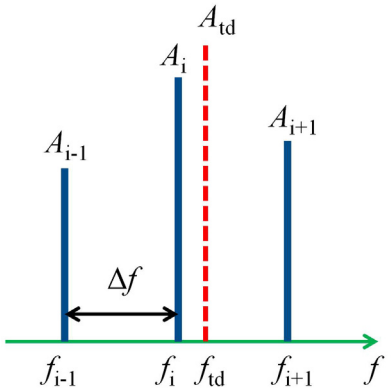

Figure 4-3: Frequency correction based on a special spectrum-line-interpolation algorithm

Here the f_i is the detected dominant frequency (i.e. f_d in Section 4.1.1) where the maximum amplitude, A_i, exists in the spectrum, while A_{i-1} and A_{i+1} are the left and right adjacent amplitudes. Hence, three spectrum lines are utilized in the correction. Δf is the frequency resolution determined by the length of the moving-time window in the MTWFFT method. Through the convolution of the FT of the original signal (just a Dirac delta distribution at f_{td}) and the FT of Hanning window, $0.5[\mathrm{sinc}(x)-(\mathrm{sinc}(x-1)+\mathrm{sinc}(x+1))/2]$, the normalized amplitude difference of the adjacent spectrum lines depends only on the normalized frequency shift between f_{td} and f_i (see Eq. (4.1) above).

Obtaining an analytical expression of f_{td} is not easy or might even be impossible. Therefore, a polynomial approximation of the solution leads to Eq. (4.2).

$$f_{td} \approx f_i + \frac{2}{3} \cdot r_A \cdot (1 - 0.327 \cdot r_A^2) \cdot \Delta f \tag{4.2}$$

With the spectrum-line-interpolation algorithm described above, the instantaneous dominant frequency can be refined with a higher resolution compared with the direct analysis result of the MTWFFT method. It can be treated as an extension or refinement. However, only frequency correction is proposed here. A consideration with possible amplitude and phase corrections can further refine the analysis result of the MTWFFT method. Here, a triple-spectrum-line-interpolation algorithm proposed by Niu[77] *et al.* is integrated into the TFA-based PIM and the evaluation method to obtain the yaw moment of inertia for the purpose of a more accurate frequency, amplitude and phase result. More details about this triple-spectrum-line-interpolation algorithm are given in Appendix A.3. The analysis result is acceptable with satisfactory accuracy.

4.3 Verification of MTWFFT

Before the integration of MTWFFT into the PIM, verification with a synthetic time varying signal is performed. Here, the extended MTWFFT method with the spectrum-line-interpolation algorithm (see Eq. (4.2)) is used to analyze the synthetic signal (see Eq. (4.3)). The analysis results were also cross-checked with the analysis results of the HT. Its validity for a time varying system is proven by this.

$$\begin{cases} s(t) = A(t) \cdot cos\,(2\pi \cdot (0.75t - 0.005t^2)) \\ A(t) = 5 + 0.25t \\ f(t) = 0.75 - 0.01t \end{cases} \tag{4.3}$$

[77] Niu et al.: An Algorithm for … Triple-spectrum-line Interpolation FFT, 2012.

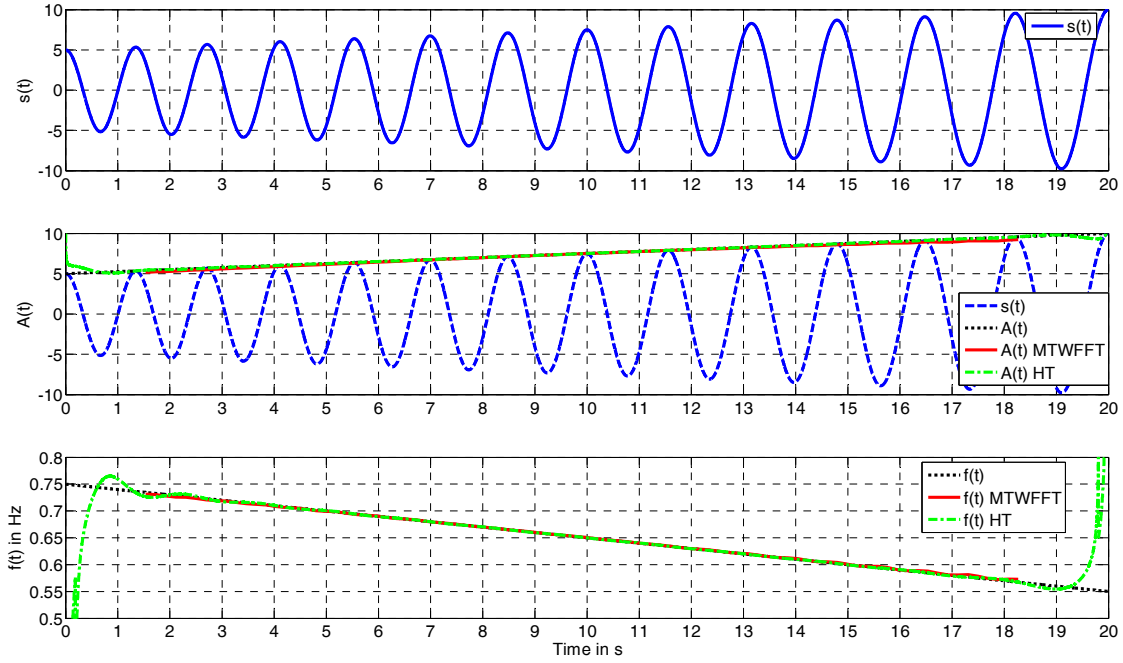

Figure 4-4: Analysis results of a synthetic time varying signal with MTWFFT and HT

The analysis result of the synthetic signal in Eq. (4.3) with MTWFFT is shown in Figure 4 above. The length of the moving-time window is defined by the detected frequency 0.65 Hz through the FFT of the complete time signal. And the length of the window is fixed in the moving process. Both the instantaneous time-variant amplitude and dominant frequency expressed in Eq. (4.3) are estimated with sufficient accuracy and resolution.

The analysis results of the synthetic signal with the two methods, MTWFFT and HT, are shown in the second and third diagrams in Figure 4-4 above. The analysis results with both methods are almost exactly the same and are consistent with the time-variant amplitude and dominant frequency expressed in Eq. (4.3).

The length of the moving-time window in MTWFFT is defined by the detected frequency 0.65 Hz obtained from the conventional Fourier transform of the complete time signal. And the length of the window is fixed in the moving process. With the help of the spectrum-line-interpolation algorithm, the instantaneous dominant frequency is identified with sufficient resolution compared with that of the Hilbert transform. But a small amplitude error from the MTWFFT method still exists due to no amplitude correction.

4.4 Integration in vehicle dynamics

In vehicle dynamics, handling and stability are concerned in the lateral dynamics. Under such circumstances, harmonic excitation and response are frequently adopted or studied. This provides a potential application space for the proposed PIM. There are two main application maneuvers. One is the harmonic response of a forced oscillation under a harmonic excitation, like a slalom test. The second case is the harmonic response of a free oscillation under a non-periodic excitation for a specific vehicle system at its dynamic critical speed, like the critical oscillations of a CTC under an impulse excitation.

4.4.1 Axle side-slip angle and axle cornering stiffness

For linear vehicle lateral dynamics, the side-slip angle and cornering stiffness are of great concern. Even without optical sensors, like Correvit® or wheel vector sensor, the axle side-slip angle can be estimated for vehicle systems with harmonic response under the small angle approximation ($\sin x \approx x$, $\cos x \approx 1$). Here a CTC is taken as an application example based on the STM derived in Chapter 2.

The axle side-slip angles in the complex frequency domain are derived with the Laplace transform and Fourier transform of the corresponding single-track equations in the time domain. The derivation of the α_f of the towing car is demonstrated by Eq. (4.4) as an example.

$$\begin{cases} a_{yf,1} = \dot{v}_{yf,1} + v_x \cdot \dot{\psi}_1 \Leftrightarrow \int a_{yf,1} = v_{yf,1} + v_x \cdot \psi_1 \Leftrightarrow v_{yf,1} = \int a_{yf,1} - v_x \cdot \psi_1 \\ \alpha_{f,1} = \dfrac{\delta_H}{i_s} - \beta_{f,1} = \dfrac{\delta_H}{i_s} - \dfrac{v_{yf,1}}{v_x} \end{cases} \Rightarrow \alpha_{f,1} = \frac{\delta_H}{i_s} - \frac{\int a_{yf,1}}{v_x} + \int \dot{\psi}_1$$

$$\xrightarrow{Laplace\ transform} \alpha_{f,1}(s) = \frac{\delta_H(s)}{i_s} - \frac{a_{yf,1}(s)}{s \cdot v_x} + \frac{\dot{\psi}_1(s)}{s} \tag{4.4}$$

$$\xrightarrow{Fourier\ transform} \alpha_{f,1}(j\omega_1) = \frac{\delta_H(j\omega_1)}{i_s} - \frac{a_{yf,1}(j\omega_1)}{j\omega_1 \cdot v_x} + \frac{\dot{\psi}_1(j\omega_1)}{j\omega_1}$$

For the towing car, the axle side-slip angles can be represented by their amplitudes in the complex frequency domain based on the STM. Here, j is the imaginary unit; ω_1 is the dominant frequency in the yaw rate of the towing car. The steering system is assumed to be rigid with a steering ratio i_s.

$$\begin{cases} \hat{\alpha}_{f,1} = \dfrac{\hat{\delta}_H}{i_s} - \dfrac{\hat{v}_{yf,1}}{v_x} = \dfrac{\hat{\delta}_H}{i_s} - \dfrac{\hat{a}_{yf,1}}{j\omega_1 v_x} + \hat{\psi}_1 = \dfrac{\hat{\delta}_H}{i_s} - \dfrac{\hat{a}_{yf,1}}{j\omega_1 v_x} + \dfrac{\hat{\dot{\psi}}_1}{j\omega_1} \\ \hat{\alpha}_{r,1} = -\dfrac{\hat{v}_{yr,1}}{v_x} = -\dfrac{\hat{a}_{yr,1}}{j\omega_1 v_x} + \hat{\psi}_1 = -\dfrac{\hat{a}_{yr,1}}{j\omega_1 v_x} + \dfrac{\hat{\dot{\psi}}_1}{j\omega_1} \end{cases} \tag{4.5}$$

Normally the acceleration sensor or an Inertial Measurement Unit (IMU) is easily installed near the rear axle in the trunk, so the lateral acceleration at the front axle can be derived in the following way.

$$\hat{a}_{yf,1} = \hat{a}_{yr,1} + j\omega_1\hat{\psi}_1 l_1 \tag{4.6}$$

Meanwhile, the axle lateral forces can be easily obtained from the sum of left/right tire forces, which can be captured by the measuring rims.

A problem exists for the trailer, once the measuring rims for trailer wheels are not available. Therefore, obtaining the true values of the lateral forces of trailer wheels is not possible. Instead, simplified estimation based on the forces at the drawbar and trailer lateral acceleration is possible. Since the system has a tandem-axle trailer, the lateral forces of the both trailer axles are simplified to be the same based on the simulation data in the CarMaker® environment. On the one hand the front axle of the trailer is closer to the COG of the trailer and bears more load; on the other hand an additional pitch moment due to the aerodynamic drag force on the trailer body induces a wheel load shift from the front axle to the rear axle. Hence, the practical distribution of the total load is approximately the same between the front axle and the rear axle of the trailer. This assumption is confirmed by the simulation data in the CarMaker® environment. With these simplifications, the axle side-slip angle and the axle lateral force follow from the equations below.

$$\begin{cases} \hat{\alpha}_{f,2} = -\frac{\hat{v}_{yf,2}}{v_x} = -\frac{\hat{a}_{yf,2}}{j\omega_2 v_x} + \hat{\psi}_2 = -\frac{\hat{a}_{y,2}}{j\omega_2 v_x} + \frac{\hat{\dot{\psi}}_2}{j\omega_2} - \frac{\hat{\dot{\psi}}_2 l_{f,2}}{v_x} \\ \hat{\alpha}_{r,2} = -\frac{\hat{v}_{yr,2}}{v_x} = -\frac{\hat{a}_{yr,2}}{j\omega_2 v_x} + \hat{\psi}_2 = -\frac{\hat{a}_{y,2}}{j\omega_2 v_x} + \frac{\hat{\dot{\psi}}_2}{j\omega_2} + \frac{\hat{\dot{\psi}}_2 l_{r,2}}{v_x} \end{cases} \tag{4.7}$$

$$\begin{cases} F_{yh,2} = -(F_{yh,1}\cos\theta_h + F_{xh,1}\sin\theta_h) \approx -(F_{yh,1} + F_{xh,1}\theta_h) \\ F_{yf,2} \approx F_{yr,2} \approx 0.5 \cdot F_{y,2} = 0.5(m_2 a_{y,2} - F_{yh,2}) \end{cases} \tag{4.8}$$

Here, $F_{y,2}$ denotes the sum of the lateral forces generated by the trailer tires. The forces at drawbar are measured by a sensor installed at the hitch of the towing car. Because the trailer lateral acceleration and yaw rate are measured based on the trailer body-fixed coordinate system, the contribution from the hitch angle is not concerned, different from Eq. (3.8). Also, the calculation of trailer axle side-slip angle is based on the trailer body-fixed coordinate system as well, different from that in the STM. Considering the lateral force at the hitch point (in Figure 3-1) based on the principle of action and reaction, a minus sign is applied in Eq. (4.8).

The dynamic amplitudes of the axle side-slip angle and axle lateral force can be obtained with the MTWFFT method based on the formulas from Eq. (4.5) to Eq. (4.8). Consequently, the instantaneous axle cornering stiffness is their complex ratio.

$$C_{\alpha,i}(t) = \frac{\hat{F}_{y,i(t)}}{\hat{\alpha}_i(t)} \tag{4.9}$$

4.4.2 Effective axle load evaluation algorithm and normalized axle cornering stiffness

Vehicle dynamics experiment with harmonic excitation or response is frequently used to determine the system characteristics, like yaw gain transfer function. Under a harmonic response, the axle load is ideally assumed to be constant. But due to some component with nonlinear characteristic, the dynamic wheel load is not perfect sinusoidal at the dominant yaw oscillation frequency (f_{yaw}), even the wheel load fluctuations (above 8 Hz) are not taken into account. Instead, it is asymmetric and consequently an induced oscillation at the 1st harmonic ($2f_{yaw}$) exists in the axle load. Actually, the f_{yaw} is more or less time varying and so is this harmonic oscillation in the axle load.

From another perspective, the mass-spring-damper system simplified from the axle is excited harmonically. The vertical body resonance reacts with the wheel load oscillation in the frequency range 1-2 Hz. The influence of axle load oscillation at about 1-2 Hz on the axle cornering stiffness is investigated here. If the fundamental harmonic is approximately half of this resonance frequency, the axle load can be effectively more or less than the average due to this oscillation. To be more in detail, in one case the side-slip angle α reaches its maximal absolute value (positive or negative) when the axle load F_z also reaches a maximum. The instantaneous axle load supports the cornering stiffness at this moment (see Figure 4-5 (a)). In this situation, the phase shift of the harmonic axle load referring to the square of the axle lateral force F_y^2 is defined as 0°. When a maximal absolute α meets with an average axle load around, the instantaneous axle load is neutral and has no influence (see Figure 4-5 (b), the phase shift of the harmonic axle load is defined as -90° or 90°). However, in case of a minimum at the maximal absolute side-slip angle, it is effectively less and the cornering stiffness has to decrease (see Figure 4-5 (c), the phase shift of the harmonic axle load is defined as -180° or 180°). The phase shift relationship between the F_y and F_z is summarized in Figure 4-5 below. Here the F_y^2 generates a signal with the same oscillation frequency as the F_z and it can serve as a phase reference signal for the 1st harmonic in the dynamic axle load.

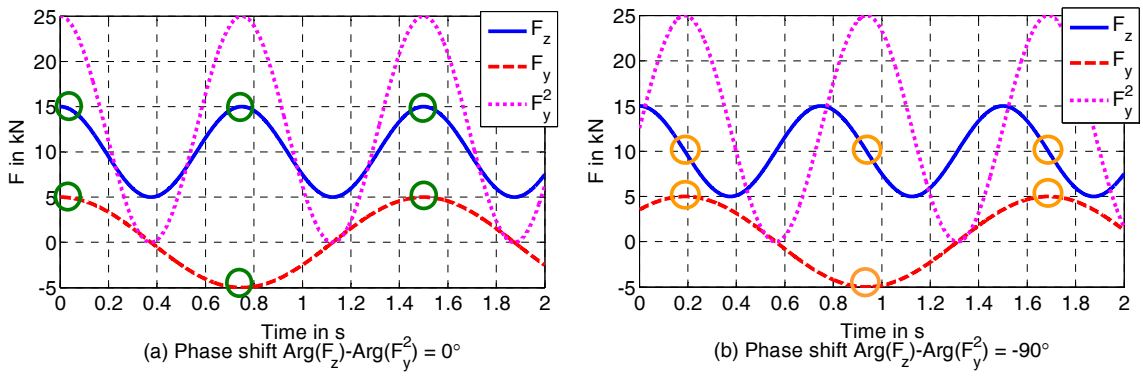

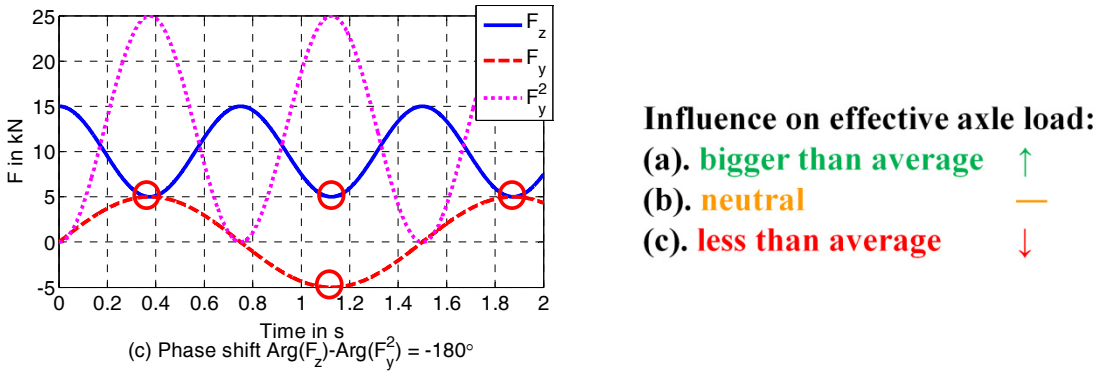

Figure 4-5: Phase shift relationship between the axle lateral force and axle load

A case study from the road test of a car-trailer combination shows a dominant oscillation frequency in the $F_{zr,1}$ which is ca. the 1st harmonic (dominated by 1.40 Hz, 1st harmonic 2ω) of the fundamental (dominated by 0.67 Hz, fundamental harmonic ω) in the $F_{yr,1}$ (see Figure 4-6) at the rear axle. Starting from 65.4 seconds, the amplitude of the dominant 1.40 Hz oscillation reaches an amount of ca. 1 kN occasionally (in the time windows). It can contribute to the effective axle load and hence influence the axle cornering stiffness $C_{\alpha r,1}$.

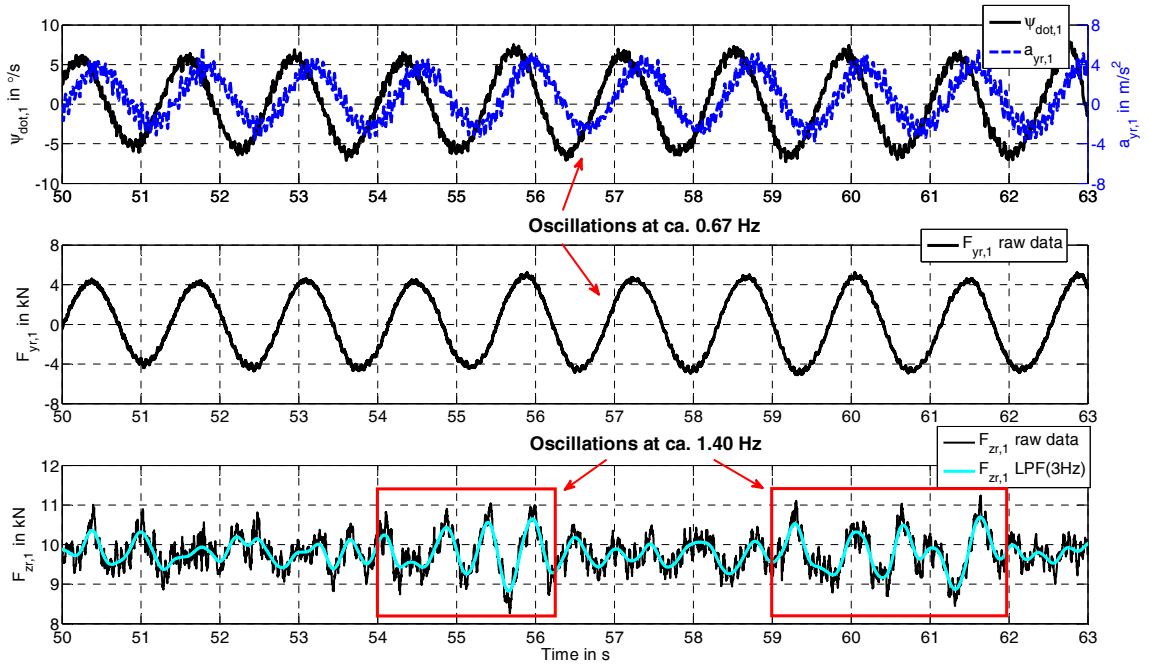

Figure 4-6: Axle load oscillation ($\psi_{dot,1}$, $a_{yr,1}$, $F_{yr,1}$ and $F_{zr,1}$, LPF: Low-pass filter)

The amplitude of this axle load oscillation indicates some degree of time varying property at this axle. Furthermore, a phase shift between the $F_{yr,1}$ and $F_{zr,1}$ also deserves attention. Both the amplitude and phase of the axle load oscillation influence the effective axle load.

The instantaneous cornering stiffness depends a lot on the wheel/axle load. Considering this influence, a weight normalized cornering stiffness ζ is defined by Eq. (4.10) below[78].

$$\zeta(t) = \frac{C_\alpha(t)}{F_z(t)} \tag{4.10}$$

The influence of axle load oscillation on the axle cornering stiffness is investigated. For the axle cornering stiffness, a constant expression in the STM in Section 3.1 is not sufficient. Here, "other effects, like load transfer, body roll, steer compliance, side force steer and initial camber and toe angles have also to be included in the ultimate expression of an effective axle cornering stiffness", proposed by Pacejka[78]. As is known, the transient wheel load is more complex in an unsteady state condition. Besides the static component and dynamic component at the dominant frequency, other contributions also exist when an effective wheel load is considered, e.g. nonlinear harmonics or wheel load fluctuations[79] resulting from road irregularities. Hence, an effective wheel load can be derived including a considerable effect for a specific use case. Only the major component resulting from the axle load oscillation (at about 1-2 Hz) discussed above is considered in the following derivation for simplification.

An evaluation algorithm for an effective axle load (static component plus additional component from axle load harmonic) is derived. It is based on modulation within the range of linear lateral dynamics and described by Eq. (4.11) below. Here, ω is the dominant angular frequency in the side-slip angle and 2ω, 3ω are its 1st ,2nd harmonics. The initial phases of the axle side-slip angle $\alpha(t)$ and the axle load harmonic $F_{z,2\omega}(t)$ are φ_y and φ_z respectively. $F_{z,0}$ denotes the static axle load at frequency $\omega_0 = 0$ s^{-1}. $F_{z,2\omega,eff}$ denotes the effective component from axle load harmonic at 2ω. $Re(F_{z,2\omega,eff})$ denotes its real part and $Im(F_{z,2\omega,eff})$ denotes its imaginary part.

$$\begin{cases} \alpha(t) = \hat{\alpha}\, cos\big(\omega t + \varphi_y\big) \\ F_z(t) = F_{z,0} + F_{z,2\omega}(t) = F_{z,0} + \hat{F}_{z,2\omega}\, cos(2\omega t + \varphi_z) \\ \Delta\varphi = \varphi_z - 2\varphi_y \\ F_y(t) = \alpha(t) \cdot C_\alpha(t) = \alpha(t) \cdot \zeta(t) \cdot F_z(t) \end{cases} \Rightarrow$$

[78] Pacejka: Tire and Vehicle Dynamics, third edition, 2012, p. 9.

[79] Heißing et al.: Chassis Handbook, 2011, p. 114.

$$\begin{cases} F_y(t) = \hat{F}_{y,\omega}\, sin\big(\omega t + \varphi_y + \Delta\varphi_\omega\big) + \hat{F}_{y,3\omega}\, sin\big(3\omega t + 3\varphi_y + \Delta\varphi_{3\omega}\big) \\ \Delta\varphi_\omega = tan^{-1}\frac{\hat{F}_{z,0}+0.5Re\big[F_{z,2\omega,eff}(j\omega)\big]}{-0.5Im\big[F_{z,2\omega,eff}(j\omega)\big]} \\ \Delta\varphi_{3\omega} = tan^{-1}\frac{Re\big[F_{z,2\omega,eff}(j\omega)\big]}{-Im\big[F_{z,2\omega,eff}(j\omega)\big]} \\ \hat{F}_{y,\omega} = \hat{\alpha}\cdot\zeta(t)\cdot\sqrt{\big(F_{z,0}+0.5Re\big[F_{z,2\omega,eff}(j\omega)\big]\big)^2+\big(0.5Im\big[F_{z,2\omega,eff}(j\omega)\big]\big)^2} \\ \hat{F}_{y,3\omega} = \hat{\alpha}\cdot\zeta(t)\cdot\sqrt{\big(0.5Re\big[F_{z,2\omega,eff}(j\omega)\big]\big)^2+\big(0.5Im\big[F_{z,2\omega,eff}(j\omega)\big]\big)^2} \end{cases} \tag{4.11}$$

Because the axle lateral force $F_y(t)$ is dominated by the fundamental harmonic ω (see Figure 4-6), its amplitude can be approximated by the main contribution at ω.

$$\begin{cases} F_y(t) \approx \hat{F}_{y,\omega}\, sin\big(\omega t + \varphi_y + \Delta\varphi_\omega\big) \\ \hat{F}_y \approx \hat{F}_{y,\omega} = \hat{\alpha}\cdot\zeta(t)\cdot\sqrt{\big(F_{z,0}+0.5Re\big[F_{z,2\omega,eff}(j\omega)\big]\big)^2+\big(0.5Im\big[F_{z,2\omega,eff}(j\omega)\big]\big)^2} \end{cases} \tag{4.12}$$

With this derivation, the relationship between the axle cornering stiffness and the corresponding effective axle load is described by the following equation.

$$C_\alpha(t) = \zeta(t)\cdot F_{z,eff} = \zeta(t)\cdot\sqrt{\big(F_{z,0}+0.5Re\big[F_{z,2\omega,eff}(j\omega)\big]\big)^2+\big(0.5Im\big[F_{z,2\omega,eff}(j\omega)\big]\big)^2} \tag{4.13}$$

Because $0.5Im\big[F_{z,2\omega,eff}(j\omega)\big] \ll F_{z,0} + 0.5Re\big[F_{z,2\omega,eff}(j\omega)\big]$

$$\begin{cases} F_{z,eff} = \sqrt{\big(F_{z,0}+0.5Re\big[F_{z,2\omega,eff}(j\omega)\big]\big)^2+\big(0.5Im\big[F_{z,2\omega,eff}(j\omega)\big]\big)^2} \approx F_{z,0}+0.5Re\big[F_{z,2\omega,eff}(j\omega)\big] \\ F_y(t) \approx \hat{F}_{y,\omega}\, sin\big(\omega t+\varphi_y+\Delta\varphi_\omega\big) \approx \hat{F}_{y,\omega}\, sin\left(\omega t+\varphi_y+\frac{\pi}{2}\right) = \hat{F}_{y,\omega}\, cos\big(\omega t+\varphi_y\big) \end{cases} \tag{4.14}$$

An approximate in-phase oscillation between $F_y(t)$ and $\alpha(t)$ is indicated by Eq. (4.14). Here, the real/imaginary part of $F_{z,2\omega,eff}$ can be obtained based on the formulas below.

$$\begin{cases} Re\big[F_{z,2\omega,eff}(j\omega)\big] = \hat{F}_{z,2\omega}\cdot cos(\Delta\varphi) = \hat{F}_{z,2\omega}\cdot cos\big(\varphi_z - 2\varphi_y\big) \\ Im\big[F_{z,2\omega,eff}(j\omega)\big] = \hat{F}_{z,2\omega}\cdot sin(\Delta\varphi) = \hat{F}_{z,2\omega}\cdot sin\big(\varphi_z - 2\varphi_y\big) \\ \varphi_z = Arg\left(F_{z,2\omega}(t)\right) \\ 2\varphi_y = Arg\big(\alpha^2(t)\big) \approx Arg\big(F_y^2(t)\big) \end{cases} \tag{4.15}$$

Here, Arg(•) denotes the phase of the harmonic signal •. The phase shift is available in this way. And $\alpha^2(t)$ or $F_y^2(t)$ generates the phase reference signal for the axle load harmonic at 2ω (ref. to Eq. (4.11)). Through the construction of $F_y^2(t)$, the problem of different dominant frequencies in F_y and F_z is solved even with a time varying ω. However, if time varying effective axle load or axle cornering stiffness is necessary, TFA-based PIM has to be considered.

Two important points have to be clarified on the derivation of effective axle load above. Firstly, because this derivation is independent on the STM, the nonlinear harmonics in axle load and its influence on the effective axle cornering stiffness can be studied with the MTWFFT. It can introduce a time varying axle cornering stiffness into the STM and makes the model time varying, too. Secondly, this derived effective axle load can serve as a linkage to investigate the coupling between the vertical dynamics and horizontal dynamics.

A time varying effective axle load $F_{z,eff}(t)$ can be obtained with the MTWFFT. Once the $C_{\alpha,i}(t)$ and $F_{zi,eff}(t)$ are obtained with the PIM, a normalized cornering stiffness $\zeta_i(t)$ can be determined as their ratio in the time domain.

$$\zeta_i(t) = \frac{C_{\alpha,i}(t)}{F_{zi,eff}(t)} \tag{4.16}$$

This coefficient $\zeta_i(t)$ provides a description of the $C_{\alpha,i}(t)$ normalized by the effective axle load and opens a discussion on the effects which are not related to the axle load.

4.4.3 Instantaneous lateral friction coefficient

For vehicle lateral dynamics, whether the tire works in the linear range or not is concerned in many cases. As a capable indicator, the lateral friction coefficient $\mu_{yi}(t)$ is also available with the MTWFFT method by the formula below.

$$\hat{\mu}_{yi}(t) = \frac{\hat{F}_{yi,sum}(t)}{F_{zi,eff}(t)} \tag{4.17}$$

It is also independent on the STM. With the advantage of TFA, the lateral friction coefficient is also an instantaneous parameter over time, which can indicate the transient tire behavior.

4.4.4 Yaw moment of inertia

Yaw moment of inertia is another important parameter in the STM, which has an influence on the yaw motion in the horizontal plane. Normally it is estimated through some experimental method in which a harmonic response is excited under a free oscillation condition[80]. An inconvenience is that additional equipment is necessary to conduct this free oscillation condition.

For a vehicle system with harmonic behavior, identification of yaw moment of inertia becomes easier with the assistance of TFA-based PIM. Based on the yaw motion equations Eq. (3.2) and Eq. (3.6) in the STM, the yaw moments of inertia of the towing car

[80] Standen: Towed vehicle aerodynamics, 1999, p. 121.

and trailer can be obtained in the complex frequency domain in the same way as the axle side-slip angle.

$$\hat{I}_{z,1} \cdot j\omega_1 \hat{\dot{\psi}}_1 = \hat{F}_{yf,1} \cdot l_{f,1} - \hat{F}_{yr,1} \cdot l_{r,1} + \hat{F}_{yh,1} \cdot l_{h,1} \tag{4.18}$$

$$\hat{I}_{z,2} \cdot j\omega_2 \hat{\dot{\psi}}_2 = \hat{F}_{yf,2} \cdot l_{f,2} - \hat{F}_{yr,2} \cdot l_{r,2} + \hat{F}_{yh,2} \cdot l_{h,2} \tag{4.19}$$

Method 1: As mentioned before, due to the absence of the measuring rims for the trailer wheels, only simplified estimation based on the forces at the drawbar and trailer lateral acceleration is possible. Under such conditions, it is assumed that the lateral forces at the two axles of the trailer are equal, i.e. half of the total amount. Based on the derivation in Eq. (4.8), the Eq. (4.19) can be replaced by the following one.

$$\hat{I}_{z,2} \cdot j\omega_2 \hat{\dot{\psi}}_2 \approx \hat{F}_{yr,2} \cdot (l_{f,2} - l_{r,2}) + \hat{F}_{yh,2} \cdot l_{h,2} \tag{4.20}$$

Method 2: There is also another evaluation method for the trailer yaw moment of inertia $I_{z,2}$ on the basis of another assumption. Because the tires at the two axles of the trailer are completely the same and the axle load has small difference, it can be assumed that the normalized axle cornering stiffness ζ_2 is the same for the two axles of the trailer. Therefore, the axle cornering stiffness $C_{\alpha i,2}$ is proportional to the axle load, which is mainly depending on the COG of the trailer. However, a wheel load shift from the front axle to the rear axle of the trailer, which is induced by an additional pitch moment due to the aerodynamic drag force on the trailer body has been ignored. Under this assumption, the trailer yaw moment of inertia $I_{z,2}$ can be described by Eq. (4.21) below.

$$\begin{cases} F_{yf,2} = C_{\alpha f,2}\alpha_{f,2} = \zeta_2 \cdot m_2 g \cdot \frac{l_{r,2}}{l_2}\left(-\frac{v_{y,2}}{v_x} - \frac{\dot{\psi}_2 l_{f,2}}{v_x}\right) \\ F_{yr,2} = C_{\alpha r,2}\alpha_{r,2} = \zeta_2 \cdot m_2 g \cdot \frac{l_{f,2}}{l_2}\left(-\frac{v_{y,2}}{v_x} + \frac{\dot{\psi}_2 l_{r,2}}{v_x}\right) \Rightarrow \\ \quad F_{yf,2} + F_{yr,2} = F_{y,2} = m_2 a_{y,2} - F_{yh,2} \\ \quad I_{z,2}\ddot{\psi}_2 = F_{yf,2} l_{f,2} - F_{yr,2} l_{r,2} + F_{yh,2} l_{h,2} \end{cases}$$

$$I_{z,2}\ddot{\psi}_2 = \frac{\dot{\psi}_2 \cdot l_{f,2} \cdot l_{r,2}}{v_{y,2}} \cdot F_{y,2} + F_{yh,2} \cdot l_{h,2} \tag{4.21}$$

Where the lateral velocity at the COG of the trailer is obtained by

$$v_{y,2} = \int a_{y,2} - v_x \cdot \psi_2 \tag{4.22}$$

Here, $F_{y,2}$ denotes the sum of the lateral forces generated by the trailer tires. Because the trailer lateral acceleration and yaw rate are measured based on the trailer body-fixed coordinate system, the contribution from hitch angle is not concerned, different from Eq. (3.7) and Eq. (3.8). And the calculation of trailer axle side-slip angle is based on the trailer body-fixed coordinate system as well, different from that in the STM.

In the same way, the trailer yaw moment of inertia $I_{z,2}$ expressed in the complex frequency domain is derived by

$$\begin{cases} \hat{I}_{z,2} \cdot j\omega_2 \hat{\dot{\psi}}_2 = \frac{\hat{\dot{\psi}}_2 \cdot l_{f,2} \cdot l_{r,2}}{\hat{v}_{y,2}} \cdot \hat{F}_{y,2} + \hat{F}_{yh,2} \cdot l_{h,2} \\ \hat{v}_{y,2} = \frac{\hat{a}_{y,2}}{j\omega_2} - \frac{v_x \cdot \hat{\dot{\psi}}_2}{j\omega_2} = \frac{\hat{a}_{y,2} - v_x \cdot \hat{\dot{\psi}}_2}{j\omega_2} \end{cases} \tag{4.23}$$

For the trailer yaw moment of inertia, the evaluation results with two methods above can be compared with each other in the application.

Therefore, the two yaw moments of inertia are available with the TFA-based PIM under such simplification. If a single-axle trailer is towed, the estimation will be more precise.

4.5 Conclusions

Inspired by the merits of Time-Frequency Analysis (TFA) in Digital signal processing (DSP), a novel Time-Frequency analysis based parameter identification method (TFA-based PIM) is proposed to investigate the potential time varying vehicle dynamics, which is related to system dynamic instability of CTCs. The TFA-based PIM proposed in this chapter is a combination of a linear single-track model (STM) and the moving-time-windowed-fast Fourier transform (MTWFFT). It can be used to estimate time-invariant and time varying system parameters. The PIM aims for the system model identification to build up simulation models. A complete block diagram of the TFA-based PIM for the application of a CTC or normal passenger car with necessary sensors is shown in Figure 4-1. The TFA-based PIM contains three components, mainly MTWFFT, a STM and an effective axle load evaluation algorithm. The former two are indispensable while the last part takes a phenomenon of nonlinearity-induced harmonic dynamic axle load into account. All the three parts are described in this chapter.

The MTWFFT proposed here has the same essence as the STFT. With a pre-defined moving time window, the instantaneous characteristics (incl. frequency, amplitude and phase) are available. Both the temporal and frequency resolutions are dependent on the length of the moving time window. The system's instantaneous transfer functions can also be calculated using the quotient of complex amplitudes. Another advantage of the MTWFFT method is that, the signal's dynamic amplitude at other frequency of interest (e.g. harmonics) is also available. A comparison of the pros and cons between the FFT, Hilbert Transform (HT) and MTWFFT is summarized, which serves as a basic guideline for the analysis of various signals. But restricted by the Fourier uncertainty principle, the frequency resolution is possibly not sufficient due to a trade-off between the temporal and frequency resolutions. A special spectrum-line-interpolation algorithm with the information near the dominant frequency is proposed as a solution for the frequency correction. Furthermore, verification with a synthetic time varying signal is performed for the MTWFFT method. Both the instantaneous time-variant amplitude and dominant

frequency are estimated with sufficient accuracy and resolution. The analysis results were also cross-checked with the analysis results of the HT. Its validity for a time varying system is proven by this.

The linear STM proposed in Section 3.1 is transformed into complex frequency domain for the purpose of integration into the TFA-based PIM. Combined with the MTWFFT, time varying vehicle dynamics can be identified and quantified within the range of linear lateral dynamics under the condition of a harmonic response. Axle side-slip angle and axle cornering stiffness can be evaluated even without optical sensors.

A theoretical analysis of the harmonic effect in dynamic axle load and its influence on the cornering stiffness is followed. And an effective axle load evaluation algorithm is proposed considering the harmonic phenomenon. Moreover, the TFA-based PIM is introduced to evaluate the normalized axle cornering stiffness, which is not related to the axle load. They establish the foundation for the impact study of nonlinearity-induced harmonic dynamic axle load on the system dynamic stability in Chapter 6.

Moreover, the instantaneous lateral friction coefficient is also available with the TFA-based PIM. It can indicate the transient tire behavior and if the tire works in the linear range or not. Besides, yaw moment of inertia, another important parameter in the STM, can be evaluated with TFA-based PIM as well. It plays an important role in the validation of a simulation model in Chapter 5.

5 Application in Vehicle Dynamics

The application scope of this novel TFA-based PIM is mainly identification of systems with time varying properties within the range of linear lateral dynamics, which aims for the model identification to build up simulation models.

In this chapter, the developed PIM is applied in a case study, a simulation model validation of a car-caravan combination. Because of the investigated critical steady state oscillation phenomenon that describes the system's stability margin, the system has a harmonic behavior under an impulse excitation at its dynamic critical speed. The driving maneuver in the road test and simulation is defined according to the lateral stability test standard ISO 9815[66] of CTCs.

A system simulation model is built in CarMaker® environment with all the system parameters delivered from the project partner. However, the model still has some problems, i.e. it is not completely validated. A further complete validation process based on the measurement data in the road test is performed in this chapter.

5.1 Test vehicle and road test

Since the simulation model of the CTC applied in the road test has already been prevalidated before our further research, much efforts and time considering the road tests are saved in the validation process. Most of the road tests are performed to observe the system dynamic critical stable state and dynamic instability phenomenon. Besides, additional road test with slalom maneuvers and steady state cornering are also performed for the purpose of model validation. All the road tests are conducted on the proving ground in Pferdsfeld, which is provided by Opel Test Center.

The test vehicle applied in the road test in shown below. The towing car is an Opel Astra J and the trailer is a Bürstner Belcanto 650TK (see Figure 5-1) with a tandem-axle caravan. The mass ratio of the towing car to the trailer is ca. 1.0. More system parameters and their corresponding values are described in Table A in Appendix A.1.

Figure 5-1: The tandem-axle trailer - Bürstner Belcanto 650TK[81] applied in the road test

A steering impulse excitation at system critical stable state serves as the main test scenario in the road test. The longitudinal velocity is fixed at the pre-defined system dynamic critical speed without the function of cruise control, which is found by some pre-tests. Two different types of damper, series damper and prototype damper, are installed in the suspension of the towing car, respectively. The corresponding system dynamic behaviors under a steering impulse excitation are shown in Figure 1-3 and Figure 1-4 in Section 1.2.2. This test scenario aiming for dynamic stability research of CTCs are defined on the basis of the lateral stability test standard ISO 9815[66]. All the necessary system parameters and measurement sensors included in Figure 4-1 are available in the road test. Besides, the vertical hitch load is also available with a force sensor installed at the hitch point on the towing car.

[81] Wohnmobile Bürstner – virtual: http://www.kfz-kleinanzeigen.com/detailanzeige-39719420.html, last access: February 28th 2015.

5.2 Validation of simulation model (I)

5.2.1 Simulation environment

The system simulation environment is the CarMaker® by IPG Company. The software has not only a user-friendly Graphical User Interface (GUI, Version 4.0.5, see Figure 5-2) but also a simply pre-defined corresponding Simulink model. Moreover, a module of any individual component can be easily implemented in Matlab/Simulink® and simulation of a specific parameter's influence incl. sensitivity analysis can be performed in this environment as well. With numerical calculation, it is easier to have minimum disturbance and great reproducibility compared with the real driving test. More importantly, some small difference or nonlinear phenomenon, which is extremely hard to be modified in the road test, e.g. a nonlinearity-induced harmonic dynamic axle load discussed in Chapter 6, can be systematically studied in the simulation environment with CarMaker®.

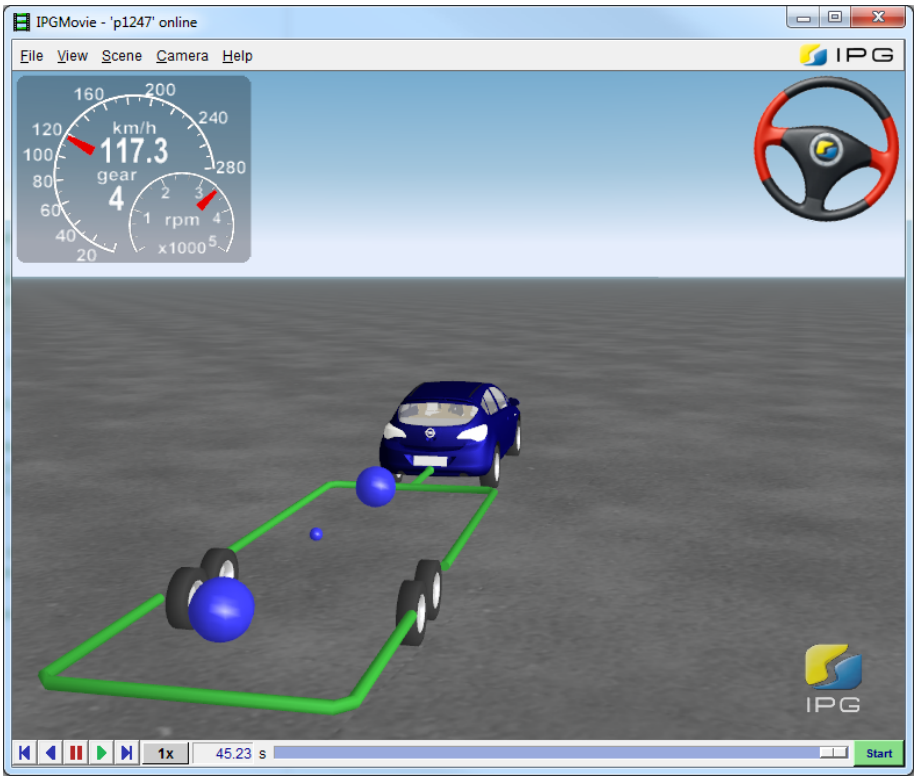

Figure 5-2: Animation of the dynamic stability of a car-trailer combination in simulation

5.2.2 Simulation model

The simulation is carried out under the combination of CarMaker® and Matlab/Simulink®. In CarMaker® a complex system model is created to describe the system behavior with numerous DOFs considering the motion of the car body, the trailer body, the suspension, the hitch point, the aerodynamics, etc. A corresponding graphical model is also created in the GUI in Matlab/Simulink® at the same time.

The Magic Formula[82,83] tire model is applied to describe the tire behavior. A big problem in the simulation model is that, the tire models do not match with the dynamic characteristics of the real tires applied in the road test. It is the main challenge in the validation process. A simple damper model based on the look-up table is built in Simulink and specific nonlinear phenomenon can also be realized in Simulink. In the simulation, the steering wheel input can also be selected and imported from the real driving test, but the gas pedal is still controlled by a driver model in CarMaker® in the simulation model of the car-caravan combination.

5.2.3 Validation method

All the system parameters in the simulation model are delivered from the project partner. The damper characteristics are provided by its supplier. Because of the different loads, inevitable changes of the tire characteristics and some other influences like temperature or aerodynamics in the real driving test, the system simulation model still behaves differently from the real experimental system. In order to reproduce the test scenario in simulation and have a comparable result, further validation of the simulation model is necessary.

The validation of the simulation model is performed in three steps. They are described by the flow diagrams below.

---

[82] Pacejka: Tire and Vehicle Dynamics, third edition, 2012, p. 165.

[83] IPG CarMaker: Reference Manual, Version 4.0.5, 2013, p. 286.

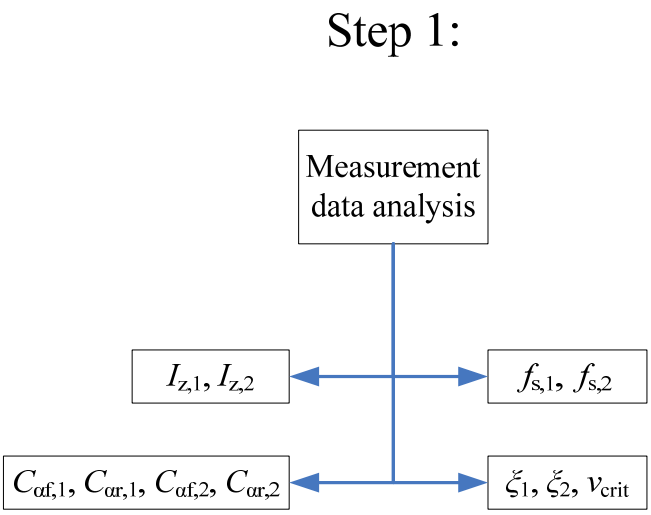

Figure 5-3: The flow diagram of the validation process of the simulation model – step 1

The first step is mainly measurement data analysis (see Figure 5-3). The analysis results include the yaw moment of inertia, axle cornering stiffness, dominant yaw oscillation frequency and yaw damping ratio, system dynamic critical speed. They are utilized in the model parameterization and validation later. The measurement data, which is analyzed in this step, is mainly the acquisition data from the driving tests under the dynamic critical stable state with a steering impulse excitation.

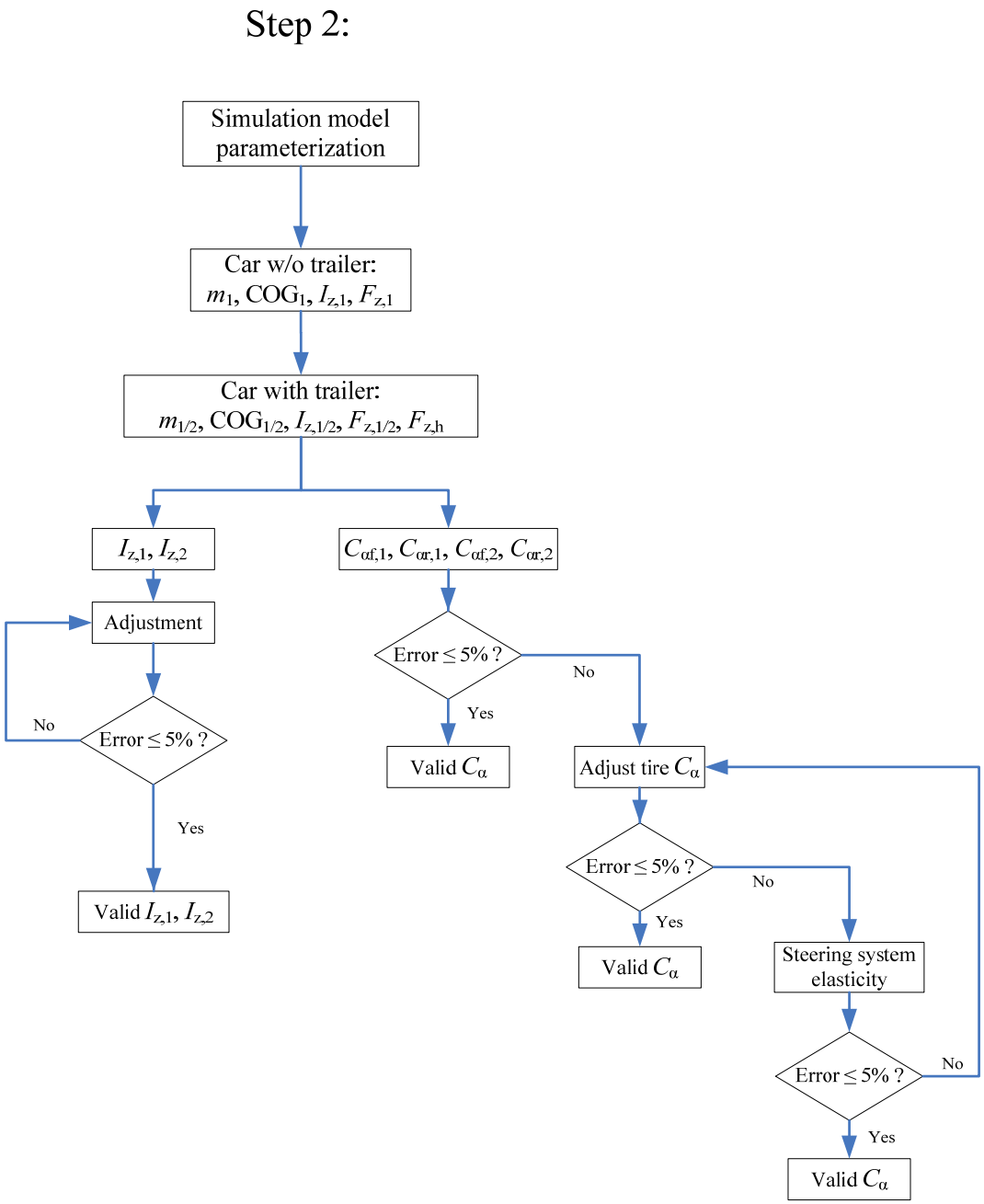

Figure 5-4: The flow diagram of the validation process of the simulation model – step 2

The second step is simulation model parameterization (see Figure 5-4). In this step, firstly the parameterization of the towing car w/o trailer is performed at stationary condition, like mass, COG, yaw moment of inertia, additional load and static wheel load. Then a similar procedure is also conducted for the CTC. For the CTC, the forces at the hitch point also have to be checked with regard to the COG of the trailer. Afterwards the yaw moments of inertia are adjusted under dynamic condition again. They are evaluated with the assistance of the TFA-based PIM described in Section 4.4.4.

Finally, a valid axle cornering stiffness is considered under dynamic condition. Axle cornering stiffnesses are parameterized with the derived TFA-based PIM described in Section 4.4.1 as well. In this process, the system dynamic variables are actually compared with the measurement data in the road test, like the wheel forces, hitch forces, etc. under the system dynamic critical stable state or even a slalom maneuver at lower speed if necessary, because they are necessary in the TFA-based PIM.

For a persuasive comparison, the steering wheel input in the simulation is guaranteed to be nearly the same as that in the real driving test. The longitudinal velocity is expected to be the system dynamic critical speed either in the simulation or in the real driving test, although a reasonable difference might still exist between the simulation and the road test. Under these conditions, the parameterization of axle cornering stiffnesses can be achieved. Some other effects should also be considered, like the aerodynamics and steering system elasticity. If the validation criteria, 5% error range, are not met, several adjustment methods are considered sequentially, e.g. adjusting the tire cornering stiffness and modeling the steering system elasticity. The system parameterization is the precondition for further model validation.

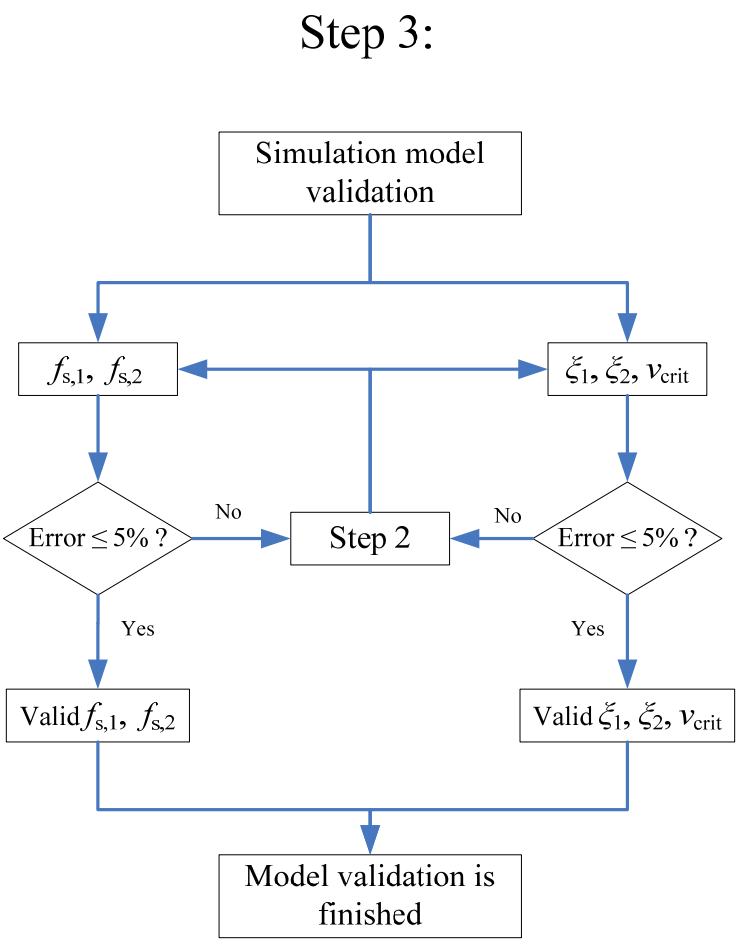

Figure 5-5: The flow diagram of the validation process of the simulation model – step 3

The third step is the simulation model validation (see Figure 5-5). Here the dominant yaw oscillation frequency and system dynamic critical speed (or yaw damping ratio) are mainly concerned. Only when the validation criteria with 5% error are met, the validation process can be finished.

Therefore, these three steps can be treated as the validation method from the model parameterization to further model validation.

5.2.4 Validation criteria

As mentioned in validation method, three steps are performed with comparison. For this purpose a general validation criterion is that, the difference of each system parameter or state variable between the experimental data and simulation data should be within 5% of the experimental data. Any bias error should be corrected before. It is a basic principle in the whole validation process.

Actually, in practice, such accurate quantification is only used for some important system parameter, like the system dynamic critical speed. In a general case, most of the system state variables are only validated through the comparison of the dynamic amplitude and oscillation frequency in the time domain, like the dynamic wheel load. If the simulation data can match with the experimental data very well in the time domain, further precise quantification for system parameters through other PIMs, e.g. MTWFFT, is not necessary. The validation criterion is guaranteed, too. However, due to a potential time varying property introduced by vertical dynamics, sometimes this critical validation criterion is difficult to be guaranteed for some quantities, e.g. a time varying dominant yaw oscillation frequency. In this case, the potential nonlinearity-induced time varying vertical dynamics and its influence on the system dynamic stability have to be further considered.

5.2.5 Validation process

In this section, the validation process of the simulation model is described in detail. The main considerations on model parameterization and validation are described sequentially. They determine the quality of the model validation.

Driver inputs

As mentioned in Section 5.2.2, the steering wheel input can be selected and imported from the real driving test. However, the real steering excitation from the real driving test is not recommended due to several reasons. Firstly, a calibration error still exists in the steering wheel sensor even a pre-calibration for the sensor is conducted. Secondly, the steering wheel input after an expected impulse still has some oscillation with a slight

amplitude, which can be explained by an obvious coupling of the steering and yaw motion between the horizontal motion of the towing car and steering wheel input introduced by the driver. That is to say, the steering wheel cannot be completely fixed by the driver under the real test condition. Although a fixation device can improve this situation, an artificial steering input generated by the CarMaker Maneuver GUI is utilized with the advantage of a pure steering excitation. It is approximately a half-sinus signal with the amplitude of 19° and the frequency of 0.675 Hz. This artificial steering input matches with that in the real driving test very well.

The speed control of the simulation is also designed in the CarMaker Maneuver GUI based on a closed-loop PI controller[84]. The car starts at a given initial speed and the driver model has ca. 40s to make the system driving at a constant longitudinal speed. Based on the energy conservation principle, a compensatory gas pedal input by the driver is necessary in the real driving test when the Cruise Control is inactive. This is the goal of the longitudinal speed control in the simulation. Therefore, the sensitivity of the speed control in the longitudinal dynamics of CarMaker Maneuver GUI is set as 0.9, which determines the reaction behavior of the gas pedal in case of a speed difference.

Even so, the longitudinal velocity of the towing car in the simulation still drops due to the yaw oscillation. To reach the desired speed, the speed controller has to change the gas pedal continually, which results in a continuous vibration in the longitudinal acceleration. This phenomenon affects the forces at the hitch point and the system yaw damping ratio will also be influenced accordingly. In order to minimize such influence, a feed-forward controller is designed and implemented in the simulation. Once the longitudinal speed drops when the yaw oscillation occurs, a compensatory driving torque is directly added by a product of the current longitudinal acceleration and a gain factor -*K* to the engine output torque regardless of any time delay. The principle of the feed-forward controller for the longitudinal velocity is shown in Figure 5-6 below.

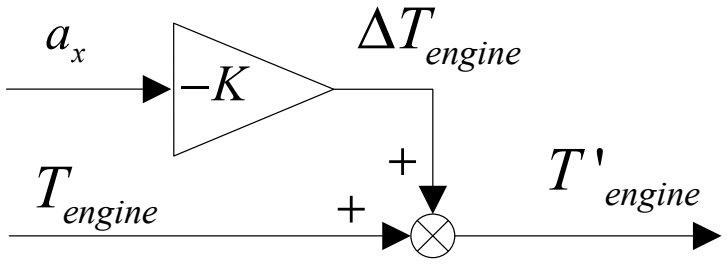

Figure 5-6: A feed-forward controller for the longitudinal velocity

The gain factor -*K* is calculated with the mass of the towing car m_1, the mass of the trailer m_2, wheel dynamic rolling radius r_d, the gearbox transmission ratio i_t and the

[84] IPG CarMaker: Reference Manual, Version 4.0.5, 2013, p. 40.

differential transmission ratio i_d. An additional gain factor K_a is utilized to adjust the control effect. The gain factor -K is determined by following equations.

$$\Delta F_{xf,1} = -(m_1 + m_2) \cdot a_x = \frac{\Delta T_{engine} \cdot i_t \cdot i_d}{r_d} \tag{5.1}$$

$$-K = -K_a \cdot \frac{\Delta T_{engine}}{a_x} = K_a \cdot \frac{(m_1+m_2) \cdot r_d}{i_t \cdot i_d} \tag{5.2}$$

With the external driving torque from the feed-forward controller, the deviation in the longitudinal speed is compensated. The longitudinal acceleration is kept nearly zero in the simulation. With this feed-forward controller, the goal of longitudinal speed control can be satisfied.

Wheel load and hitch force

In the road test, the wheel dynamic forces of towing car are measured with the four measuring rims. Besides, the real static wheel loads of the towing car or the trailer are measured by the mobile wheel load scale under stationary condition. Because of the additional weight of the test equipment and passengers, the wheel loads and COG change accordingly. For the model parameterization, the static wheel loads of the towing car and trailer are readjusted based on the measurement data. As a result, the individual wheel load and hitch forces match with the measurement data in the road test very well after the system rebalance.

Aerodynamics

System aerodynamics has significant influence on the longitudinal force at the hitch point while the longitudinal dynamics, i.e. acceleration or deceleration, also have influence on system dynamic stability[85]. Therefore, the system aerodynamics definitely influences the system dynamic stability. Under such condition, the system aerodynamics should also be considered as well in the validation of the simulation model. The aerodynamic characteristics of the towing car and the trailer are described with look-up tables in relation to the different angles of attack of wind[86].

The longitudinal hitch force in the simulation is much bigger than the measurement data in the road test. The rolling resistance of the wheels cannot cause such a big difference. The aerodynamic drag acting on the trailer is relatively much smaller in a CTC than that acting on a single trailer at the same relative wind speed. It results in a much smaller longitudinal force at the hitch point in the road test. Since it is infeasible to perform the

[85] Fischer et al.: Aktive Gespannstabilisierung beim BMW X 5, 2002, p. 333.

[86] IPG CarMaker: Reference Manual, Version 4.0.5, 2013, p. 132.

wind-tunnel experiment for the purpose of a refined look-up table to represent a more precise aerodynamic drag coefficient of the trailer, the easiest way to adjust the aerodynamics of the simulation model is to change the aerodynamic reference point and area of the trailer reasonably. According to the measurement data, the aerodynamic reference area is reduced from 5.0 m^2 to 1.5 m^2. After the adjustment, the longitudinal force at hitch point in the simulation is very close to that in the road test. The system aerodynamics has been adjusted as much as it can be to fit the real experimental data. However, the system aerodynamics of CTCs is too complex to be modified without the assistance of wind-tunnel experiments[87] and further validation is infeasible in our research either.

Damper characteristics

Because the CDC dampers installed in the towing car in the road test are utilized in extreme hard or soft mode, a corresponding damper module has to be considered in the simulation as well. The bench test data of CDC dampers are provided by its supplier, by which the damper characteristics are described by its corresponding F_d-v_d diagram. Other damper characteristics like the elasticity, hysteresis, etc, are not considered in the simulation model at the first step. On this basis, a simple damper module described by look-up tables in Matlab/Simulink® are built and embedded into the complete system model. Moreover, variations of damper behavior incl. some failure phenomenon are also possible and easy to be realized in further simulation.

Yaw moment of inertia

In the driving test, the yaw moment of inertia of the trailer has a given measured value while that of the towing car is unknown. In the simulation model, both the yaw moments of inertia of the towing car and trailer are given. There is a big difference in that of the trailer between the measured one and the one used in the simulation. Since the wheel forces, hitch forces and yaw rates are captured in the road test and also available in the simulation, an evaluation algorithm for the yaw moment of inertia is necessary for further model validation. Based on the TFA-based PIM, this evaluation algorithm is detailedly described in Section 4.4.4. Because they are estimated in the complex frequency domain, the argument information can be used to check the evaluation algorithm. A comparison between the given values (incl. measured ones) and the estimated values derived from the measurement data or simulation data is given in Table 5-2 in Section 5.2.6.

[87] Standen: Towed vehicle aerodynamics, 1999.

Axle cornering stiffness

Tire model is always one of the most important parts in vehicle dynamics simulation. The Magic Formula tire model is applied for the tires of the towing car in the simulation model, and it contains hundreds of parameters, which depend on the wheel alignment, tire pressure, friction coefficient, etc. A "RealTime Tire" model, a modified version of IPGTire that is mainly based on measurements[88], is applied for the tires of the trailer in the simulation model. The parameterization of the axle cornering stiffness plays a decisive role in the validation of the simulation model in horizontal plane. The adjustment of axle cornering stiffness can be achieved with the modification of individual tire cornering stiffness, which can be achieved through a scaling factor "F_y cornering stiffness" in the CarMaker GUI for the tire model.

With the help of the measuring rims and other measuring equipment, a large number of system dynamics variables are obtained in the road test. Based on the TFA-based PIM proposed in Section 4.4.1, the axle cornering stiffnesses of the towing car and trailer in either the measurement data or the simulation data can be evaluated respectively. A comparison between the estimated values from measurement data and the simulation data indicates that, there is a big difference in cornering stiffness, particularly in the $C_{\alpha r,1}$ (about 50% smaller in the simulation data). The axle cornering stiffness of the trailer is also much smaller in the simulation compared to that derived from the measurement data. Accordingly, the dominant yaw oscillation frequency and the amplitude of the lateral acceleration or yaw rate cannot match the experimental data either. Because the front axle cornering stiffness of the towing car might be affected by other factors like the steering system, the rear axle cornering stiffness of the towing car is served as a reference for the adjustment in this step. Because the tire model for both axles of towing car is completely the same, a same adjustment is also done for the front axle. On this basis, the scaling factor "***F*****$_y$ cornering stiffness**" in the Magic Formula tire model for both axles of the towing car is changed from 1.0 to 1.47. The scaling factor "**Lateral force stiffness**" in the "RealTime Tire" model for both axles of the trailer is changed from 1.0 to 1.36.

After the adjustment of the tire cornering stiffness, the dominant yaw oscillation frequency in the simulation has become closer to the measurement data and so is the lateral acceleration. However, the dominant yaw oscillation frequency still has a considerable deviation. The axle cornering stiffness is also closer to the measurement data, but it still has a significant difference between the measurement data and the simulation data.

The new analysis result of the axle cornering stiffness after the adjustment of the tire model gives a hint that the remaining difference possibly results from a smaller wheel

[88] IPG CarMaker: User's Guide, Version 4.0.5, 2013, p. 232.

steering angle δ_w at the front axle of the towing car due to the existence of the steering system which does not exist at the rear axle.

Steering system elasticity

Since the estimated front axle cornering stiffness $C_{\alpha f,1}$ is much smaller than the rear one $C_{\alpha r,1}$ in the measurement data, an additional influence on the front axle side-slip angle due to the steering system elasticity is a potential reason. In this way, the wheel steering angle δ_w at front axle is actually less than that with a rigid steering system. Therefore, the front axle lateral force also decreases due to a smaller side-slip angle. Nevertheless, a rigid steering system with a constant steering ratio is utilized in the TFA-based PIM in Section 4.4.1. The estimated axle cornering stiffness will decrease when the steering system elasticity is introduced.

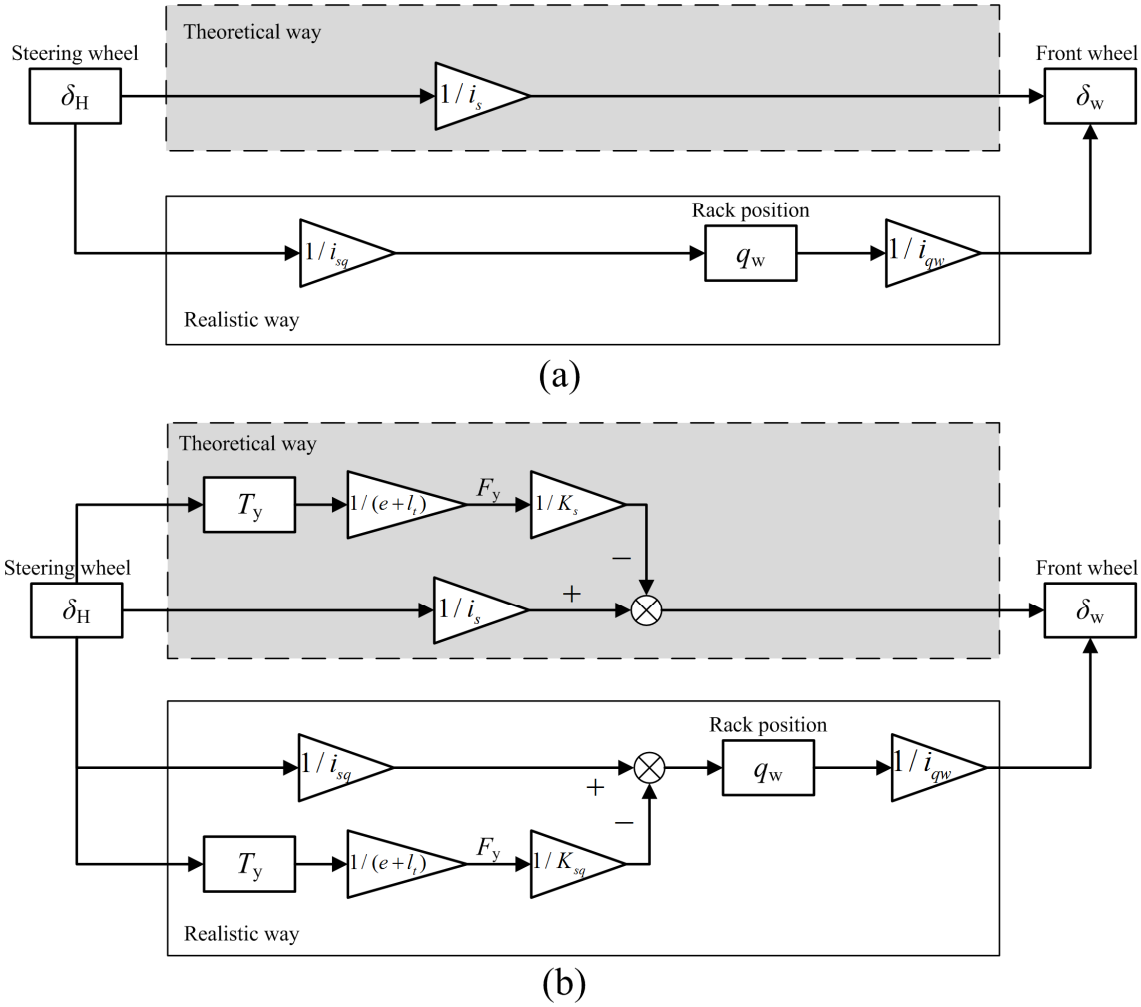

Figure 5-7: Modeling of steering system: (a) Steering system without elasticity (b) Steering system with elasticity

The modeling of the steering system with elasticity is shown in Figure 5-7 above. As a comparison, the steering system without elasticity is also shown in Figure 5-7 (a). Both

models in the theoretical way and the realistic way implemented in CarMaker are illustrated in block diagrams. Here, δ_H is steering wheel angle by hand. δ_w is front wheel steering angle (same for the left and right wheels). q_w denotes the rack position. i_s is the steering ratio from the steering wheel to the front wheel (15). i_{sq} is the steering gear ratio from the steering wheel δ_H to the rack (107 rad/m) and i_{qw} is the steering ratio from the rack to the front wheel steering δ_w.

For the steering system with elasticity in Figure 5-7 (b), the self-aligning torque T_y results from the lateral force F_y that exerts a moment about the kingpin (steering axis) through the moment arm which is composed of the caster length e and the pneumatic trail l_t[89]. The front wheel steering angle δ_w is assumed to be influenced by the front axle lateral force. This additional component is assumed to be proportional to the front axle lateral force and same for the left wheel and right wheel. The physical mechanism is described by the following equation.

$$\delta_w = \frac{\delta_H}{i_s} - \Delta\alpha_s = \frac{\delta_H}{i_s} - \frac{1}{K_s}(F_{yfL,1} + F_{yfR,1}) \tag{5.3}$$

$\Delta\alpha_s$ is the additional component of side-slip angle due to the steering system elasticity. K_s is the lateral stiffness related to the wheel side-slip angle due to steering system elasticity (unit: kN/rad). $F_{yfL,1}$ and $F_{yfR,1}$ are the lateral forces at the front left wheel and front right wheel, respectively.

In the practical steering mechanism, only the steering gear ratio can be adjusted by the rack position q_w in the steering system. Therefore, the Eq. (5.3) is replaced by

$$\begin{cases} \delta_H = \delta_w \cdot i_s = q_w \cdot i_{sq} \\ q_w = \frac{\delta_H}{i_{sq}} - \Delta q_w = \frac{\delta_H}{i_{sq}} - \frac{1}{K_{sq}}(F_{yfL,1} + F_{yfR,1}) \end{cases} \tag{5.4}$$

A corresponding stiffness K_{sq} (10251, unit: kN/m) related to the rack position is proportional to the lateral stiffness K_s related to the wheel side-slip angle. Hence, their relationship is defined by the equation below.

$$K_s = \frac{K_{sq} \cdot i_s}{i_{sq}} \tag{5.5}$$

Under this consideration, a simple module describing the steering system elasticity (described in the realistic way in Figure 5-7 (b)) is designed and embedded into the simulation model in Simulink. The physical fundamental is that, the effective front wheel side-slip angle consists of two parts. One is due to original tire cornering characteristic defined by the Magic Formula tire model and the other is due to the steering system elasticity. The effective front wheel side-slip angle is described by the equation below.

[89] Pacejka: Tire and Vehicle Dynamics, third edition, 2012, p. 10.

$$\alpha_{f,eff,1} = \alpha_{f,tire,1} - \Delta\alpha_s \tag{5.6}$$

The Eq. (5.6) can also be transformed to an expression with the cornering stiffness, Eq. (5.7). One point has to be pointed out. If the C_α is a negative coefficient regarding the physical mechanism of lateral force, i.e. a tire with a negative side-slip angle generates a positive lateral force, the K_s is a positive coefficient due to the physical mechanism of the steering system elasticity considered here. They have different signs.

$$C_{\alpha f,eff,1}^{-1} = C_{\alpha f,tire,1}^{-1} + K_s^{-1} \tag{5.7}$$

After the adjustment with the module describing the steering system elasticity above, any axle cornering stiffness is nearly the same as that in the measurement data, especially at the responsive beginning with a steady state oscillation. The dominant yaw oscillation frequency in the simulation becomes even closer to that in the measurement data and so are the lateral acceleration and both yaw rates. However, the dominant yaw oscillation frequency shows a time varying property after the steady state oscillation. This corresponds with a slightly bigger amplitude in the yaw rate or the lateral acceleration. Accordingly, the axle cornering stiffness shows some degree of time varying property as well, particularly in the rear axle cornering stiffness of the towing car $C_{\alpha r,1}$. This deviation resulting from the time varying property cannot be simulated if its source is not clear. This problem is discussed in detail in Chapter 6.

With the designed steering system elasticity module, the simulation model can describe the system dynamic behavior even better. This module is effective in the model validation. As a result, a comparison between the estimated axle cornering stiffness derived from the measurement data and the estimated values derived from the simulation data is given in Table 5-1 in Section 5.2.6.

5.2.6 Validated model without time-varying property

Both the experimental system and simulation model can be simplified and represented well by the STM within the range of linear lateral dynamics. The motivation in this application is to compare the system parameters from both systems, including the dominant yaw oscillation frequency, axle cornering stiffness, instantaneous lateral friction coefficient, etc. Through this comparison, the validation of a complex simulation model can be completed within the range of linear lateral dynamics at the first step. Furthermore, identification of potential time varying system parameters is of special interest in the experimental system. Such new discovery can give a hint for the further investigation on system handling and stability.

The simulation model has a non-validated aerodynamic module but no road surface module (i.e. just a perfectly flat road). The values of main system parameters are also in Table A in Appendix A.1. The vehicle longitudinal velocity is set to the previously

determined critical speed of 107.9 km/h in the road test. Under an impulse steering excitation with amplitude ca. 19°, the system exhibits a steady state oscillatory motion. The system critical speed is ca. 117.3 km/h in the simulation with a complete model in CarMaker. The lateral accelerations of the towing car and the trailer have nearly the same amplitudes between the experiment and simulation. They are shown in Figure 5-8 below. After the time point 62.5s, a correction signal with high frequency disturbances is applied to the steering wheel by the driver to stop the critical stable state in the experiment.

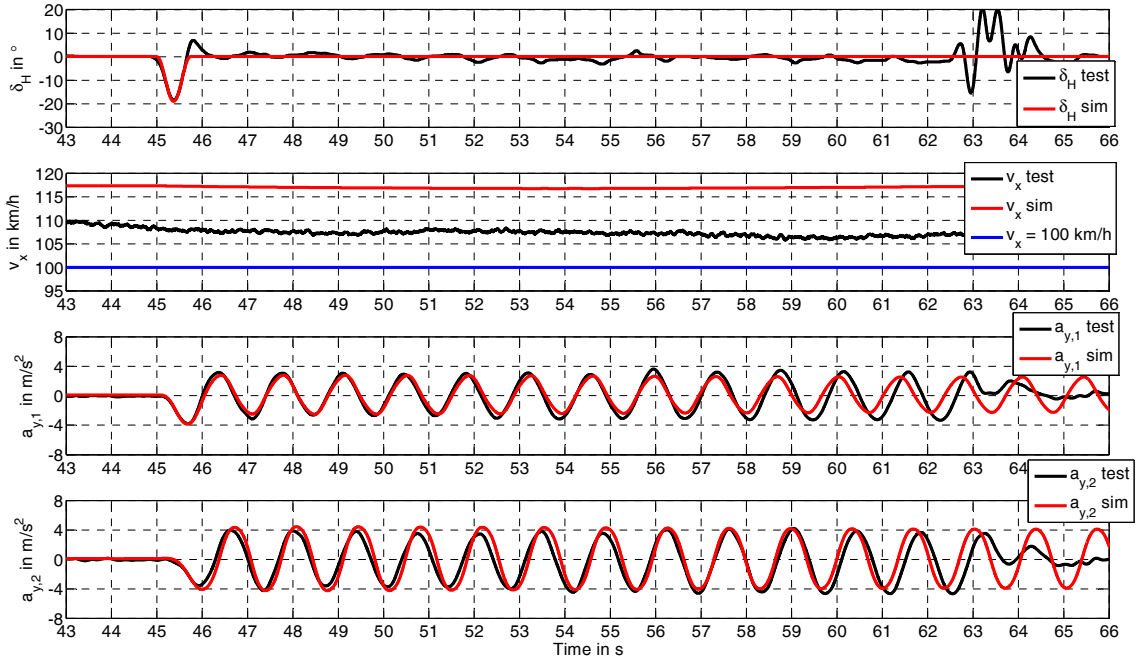

Figure 5-8: First-phase validation of δ_H, v_x and a_y

The yaw rates of the towing car and trailer are illustrated in Figure 5-9. With the assistance of the TFA-based PIM, an instantaneous dominant yaw oscillation frequency ($f_{s,1}$ for the towing car, $f_{s,2}$ for the trailer) is obtained. For a compromise between the temporal and frequency resolutions, the length of the moving time window is determined as roughly two yaw oscillations (T=2/$f_{s,1}$≈2/$f_{s,2}$≈2.7s). The overlap is fixed by the moving step Δt (Δt=T/16≈0.17s). The real experimental system has some time varying property which is indicated by a slight decrease in the $f_{s,1}$ or $f_{s,2}$. Consequently, it leads to slightly bigger amplitude in the lateral acceleration or yaw rate. This phenomenon is not found in the simulation model. Instead, the $f_{s,1}$ or $f_{s,2}$ in the simulation is approximately constant.

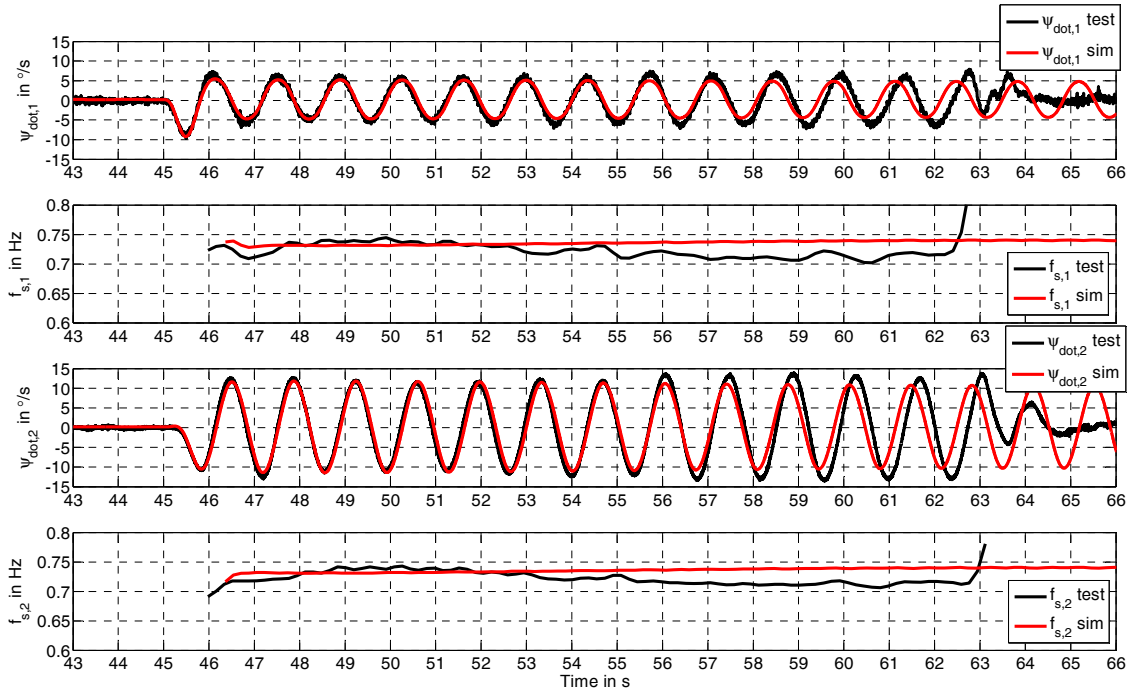

Figure 5-9: First-phase validation of yaw rate and dominant yaw oscillation frequency

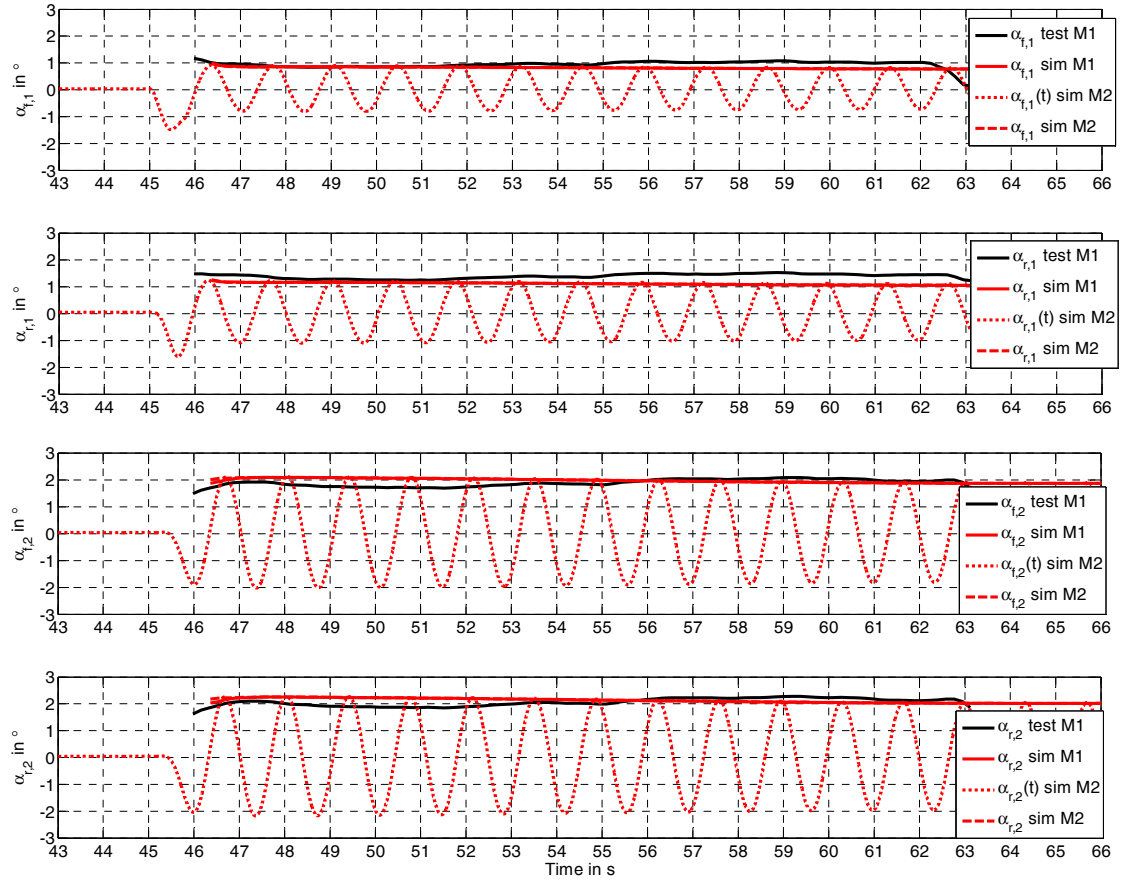

Figure 5-10: First-phase validation of axle side-slip angle

The axle side-slip angles are evaluated with the developed TFA-based PIM at the dominant yaw oscillation frequency. Based on the derived formulas in Section 4.4.1, the axle side-slip angle of the towing car or trailer is described in the time domain with the solid lines (M1: Method 1) in Figure 5-10. For comparison, their time domain signals in simulation (i.e. time domain signal of body side-slip angle is available) are described with the dotted lines (M2: Method 2, also based on the STM). Besides, their amplitudes are also evaluated with the TFA-based PIM and expressed with dashed lines (M2: Method 2, also based on the STM). Due to the available body side-slip angle and the wheel lateral forces in simulation, both axle side-slip angles and axle cornering stiffnesses of the trailer can be obtained. The analysis results match with each other very well between the experiment and simulation. A relatively bigger deviation, especially for $\alpha_{r,1}$, starts from the time point 52s, which is consistent with slightly bigger amplitude in the lateral acceleration or yaw rate in Figure 5-8 or Figure 5-9 above.

The axle cornering stiffnesses are also evaluated with the TFA-based PIM at the dominant yaw oscillation frequency (see Figure 5-11). The analysis results match with each other very well between the experiment and simulation. For the trailer, the cornering stiffness of the rear axle is taken as the reference in the validation based on the simplification (see Eq. (4.7) and (4.8)) in Section 4.4.1. The real front axle cornering stiffness of the trailer is ca. 8-10 kN/rad bigger than that of the rear axle of the trailer, because it is closer to the COG of the trailer and bears more load. It is confirmed by the data analysis that, the lateral force of the trailer front axle is ca. 2.2% smaller while its side-slip angle is ca. 7.2% smaller when comparing to those of the trailer rear axle. This difference is indicated by the analysis result of the simulation data with Method 2. Besides, a small deviation of ca. 3 kN/rad between Method 1 and Method 2 still remains in the front axle cornering stiffness of the trailer, possibly owing to the simplification in Section 4.4.1.

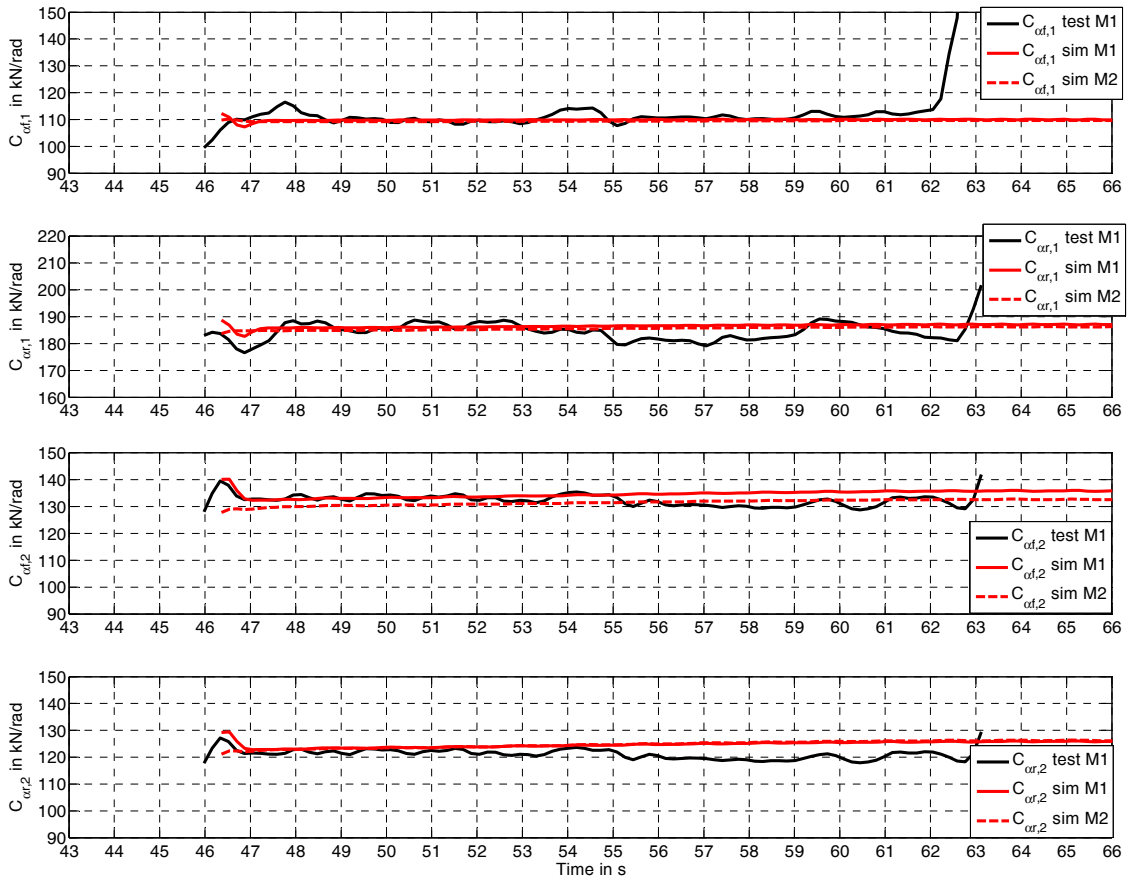

Figure 5-11: First-phase validation of axle cornering stiffness

The instantaneous lateral friction coefficient $\mu_{yf,1}$, effective axle load $F_{zf,eff,1}$ and normalized cornering stiffness $\zeta_{f,1}$ of the front axle of the towing car are estimated with the TFA-based PIM. Their variation trends at the dominant yaw oscillation frequency are shown in Figure 5-12 below. The $\mu_{yf,1}$ works always in the tire linear range in simulation. Although a slight increase in $\mu_{yf,1}$ starts from the time point 52s, there is no significant change in others in the experiment.

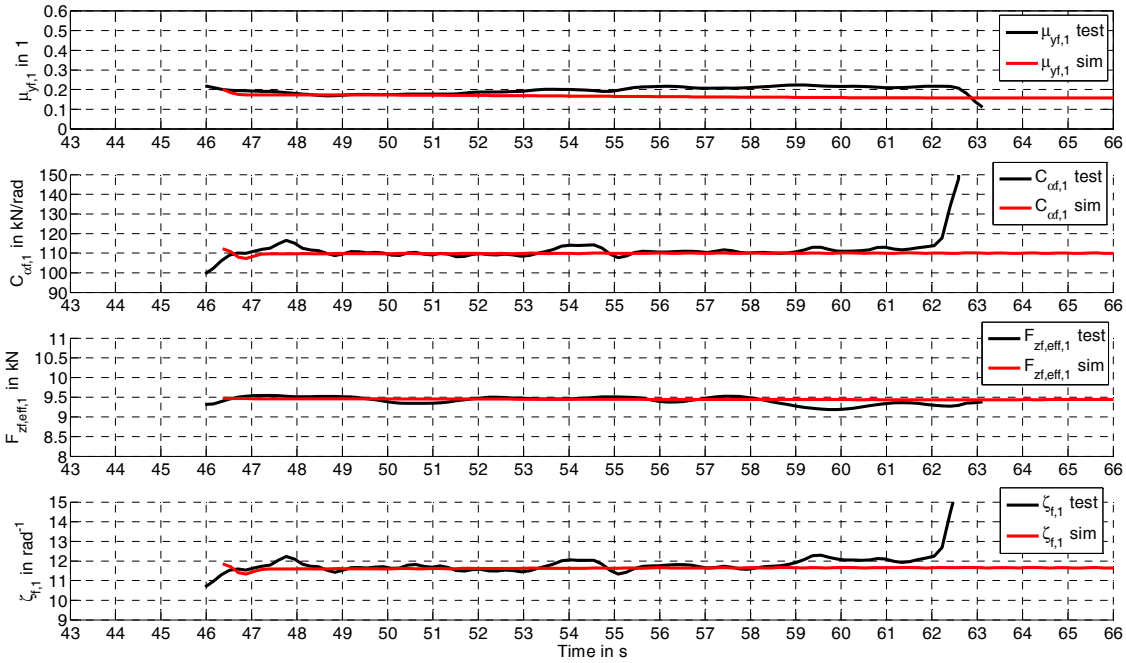

Figure 5-12: First-phase validation of $\mu_{yf,1}$, $C_{\alpha f,1}$, $F_{zf,eff,1}$ and $\zeta_{f,1}$ of the front axle of the towing car

Furthermore, the instantaneous lateral friction coefficient $\mu_{yr,1}$, effective axle load $F_{zr,eff,1}$ and normalized cornering stiffness $\zeta_{r,1}$ of the rear axle of the towing car are also estimated with the TFA-based PIM. Their variation trends at the dominant yaw oscillation frequency are shown in Figure 5-13 below. One point has to be mentioned here: while the $\mu_{yr,1}$ works always in the tire linear range in simulation, it works mostly on the boundary of the tire nonlinear range in the experiment. The possible reason is the different tire characteristics or slight difference in the axle cornering stiffness due to slight difference in the dynamic wheel/axle load.

Besides, an obvious and significant time varying property exists in the rear axle cornering stiffness $C_{\alpha r,1}$ in two time windows, e.g. in 54-56s or 59-61s. This instantaneous change can be explained partly by the corresponding change in the rear axle effective axle load $F_{zr,eff,1}$. However, the remaining change that is transferred to the normalized cornering stiffness $\zeta_{r,1}$ still deserves special attention. It indicates some potential difference in the tire characteristics described by the Magic Formula tire model as well.

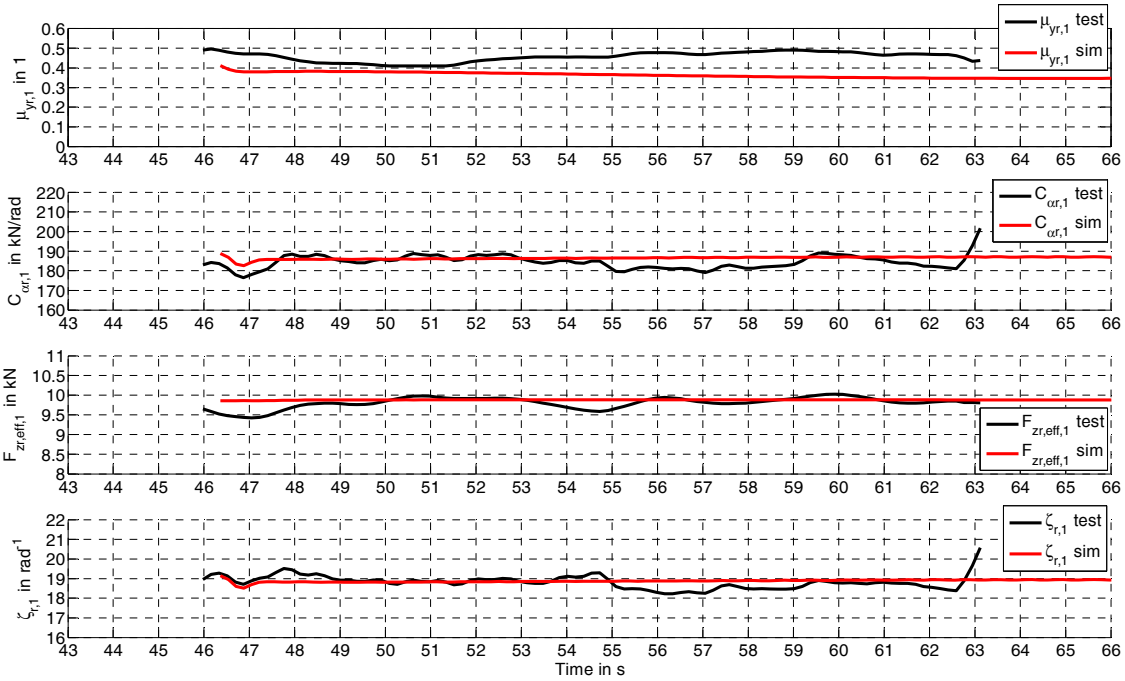

Figure 5-13: First-phase validation of $\mu_{yr,1}$, $C_{\alpha r,1}$, $F_{zr,eff,1}$ and $\zeta_{r,1}$ of the rear axle of the towing car

Table 5-1: Comparison of axle cornering stiffness (amplitude and phase) and system dynamic critical speed after model validation

System Parameter	Description	Experiment M1	Simulation		Unit
			M1	M2	
$C_{\alpha f,1}$	Front axle cornering stiffness	109.2 (-8.0°)	109.2 (-7.6°)	109.3 (-8.0°)	kN/rad
$C_{\alpha r,1}$	Rear axle cornering stiffness	184.9 (-6.7°)	184.9 (-5.2°)	185.2 (-5.4°)	kN/rad
$C_{\alpha f,2}$	Front axle cornering stiffness	134.2 (-0.8°)	134.2 (-13.9°)	131.2 (-15.9°)	kN/rad
$C_{\alpha r,2}$	Front axle cornering stiffness	123.4 (-6.9°)	123.4 (-18.3°)	124.4 (-16.5°)	kN/rad
v_{crit}	System dynamic critical speed	107.9	117.3	117.3	km/h
v_{crit} in STM	System dynamic critical speed	123.0	123.0	123.3	km/h

After a complete simulation model validation, a comparison of the axle cornering stiffness (amplitude and phase) and the system dynamic critical speed is given in Table 5-1 above. No significant difference exists in either of the axle cornering stiffness between the experiment and simulation except a deviation of ca. 3 kN/rad in the $C_{\alpha f,2}$ due to the simplification related to the tandem-axle trailer in the TFA-based PIM. Also, in the

evaluation results with Method 1, there is a deviation of ca. 13° in the phases of the axle cornering stiffnesses of the trailer between the experiment and simulation. Moreover, there is no significant difference in v_{crit} in STM with the system parameters evaluated from the experiment or simulation data. It is consistent with the small sensitivity of $C_{\alpha f,2}$ to v_{crit} based on the analysis of system dynamic stability with the analytical STM (see Figure 3-7). However, there is still ca. 10 km/h deviation in the system dynamic critical speed v_{crit} between the experiment and the CarMaker simulation. But this deviation in v_{crit} disappears in the linear STM with the estimated axle cornering stiffnesses, although the v_{crit} in the linear STM without aerodynamics module is even ca. 6 km/h larger than that in the CarMaker simulation. It gives a strong indication that, such a deviation in v_{crit} might result from two sources: an aerodynamic effect and the coupling between the vertical dynamics and the horizontal dynamics. Some preliminary simulation results[90] show that, the v_{crit} reduces by ca. 3.0 km/h when a module representing the ambient aerodynamics is integrated as well. Also, theoretical analysis on this point is given by Schütz and Hucho[91]. Experiment results in wind tunnel tests and road tests by Peschke and Mankau[92] revealed the aerodynamic drag force induced an additional pitch moment on the trailer, by which the vertical hitch load is reduced significantly. Also, through experiments Zomotor[93] found that, the vertical hitch load influences the v_{crit} significantly as well. When the vertical hitch load increased from 0 to 500 N, the v_{crit} can be increased by ca. 20 km/h. Therefore, either the deviation in v_{crit} between the experiment and the CarMaker simulation or the deviation in v_{crit} between the linear STM and the CarMaker simulation might be owed to a non-validated aerodynamic module or its complete absence. Moreover, the coupling between the vertical dynamics, in which the suspension forces are involved, and the horizontal dynamics also deserves specific attention. The deviation of ca. 13° in the phases of the axle cornering stiffnesses of the trailer might be attributed to different system roll behaviors between the experiment and simulation, especially the difference in the trailer roll behavior. Further simulation shows that, through the change of system roll characteristics (i.e. increasing the total roll stiffness of the towing car as ten times stiff as the original value) the v_{crit} can be increased by ca. 6.0 km/h. In this situation, the influence from the aerodynamic effect is also combined owing to a bigger aerodynamic drag force. These point out a further potential for the simulation model validation.

Moreover, the yaw moment of inertia of the towing car or trailer is obtained in the same way (see Section 4.4.4) with the TFA-based PIM (see Figure 5-14 below). Due to the

[90] Gao: Modeling and Simulation of Aerodynamics…, Master's thesis supervised by Zhang, 2013.

[91] Schütz: Hucho-Aerodynamik des Automobils, 2013, p. 341.

[92] Peschke et al.: Auftriebskräfte am Wohnanhänger…, 1982.

[93] Zomotor et al.: Untersuchungen über die Stabilität und das aerodynamische Störverhalten…, 1982.

advantage of TFA, an instantaneous argument is served as a helpful tool to check if the calculation formulas in Section 4.4.4 are correct or not. However, an extended phase correction algorithm, triple-spectrum-line-interpolation algorithm proposed by Niu[94] *et al*., is considered and applied here to compensate a significant error in [-90°, 90°] led by phase without correction[95] due to the well-known leakage effect in spectral analysis. More details about this triple-spectrum-line-interpolation algorithm are given in Appendix A.3.

For the towing car, the estimated amplitudes match with each other very well between the experiment and simulation, but the arguments have ca. -20° delay. This indicates the yaw rate of the towing car has a phase delay of ca. 20° at the dominant yaw oscillation frequency compared to the tire lateral force. This phase delay is attributed to the suspension kinematics and compliance of the towing car.

For the trailer, the arguments of the yaw moments of inertia with Method 1 are nearly zero, but the estimated amplitudes with Method 1 have a clear deviation of ca. 580 kgm^2 (ca. 5.5 %) between the experiment and simulation. This deviation can be attributed to the simplification that the lateral forces at the two axles of the trailer are equal, i.e. half of the total amount, and the consequent amplification effect by the lever arm in Eq. (4.20). The arguments of the yaw moments of inertia with Method 2 have ca. -10° delay, and the estimated amplitudes with Method 2 have a bigger deviation of ca. 1000 kgm^2 (ca. 10.9 %) between the experiment and simulation. Therefore, the evaluation Method 1 for the trailer yaw moment of inertia seems to be more precise by this comparison.

Due to the absence of trailer wheel measuring rims, an accurate estimation of the yaw moment of inertia is only possible for the towing car with the TFA-based PIM. If the measuring rims for the trailer wheels are also available, an accurate estimation of the yaw moment of inertia is also possible. The estimated result can be refined further.

After a complete simulation model validation, a comparison of the yaw moment of inertia is given in Table 5-2 below. A measured value for the yaw moment of inertia of the trailer is delivered from the project partner, but the one for that of the towing car is unknown. In the system simulation model, both of them are given as the system input parameters. They are taken into account as the reference values in the comparison.

---

[94] Niu et al.: An Algorithm for … Triple-spectrum-line Interpolation FFT, 2012.

[95] Ming et al.: Corrections for Frequency, Amplitude and Phase in A Fast Fourier Transform…, 1996.

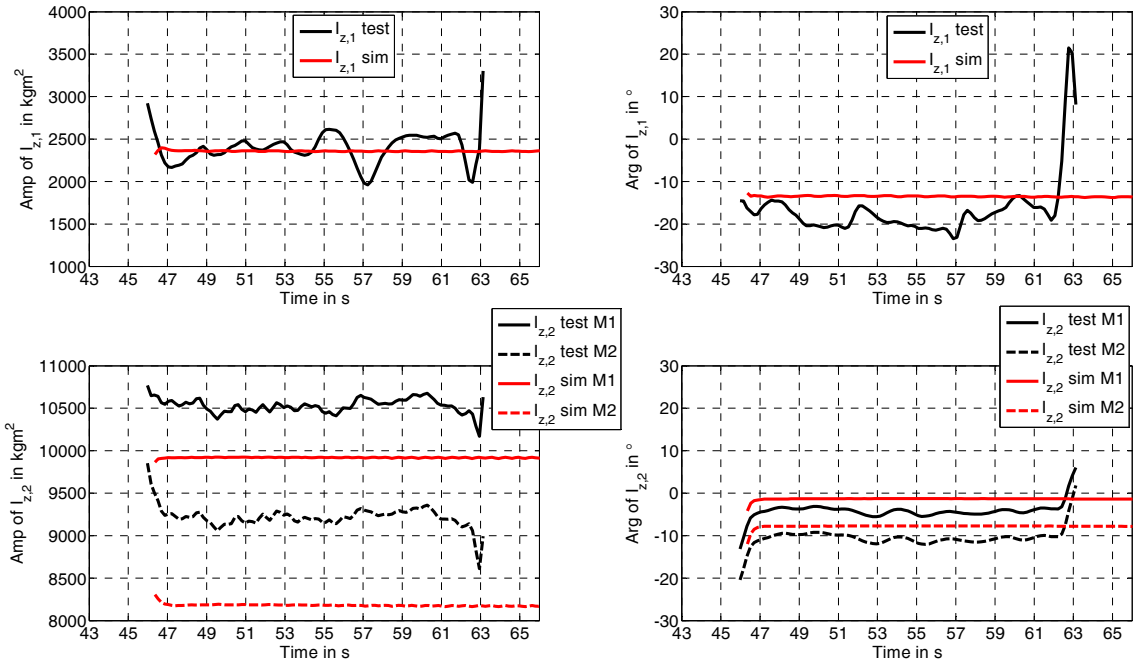

Figure 5-14: Validation of yaw moment of inertia

An error defined by Eq. (5.8) is calculated based on the estimated values with the TFA-based PIM. It aims for a comparison between the experiment and simulation. No significant difference exists in the yaw moment of inertia of the towing car $I_{z,1}$ between the experiment and simulation. However, there is still a deviation (ca. 580 kgm^2 with Method 1, ca. 1000 kgm^2 with Method 2) in the yaw moment of inertia of the trailer $I_{z,2}$ between the experiment and simulation.

$$\Delta = \left| \frac{I_{z,i,exp} - I_{z,i,sim}}{I_{z,i,exp}} \right| \times 100\% \tag{5.8}$$

Table 5-2: Comparison of yaw moment of inertia after model validation

Yaw moment of Inertia	**Experiment**			**Simulation**			**Error Δ**			
Towing car $I_{z,1}$ (kgm^2)	measured	estimated		input	estimated		absolute		percent	
	unknown	2360		2690	2360		0		0%	
Trailer $I_{z,2}$ (kgm^2)	measured	estimated		input	estimated		absolute		percent	
		M1	M2		M1	M2	M1	M2	M1	M2
	10352.8	10500	9185	10350	9920	8185	580	1000	5.5%	10.9%

There is no significant deviation for either yaw moment of inertia between the measured value and simulation input. However, for the towing car, a deviation of ca. 330 kgm^2 (ca. 12.3 %) exists between the simulation input and estimated value. For the trailer, a deviation of ca. 140 kgm^2 (ca. 1.4 %) with Method 1 is smaller when a mean estimated value between the experiment and simulation is compared (the deviation of ca. 1665 kgm^2 (ca. 16.1 %) with Method 2 is much bigger). This also points out a further potential for the simulation model validation.

By now, the complex simulation model in IPG CarMaker® software is validated within the range of linear lateral dynamics at the first step. Therefore, an explanation of ca. 10 km/h difference in the system dynamic critical speed between the experiment and simulation can be possibly achieved when the validation of aerodynamics[96,97], road irregularities and vertical dynamics[98] are considered in the future.

5.3 Conclusions

This chapter focuses on the potential application scope of the proposed TFA-based PIM in vehicle dynamics. The application scope of this novel TFA-based PIM is mainly system identification with time varying properties within the range of linear lateral dynamics, which aims for the model identification to build up simulation models.

In this chapter, the developed PIM is applied in a case study, a simulation model validation of a car-caravan combination. Because of the investigated critical steady state oscillation phenomenon that describes the system's stability margin, the system has a harmonic behavior under an impulse excitation at its dynamic critical speed. The driving maneuver in the road test and simulation is defined according to the lateral stability test standard ISO 9815 of CTCs.

A system simulation model is built in CarMaker® environment with all the system parameters delivered from the project partner. However, the model is not completely validated. A further complete validation process based on the measurement data in the road test is performed in detail. The validation method is defined with three steps in detail. A general validation criterion is that, the difference of each system parameter or

[96] Standen: Towed vehicle aerodynamics, 1999.

[97] Gao: Modeling and Simulation of Aerodynamics…, Master's thesis supervised by Zhang, 2013.

[98] Wu: Analysis of Wheel Load Fluctuations…, Master's thesis supervised by Zhang, 2013.

state variable between the experimental data and simulation data should be within 5% of the experimental data.

After a complete validation process in which many specific aspects are considered, no significant difference exists in either of the axle cornering stiffness between the experiment and simulation except a ca. 8 kN/rad deviation in the $C_{\alpha f,2}$ due to a simplification of a single-axle trailer in the TFA-based PIM. However, there is still ca. 10 km/h deviation in the system dynamic critical speed v_{crit} between the experiment and simulation. But this deviation in v_{crit} disappears in a linear STM with the estimated axle cornering stiffnesses. It gives a strong indication that, such a deviation in v_{crit} might result from the coupling between the vertical dynamics and horizontal dynamics, an aerodynamic effect or even both. This points out a further potential for the simulation model validation.

There is no significant deviation for either yaw moment of inertia between the measured value and simulation input. However, for the towing car, a deviation of ca. 330 kgm^2 (ca. 12.3 %) exists between the simulation input and estimated value. For the trailer, a deviation of ca. 140 kgm^2 (ca. 1.4 %) is smaller when a mean estimated value between the experiment and simulation is compared. This also points out a further potential for the simulation model validation.

By now, the complex simulation model in IPG CarMaker® software is validated within the range of linear lateral dynamics at the first step. Therefore, an explanation of ca. 10 km/h difference in the system dynamic critical speed between the experiment and simulation can be possibly achieved when the validation of aerodynamics, road irregularities and vertical dynamics are considered in the future. This first-phase validation of the simulation model also lays a good foundation for the simulation study of the system dynamic stability.

However, two problems still have to be considered if the further refinement of the simulation model is of concern. The first problem is that, the real experimental system has some time varying property which is indicated by a slight decrease in the $f_{s,1}$ or $f_{s,2}$. Consequently, it leads to slightly bigger amplitude in the lateral acceleration or yaw rate. This phenomenon is not found in the simulation model. An corresponding obvious time varying property also exists in the rear axle cornering stiffness $C_{\alpha r,1}$ in some time frame. This instantaneous change can be explained partly by the corresponding change in the rear axle effective axle load $F_{zr,eff,1}$. However, the remaining change that is transferred to the normalized cornering stiffness $\zeta_{r,1}$ still deserves special attention. It indicates some potential difference in the tire characteristics described by the Magic Formula tire model as well. This is the second problem, which is indicated by the deviation in the instantaneous lateral friction coefficient $\mu_{yr,1}$ between the experiment and simulation as well.

6 Impact Study of Nonlinearity-induced Harmonic Dynamic Axle Load

Any device with nonlinear characteristics can introduce harmonics to a system. This so-called harmonic effect is particularly prevalent in the electric power systems due to the existence of current harmonics, which is induced by nonlinear electric load. Because of the similarity principle between the electrics and mechanics, such harmonic effect also exists in mechanical systems, e.g. in a mass-spring-damper system with a nonlinear spring or damper. Furthermore, in the suspension design of automotive engineering, the characteristics of practical spring or damper is always designed as nonlinear and asymmetric. In such cases, this nonlinear harmonic effect can be transferred into the dynamic wheel load and hence causes stability problems for vehicle systems.

Considering the nonlinearity-induced harmonic dynamic axle load in vehicle systems, asymmetric characteristic of suspension component is a major source. The sources for the asymmetric characteristic of suspension component can be sorted into two categories. One can be called as expected asymmetry, which means different spring or damping coefficients between the compression and rebound process in the design curve. This expected asymmetry aims for a compromise between the stability/safety and comfort. The other can be called as undesired asymmetry or failure, which means unexpected low spring or damping force existing particularly in a hydraulic or pneumatic component, e.g. a hydraulic damper or gas spring. This unexpected asymmetry or failure becomes severer at specific positions in a motion cycle due to the effect of compressibility, cavitation[99] or even failure of electrical or mechanical component[100]. It is undesired but really exists in practice. It cannot be neglected at critical maneuvers[100].

In order to explain the physical mechanism of the nonlinearity-induced harmonic in vehicle systems, harmonic dynamic axle load induced by damper nonlinear characteristics is summarized in Table 6-1 below. Here damper means the shock absorber installed in the vehicle suspension. The characteristic of an ideal linear damper is illustrated by its corresponding F_d-v_d diagram, F_d-s_d diagram and relevant F-t diagram simultaneously in column (1). Under this condition, there is no asymmetry and no harmonic dynamic axle load exists accordingly. Once a bilinear damper is applied, harmonic dynamic axle load exists due to the introduced asymmetric characteristic between the rebound and compression (see column (2)). A more practical “normal” damper (see column (3)),

[99] Dixon: The Shock Absorber Handbook, second edition, 2007, p. 276-277.

[100] Bedük et al.: Effects of damper failure on vehicle stability, 2013, p. 1024-1039.

which is characterized by a piecewise linear function, induces a similar asymmetry and harmonic dynamic axle load. In this case, the harmonic dynamic axle load is caused by the original existing nonlinear property, i.e. expected asymmetry. However, damper failure can introduce harmonic dynamic axle load as well. An extremely common damper failure[101] (see column (4)) is firstly considered. A very low damping force exists at the beginning of compression. For a vehicle system with harmonic response, only one-side damper at the same axle has the phenomenon of failure I at every moment. If dampers at both sides are considered, a periodic and asymmetric axle load is induced. Furthermore, a more complicated phenomenon of damper failure II can induce a periodic and symmetric axle load (see column (5)).

It is clear that, both phenomena, "(3) Normal" and "(5) Failure II", can introduce harmonic dynamic axle load into a vehicle system. However, nonlinearity-induced harmonic dynamic axle load by "(3) Normal" exists always due to the expected asymmetry in the damper design, while that induced by "(5) Failure II" is undesired. Moreover, it leads to the impact study of nonlinearity-induced harmonic dynamic axle load on vehicle stability. This chapter covers some original contribution on this topic.

Research of nonlinear harmonic effect in dynamic axle load and its influence on system stability serves as a linkage between the horizontal dynamics and vertical dynamics for the purpose of understanding the dynamic coupling. It is only beneficial for the influence study on the system dynamic stability, particularly for a specific vehicle system like a CTC. Therefore, the impact of the harmonic dynamic axle load on dynamic stability of CTCs is the focus in this chapter. However, one point has to be mentioned before further investigation. Although impact study of harmonic dynamic axle load induced by "(5) Failure II" on the dynamic stability of a CTC is the objective of this chapter, interaction from harmonic dynamic axle load induced by original existing nonlinear property cannot be excluded because of many possible sources like "(3) Normal" in the system.

[101] Winner: Skriptum zur Vorlesung "Kraftfahrzeugtechnik", 2014.

Table 6-1: Harmonic dynamic axle load induced by damper nonlinear characteristics

Phenomenon	(1) Linear	(2) Bilinear	(3) Normal	(4) Failure I	(5) Failure II
F_d-v_d diagram	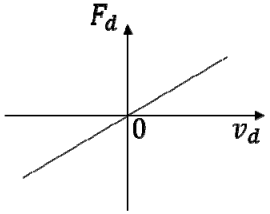	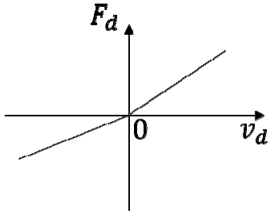	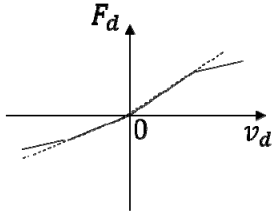	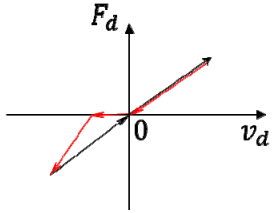	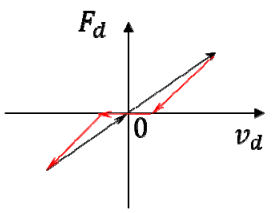
F_d-s_d diagram	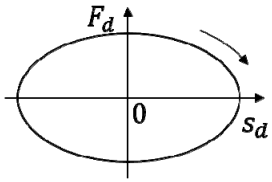	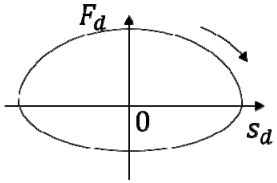	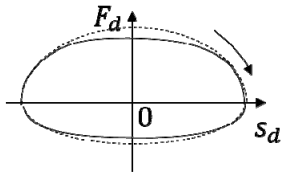	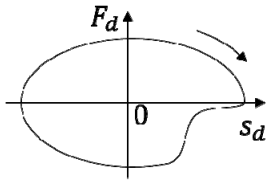	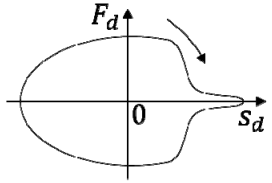
F-t diagram $F_{z,sum}$ $F_{d,L}$ $F_{d,R}$ $F_{d,sum}$	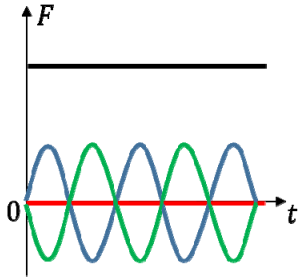	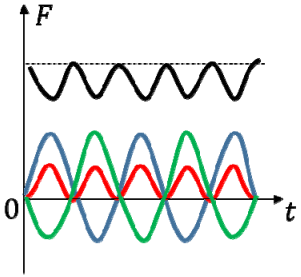	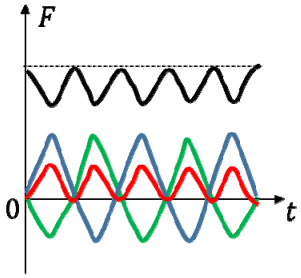	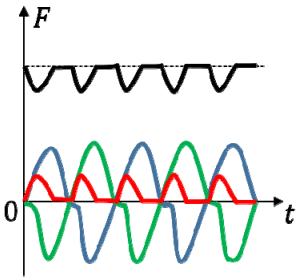	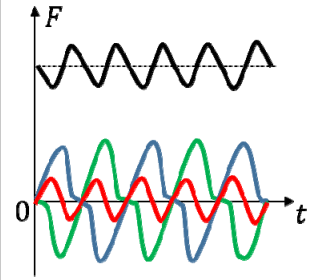

6.1 Experimental study

Because a harmonic effect in the dynamic axle load is obviously found in the road test, quantification of effective axle load indicates the axle cornering stiffness can be changed by this harmonic effect. In Section 3.2.2, the sensitivity analysis of axle cornering stiffness to system dynamic critical speed v_{crit} is already obtained. Therefore, the axle cornering stiffness is a connection to study the influence of the harmonic effect on system dynamic stability. Since the harmonic effect in the dynamic axle load is taken into account in the quantification of effective axle load in Section 4.4.2, axle cornering stiffness and effective axle load can be evaluated. Because the harmonic dynamic axle load is possibly induced by nonlinear property of some component, and such harmonic effect is time varying, the TFA-based PIM becomes necessary in such situation.

The experimental data of a typical road test with a car-caravan combination, which is the same one as that used in Section 5.2, is utilized for comparison in this chapter. The system response in the steady state oscillation is shown in Figure 6-1 below. The steering wheel impulse has amplitude of 19°. The longitudinal velocity defined by the system dynamic critical speed is ca. 107.3 km/h without significant variation. The amplitude of the yaw rate or lateral acceleration of the towing car has nearly constant oscillation amplitude at ca. 0.67 Hz, but small changes still exist (e.g. in 54-56s or 59-61s). The raw and filtered data of the rear axle load of the towing car are also shown in Figure 6-1 below. A time varying harmonic oscillation of ca. 1.40 Hz is obvious. It has relatively bigger amplitude when small changes occur in the amplitude of the yaw rate or lateral acceleration after the steering excitation, i.e. in 54-56s or 59-61s. Because the lateral acceleration is always within the range of ±4 m/s^2, a linear STM is valid to describe the system dynamic stability. More attention is paid here to the harmonic oscillation in the rear axle load due to the vital influence of the rear axle cornering stiffness $C_{\alpha r,1}$ on the system dynamic critical speed, which is quantified in the sensitivity analysis in Section 3.2.2.

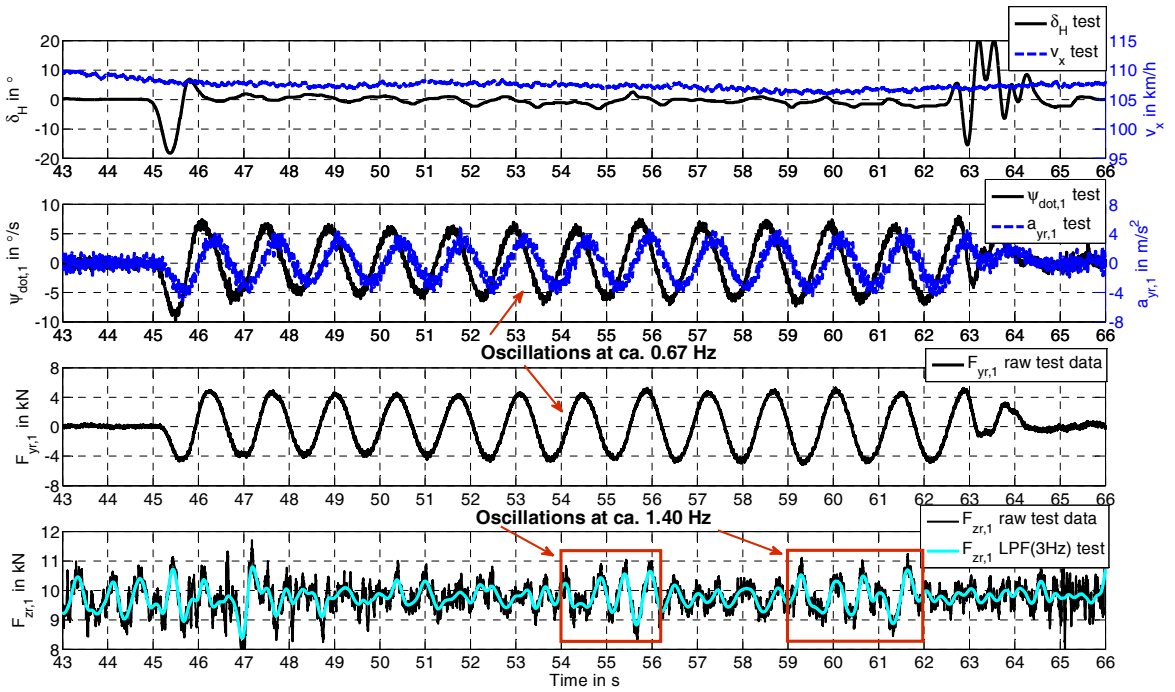

Figure 6-1: System response in steady state oscillation (δ_H, v_x, $\psi_{dot,1}$, $a_{yr,1}$, $F_{yr,1}$ and $F_{zr,1}$)

With the TFA-based PIM, rear axle cornering stiffness $C_{\alpha r,1}$, effective axle load $F_{zr,eff,1}$ and normalised axle cornering stiffness $\zeta_{r,1}$ can be evaluated and shown in Figure 6-2 below. One point has to be mentioned here, the big change at the boundary value can be neglected due to the limitation of the PIM when no harmonic oscillations exist. Three points can be concluded. Firstly, changes of $C_{\alpha r,1}$ correspond to the small changes in the amplitude of the yaw rate or lateral acceleration in Figure 6-1. To be more precise, harmonic effect in the rear axle load in 54-56s reduces the effective axle load $F_{zr,eff,1}$ and causes a corresponding reduction in $C_{\alpha r,1}$ and yaw damping ratio or v_{crit}. Therefore, the amplitude of the yaw rate or lateral acceleration increases slightly. An opposite case occurs in 59-61s. Secondly, some changes of $C_{\alpha r,1}$ can be explained by the corresponding change of $F_{zr,eff,1}$. For instance, the reduction of $C_{\alpha r,1}$ in 53-54.8s can be attributed to a reduction in $F_{zr,eff,1}$. An opposite case also occurs around 59-61s. But some changes of $C_{\alpha r,1}$ cannot be explained by the corresponding change of $F_{zr,eff,1}$, e.g. the reduction of $\zeta_{r,1}$ or $C_{\alpha r,1}$ at around 55s. Lastly, effective axle load $F_{zr,eff,1}$ changes so rapidly that even within one oscillation cycle it can have different variation tendency. For instance, it firstly decreases and then increases in the oscillation cycle around 54-56s. That implies the potential influence from a time varying phase shift of the harmonic effect in the rear axle load, while the amplitude does not change significantly.

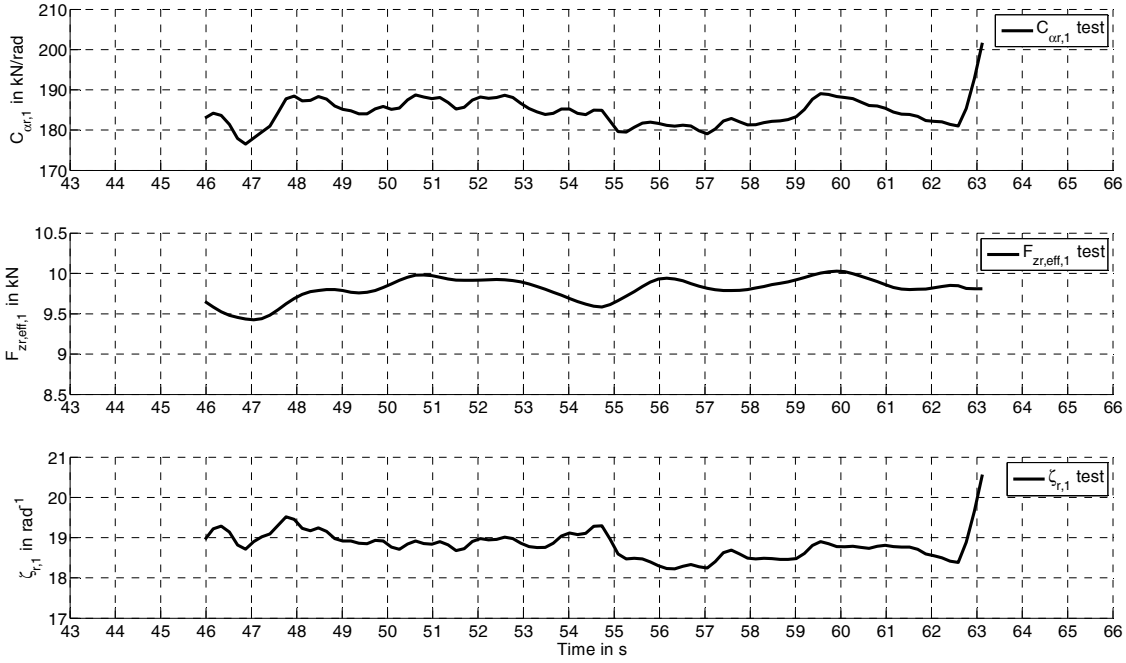

Figure 6-2: Time-frequency analysis result including $C_{\alpha r,1}$, $F_{zr,eff,1}$ and $\zeta_{r,1}$

For CTCs, the harmonic effect in dynamic axle load is clearly found, although the root cause for such effect has many possibilities. The TFA result shows that, it can indeed affect the effective axle load and axle cornering stiffness. Besides, the discovered harmonic effect in dynamic axle load is time varying and changes rapidly over time. However, through the experimental study, the influences of its amplitude and phase cannot be studied separately. Therefore, a simulation study based on innovative design is another option to achieve this goal.

6.2 Simulation method

Although Chapter 5 describes the first phase of the validation of a complex simulation model for the car-caravan combination applied in the road test, it shows that (see Section 5.2.6) nonlinearity-induced harmonic dynamic axle load cannot be simulated. Consequently, its impact on the system dynamic stability cannot be accomplished either. Although the simulation model is completely validated in the horizontal plane, further study on the coupling between the vertical dynamics and horizontal dynamics and their interactions is still a constructive extension.

In order to simulate the nonlinearity-induced harmonic dynamic axle load, modeling method for the harmonic effect is a key point in the simulation. Because this harmonic axle load is dominated by the 1st harmonic of the dominant yaw oscillation frequency, square of the yaw rate can generate this harmonic even when the dominant yaw oscillation frequency is time varying. The principle can be explained by the following Eq.

(6.1). Here, $\dot{\psi}_1$ is the yaw rate of the towing car, f_d is the dominant oscillation frequency in the yaw rate, A and φ_0 are its amplitude and initial phase, respectively.

$$\begin{cases} \dot{\psi}_1(t) = A\cos(2\pi f_d t + \varphi_0) \\ \dot{\psi}_1^2(t) = 0.5A^2[\cos(2\pi \cdot 2f_d t + 2\varphi_0) + 1] \end{cases} \tag{6.1}$$

In principle, other signals like body lateral acceleration or axle lateral force can also be selected to generate the harmonic. However, the measured body lateral acceleration is not accurate and always smeared by environmental noise. The problem of the axle lateral force is the phase shift between the front and rear axles if the harmonic effect in the front axle load is also taken into account. Therefore, the yaw rate of the towing car is utilized here.

The square also introduces an undesired DC value in the harmonic. That is the reason why a high-pass filter is followed in the flow diagram of the modeling method shown in Figure 6-3 below. With the advantage of this digital IIR filter, the DC value in the harmonic can be effectively separated. Then a variable time delay block is used to adjust the phase relationship between the harmonic and the axle lateral force. With this function, the influence of the harmonic phase on system dynamic stability can be studied. And the following gain block makes the influence study of the harmonic amplitude available, too. To integrate the module into the complete simulation model, the harmonic force designed for the axle load has to be distributed between the left and right wheels. This real-time distribution depends on the direction of the yaw rate. Here, math operations including unary minus and Heaviside step function are applied in the implementation. When the yaw rate is negative, extra harmonic force is added to the rear left wheel. Otherwise, it is added to the rear right wheel. Therefore, at every moment only one side at the rear axle has the harmonic phenomenon.

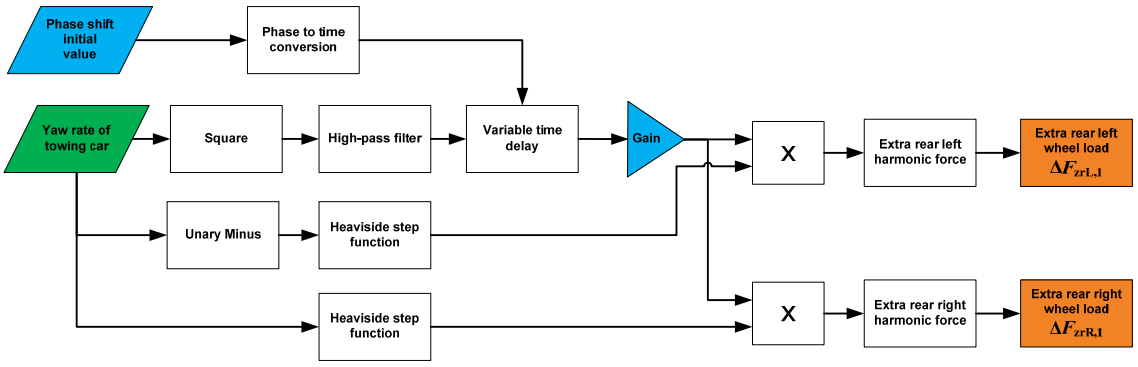

Figure 6-3: Modeling method for the harmonic axle load in the simulation

With the modeling method above, the harmonic effect in the dynamic axle load can be simulated. And both the amplitude and phase can be modified respectively in the simulation. A typical simulation result is shown in Figure 6-4 below. With appropriate modification, the maxima of the absolute axle lateral force meet around the minima of the

axle load. Under such condition, the relative phase of harmonic force to the axle lateral force is set as -180° and the effective rear axle load can be less than the average according to the analysis in Figure 4-5. The relationship between the extra harmonic rear left/right wheel load and the extra harmonic rear axle load is described by the equation below.

$$\Delta F_{\mathrm{zr},1}(t) = \Delta F_{\mathrm{zrL},1}(t) + \Delta F_{\mathrm{zrR},1}(t) \tag{6.2}$$

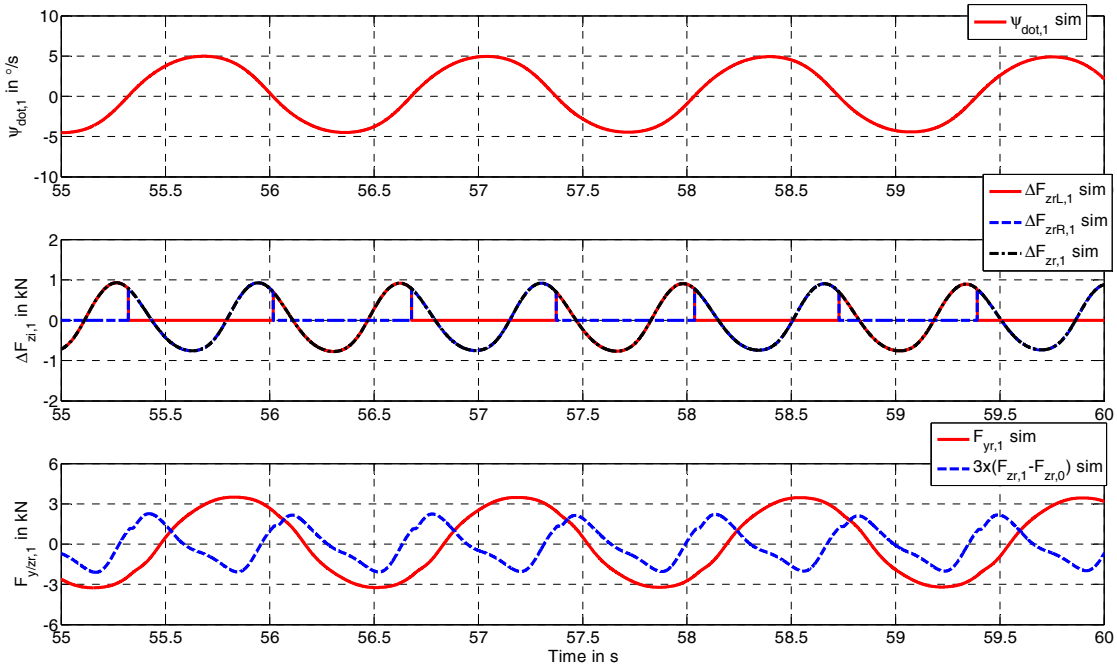

Figure 6-4: Simulation result of the harmonic phenomenon in the wheel/axle load

6.3 Simulation study

Sensitivity analysis of the influence of the harmonic amplitude or phase on the system dynamic stability is studied in this section. Since the harmonic effect is severer at the rear axle than that at the front axle of the towing car, sensitivity analysis of the harmonic impact is only performed when it exists at the rear axle of the towing car. And a precondition is that modeling of the extra harmonic axle load is only implemented at the rear axle of the towing car in the system simulation model as well.

The v_{crit} is used to describe the system dynamic stability. As a connection between the system vertical dynamics and horizontal dynamics, axle cornering stiffness $C_{\alpha\mathrm{r},1}$ (derived from Eq. (4.5)) serves to build the relationship and understand the dynamic cou-

pling based on the sensitivity analysis of system parameters in the linear STM. The effective axle load $F_{zr,eff,1}$ (derived from Eq. (4.14)) is used to quantify the harmonic dynamic axle load. Moreover, the normalized axle cornering stiffness $\zeta_{r,1}$ (derived from Eq. (4.16)) is also evaluated to investigate other effects on the $C_{\alpha r,1}$ which are not related to the main effect from the axle load.

Sensitivity analysis of the influence of the harmonic amplitude or phase on the system dynamic stability is shown in Figure 6-5 below. While the analysis result for the amplitude influence is described in the left column (see Figure 6-5 (a1)-(d1)), the analysis result for the phase influence is in the right column (see Figure 6-5 (a2)-(d2)).

One point about the sensitivity analysis for harmonic amplitude influence in Figure 6-5 (a1)-(d1) below has to be mentioned here. Because the amplitude of the extra harmonic force has to be modified by the gain factor in Figure 6-3 above, the amplitude of the total nonlinearity-induced harmonic dynamic axle load Amp($F_{zr,1}$) is different in the three cases with 0°, -90° and -180° phase shift conditions even when the gain factor is same. This is because an interaction between the extra harmonic force and the original existing nonlinearity-induced harmonic force is different from case to case. The modifications of the gain factor for different extra harmonic force in the three cases with 0°, -90° and -180° phase shift conditions are listed in Table 6-2 below.

Table 6-2: Gain factors for different extra harmonic forces

Phase shift condition	**Gain factor for different extra harmonic force**							
0°	0	0.5	1.0	2.0	2.5	3.0	4.0	5.0
-90°	0	0.5	1.0	2.0	2.5	3.0	4.0	5.0
-180°	0	0.5	1.0	2.0	2.5	3.0	4.0	5.0

For the amplitude influence, three cases with 0°, -90° and -180° phase shift conditions for the harmonic axle load are studied. The theoretical fundamental is described in Section 4.4.2. It shows that, the changes of v_{crit} in (a1) and $C_{\alpha r,1}$ in (b1) agree with the expectation well except the case with -90° phase shift condition. For the case with -90° phase shift condition, a dramatically decreasing v_{crit} in (a1) corresponds with the reduction in $C_{\alpha r,1}$ in (b1), which cannot be completely explained by the decrease in $F_{zr,eff,1}$ in (c1). This may be due to an interaction with the original existing nonlinear property of some component. The analysis results of $F_{zr,eff,1}$ in (c1) and $\zeta_{r,1}$ in (d1) indicate a potential inverse proportional relationship between them. Because the tires still work within the linear range, it raises a doubt that for the Magic Formula tire model, the cornering stiffness still has a small degressive characteristic even within the tire linear range.

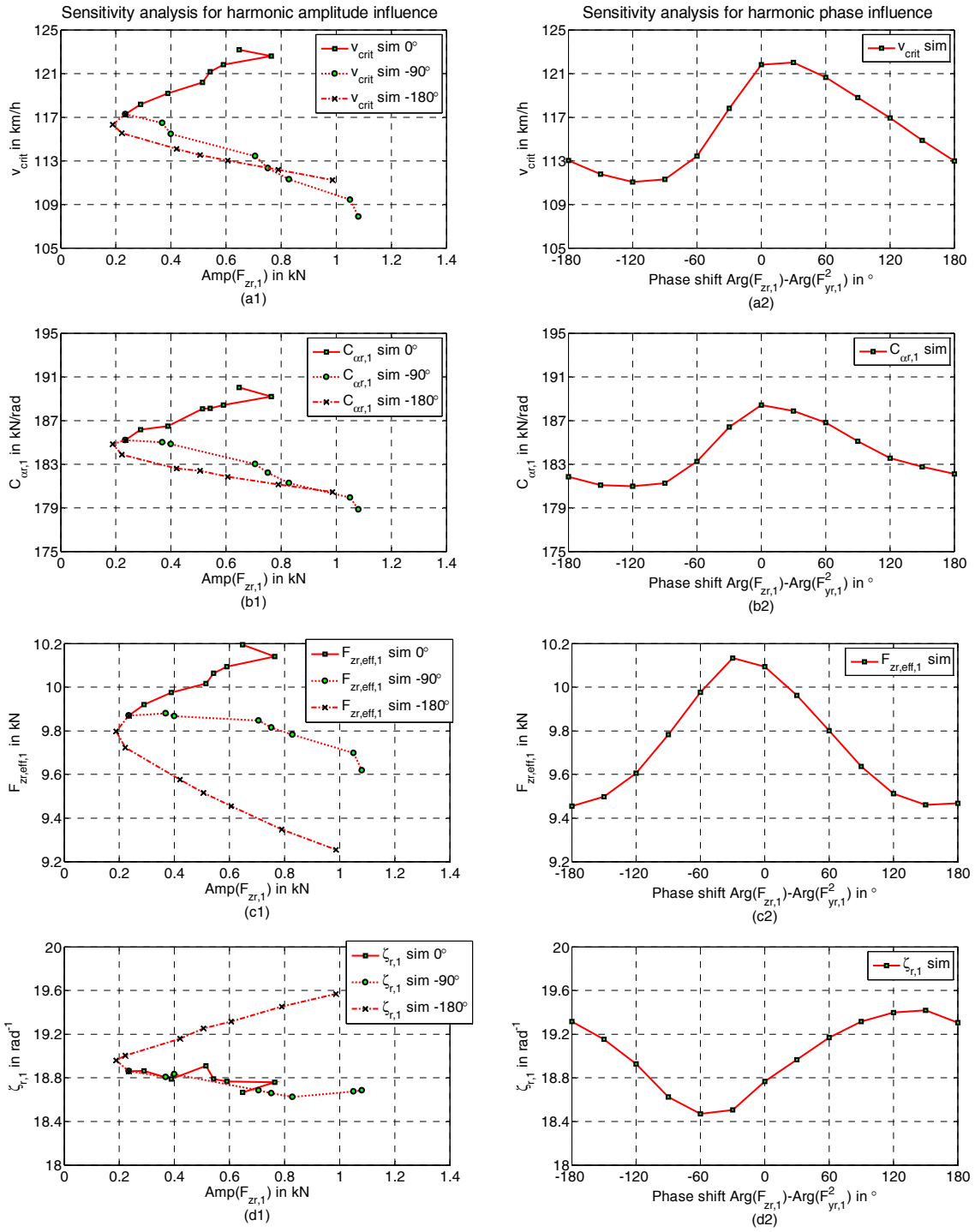

Figure 6-5: Simulation result for sensitivity analysis of the influence of the harmonic amplitude or phase

For the phase influence, it is relatively complicated because the amplitude of the harmonic force also depends on its phase at the harmonic of ca. 1.40 Hz (see Figure 6-6 below), i.e. both the extra harmonic axle force and the original existing nonlinearity-induced harmonic force are included. However, both the amplitude and phase information are included in the quantification of effective axle load $F_{zr,eff,1}$. Besides, there is a

clear dependency between the v_{crit} in (a2), $C_{\alpha r,1}$ in (b2) and $F_{zr,eff,1}$ in (c2). They have a strong correlation in Figure 6-5 (a2)-(d2).

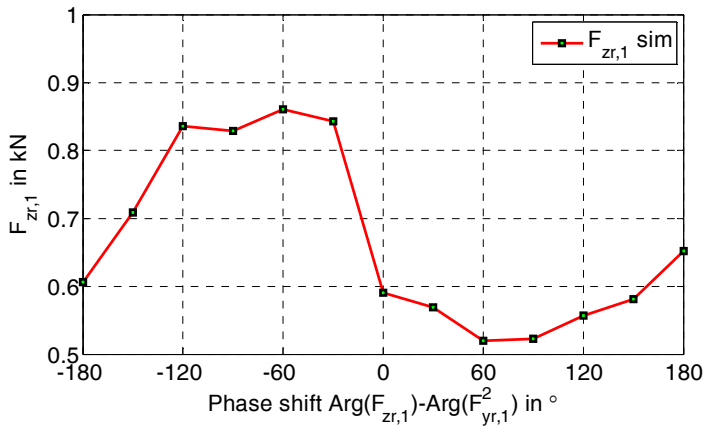

Figure 6-6: Amplitude and phase dependency in the sensitivity analysis for phase influence

Moreover, the relative phase shift of the harmonic force can induce a change of ca. 10 km/h in v_{crit} while the amplitude change of the harmonic force can induce a change of ca. 10 km/h in v_{crit} as well (amplitude of the harmonic force is within 0.2-1.2 kN). It follows that, on the one hand the simulation result is consistent with the analysis of the effective axle load described in Figure 4-5. On the other hand, the quantification of the effective axle load described in Section 4.4.2 seems to be effective as well.

The doubt about the Magic Formula tire model in the amplitude influence is proved by another simulation study on the sensitivity analysis for the axle load and steering amplitude influences under a slalom scenario, in which only the amplitude of the axle load or steering harmonic excitation is changed. The v_x is set as 90 km/h and the steering frequency is 0.75Hz, nearly the same as that in the critical stable state. A comparison of the axle load and steering amplitude influences between the critical stability (in Figure 6-7 (a) and (b)) and slalom scenario (in Figure 6-7 (c) and (d)) is shown in Figure 6-7 below. The simulation model of the CTC validated in Chapter 5 is applied in both simulation scenarios here. Sensitivity analysis results show that, the degressive (normalized) cornering stiffness depends on both the wheel/axle load and side-slip angle even within the tire linear range for the Magic Formula tire model. And the two effects are combined in the sensitivity analysis result for harmonic amplitude influence, which is indicated by the comparison of the curves' slopes. For example, for the harmonic amplitude influence with -180° phase shift condition in (a), the change of $\zeta_{r,1}$ mainly attributes to the change of $F_{zr,eff,1}$. Because the curves of $\zeta_{r,1}$ vs. $F_{zr,eff,1}$ have nearly same slopes between (a) and (c) due to a slight change of $\alpha_{r,1}$ in (b), while a relatively big difference exists between the curves' slopes of $\zeta_{r,1}$ vs. $\alpha_{r,1}$ between (b) and (d) due to the main influence from the effective axle load. The other two cases can be explained in the same way. This is the reason why the change of v_{crit} can be nearly completely explained by the change of $C_{\alpha r,1}$, but the change of $C_{\alpha r,1}$ cannot be totally explained by the corresponding change

of $F_{zr,eff,1}$ in Figure 6-5 (a1)-(d1). However, both the effects cannot be studied separately once the Magic Formula tire model is applied in the simulation. Because the harmonic axle load has a close dependency on the axle side-slip angle, neither of them can be controlled as an invariant in the critical stable state of a CTC.

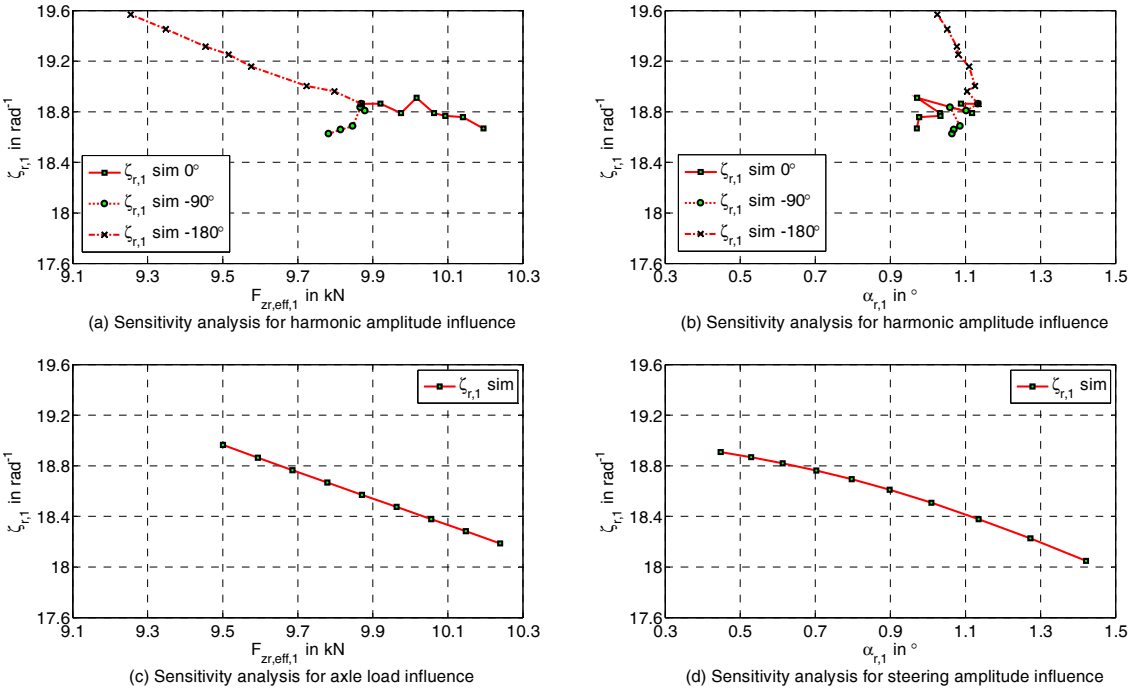

(a) Sensitivity analysis for harmonic amplitude influence

(b) Sensitivity analysis for harmonic amplitude influence

(c) Sensitivity analysis for axle load influence

(d) Sensitivity analysis for steering amplitude influence

Figure 6-7: Comparison of the axle load and steering amplitude influences between the critical stability and slalom scenario

6.4 Validation of simulation model (II)

Based on the simulation method and simulation study above, the time varying system response observed in Section 6.1 can be achieved when the simulation model has a module with which the harmonic dynamic axle load can be generated. For the typical road test utilized in Section 5.2.6, after the steering excitation the harmonic effect in rear axle load becomes abnormal in the two time windows, i.e. in 54-56s and 59-61s. Inspired by this abnormal phenomenon, the designed harmonic effect is introduced to function only at the rear axle of the towing car within the two time windows. Their amplitudes and phases can be easily modified to match with the real phenomenon in the road test. Finally, the gains and phase shift initial values are set as the ones in Table 6-3.

Table 6-3: Gains and phase shift initial values for the harmonic forces in two time windows in simulation

Designed harmonic effect at rear axle of the towing car	Time window	Amplitude gain in 1	Phase shift initial value in °
Harmonic force in the 1st time window	54-56s	2.5	-120
Harmonic force in the 2nd time window	59-61s	2.0	30

In the same way as that in Section 5.2.6, the TFA-based PIM provides an easy way to compare the system characteristics delivered from the experimental data and simulation data. A systematic comparison of the system characteristics is performed and illustrated below. And the first-phase validation result of the simulation model without extra harmonic force is also shown for comparison.

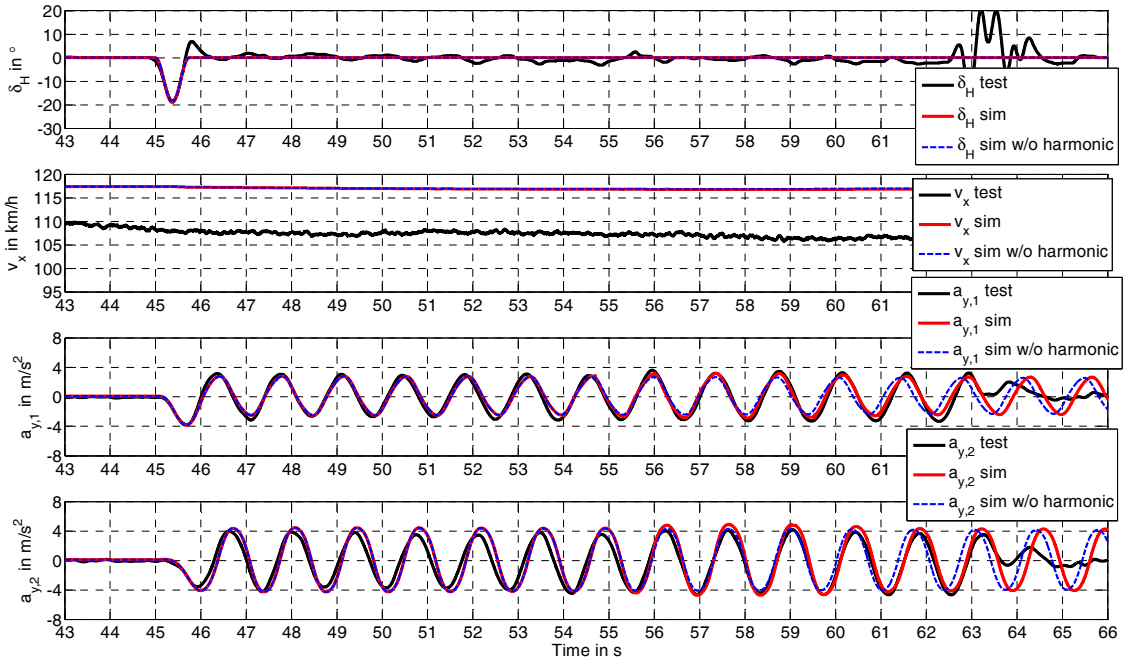

Figure 6-8: Second-phase validation of δ_H, v_x and a_y

A second-phase validation of δ_H, v_x and a_y is shown in Figure 6-8 above. Both the impulse steering excitation with amplitude ca. 19° and the longitudinal velocity ca. 117.3 km/h are totally the same as before. The system response under the steady state oscillation changes slightly in the first time window, 54-56s. The lateral acceleration of the towing car incl. its corresponding oscillation frequency matches with that in the experimental data even better. Although the amplitude of trailer's lateral acceleration is slight-

ly bigger than that in the experimental data, its frequency matches with the experimental data better. This improvement in the oscillation frequency is clearer in the dominant yaw oscillation frequency shown in Figure 6-9 below.

The yaw rate and dominant yaw oscillation frequency for the towing car ($f_{s,1}$) or trailer ($f_{s,2}$) are shown in Figure 6-9 respectively. A time varying phenomenon is found in the two time windows (54-56s and 59-61s). The system behaves a slight change in the amplitude of the yaw rate, which matches with that from the experimental data quite better than that from the simulation data without the harmonic phenomenon. Moreover, a time varying dominant yaw oscillation frequency is also available now and matches with that from the experimental data much better.

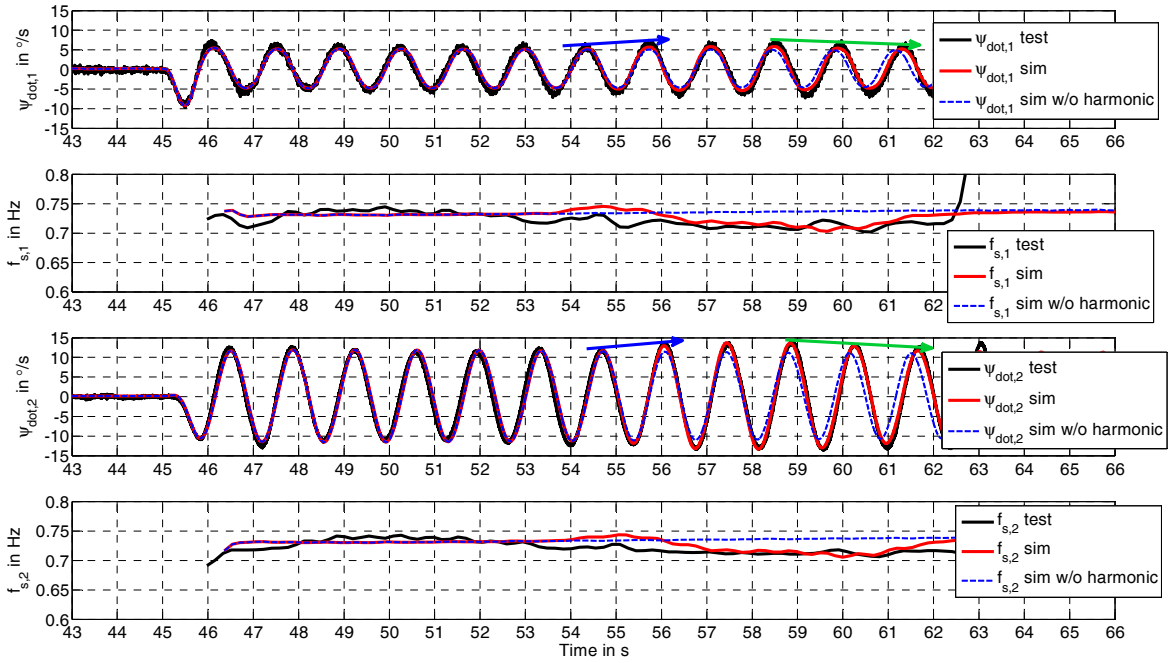

Figure 6-9: Second-phase validation of yaw rate and dominant yaw oscillation frequency

A second-phase validation of axle side-slip angle is shown in Figure 6-10 below. With the harmonic force generator, the time varying property in any axle side-slip angle is realized based on the harmonic effect functioned in the two time windows. The variation trend of any axle side-slip angle is consistent between the experimental data and simulation data.

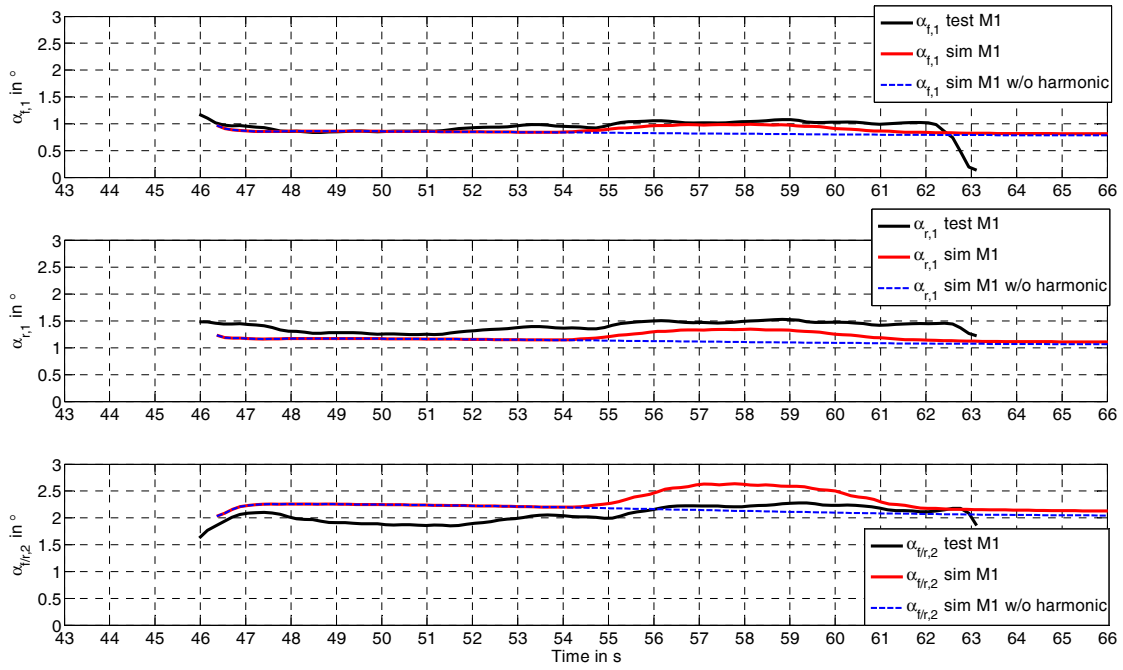

Figure 6-10: Second-phase validation of axle side-slip angle

For the axle cornering stiffness (see Figure 6-11), the rear axle cornering stiffness of the towing car and the trailer axle cornering stiffness match with that in the road test much better. However, a clear bigger deviation exists in the front axle cornering stiffness of the towing car. Since the artificial harmonic effect only functions at the rear axle of the towing car, coupling of the vertical dynamics between the front axle and rear axle of the towing car might be different between the experimental system and the simulation model. Quantification of the coupling mass[102] between the front axle and rear axle is a possible way for further refinement of the simulation model. However, it is a big challenge because the validation of the vertical dynamics will also change the horizontal dynamics for the simulation model. They cannot be validated separately in this situation.

[102] Winner: Skriptum zur Vorlesung “Fahrdynamik und Fahrkomfort” (Ride and Handling), 2014.

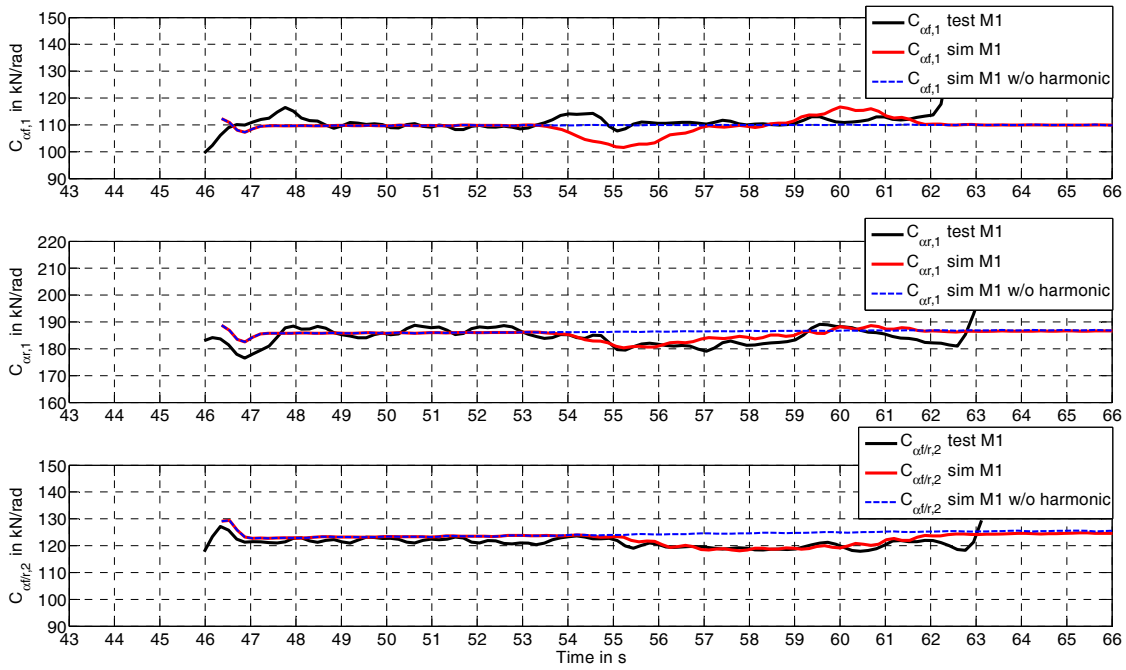

Figure 6-11: Second-phase validation of axle cornering stiffness

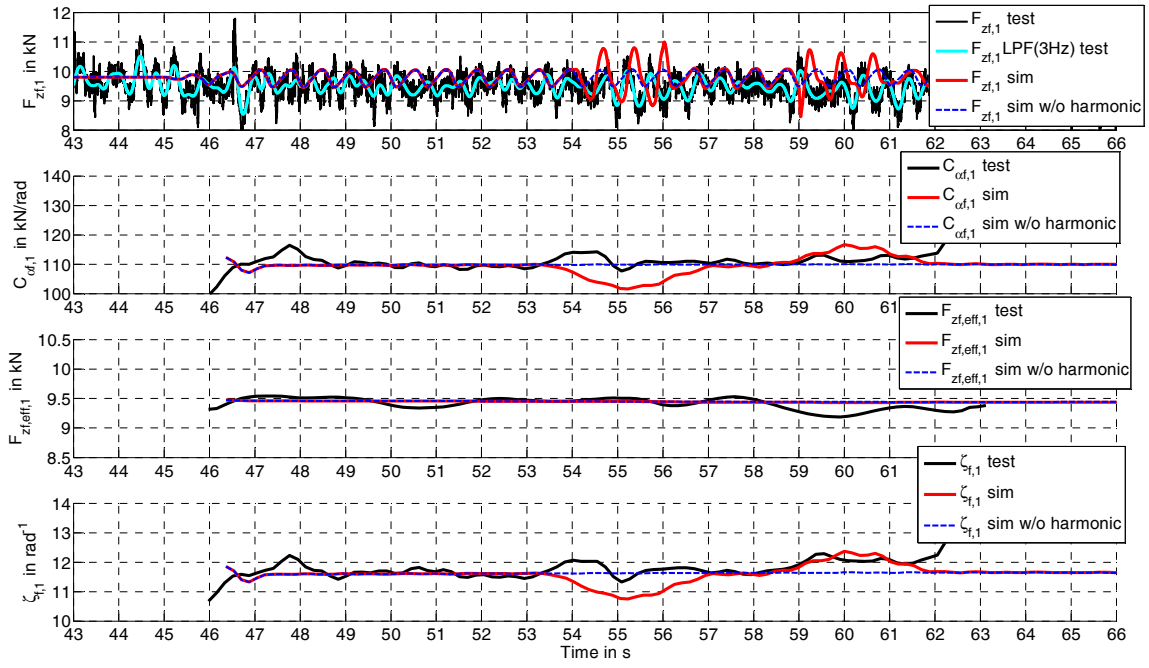

Figure 6-12: Second-phase validation of $F_{zf,1}(t)$, $C_{\alpha f,1}$, $F_{zf,eff,1}$ and $\zeta_{f,1}$ of the front axle of the towing car

The system characteristics at the front axle of the towing car, incl. $F_{zf,1}(t)$, $C_{\alpha f,1}$, $F_{zf,eff.1}$ and $\zeta_{f,1}$, are shown in Figure 6-12 respectively. The effective axle load $F_{zf,eff.1}$ shows exactly no change compared with that in the simulation data without the harmonic phenomenon. It indicates that the reduction of the axle cornering stiffness $C_{\alpha f,1}$ results

from a corresponding decrease in the normalized axle cornering stiffness $\zeta_{f,1}$, which is possibly due to different characteristics between the Magic Formula tire model and the real tire. Besides, it also shows that the coupling of the vertical dynamics between the front axle and rear axle of the towing car in the simulation data is much bigger than that in the experimental data.

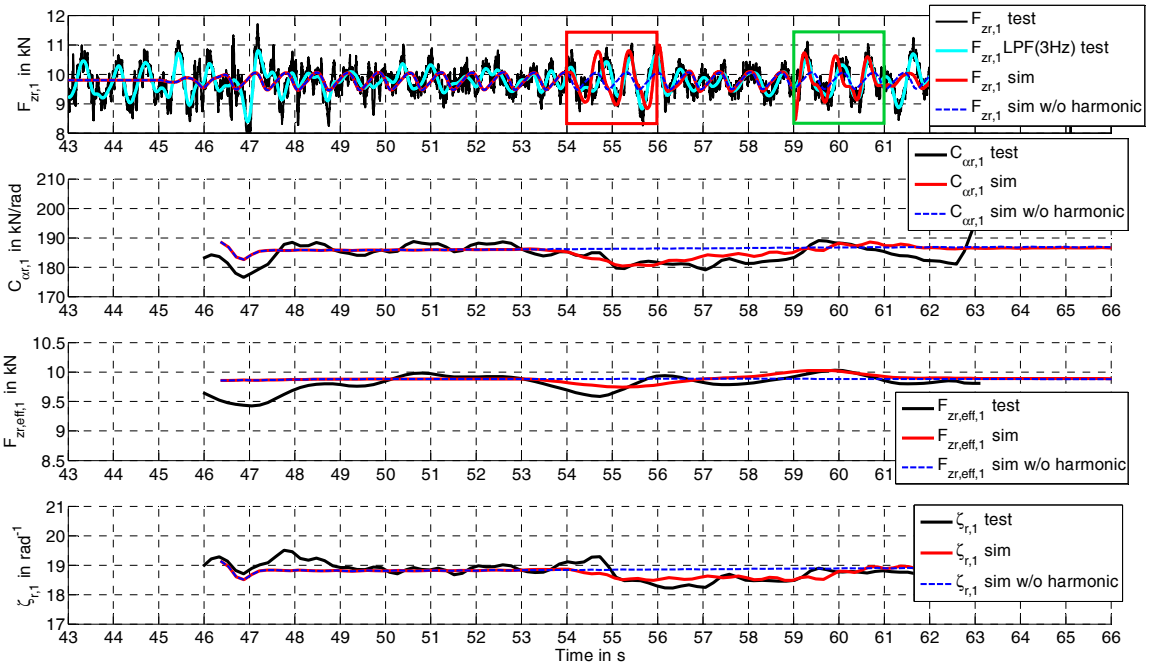

Figure 6-13: Second-phase validation of $F_{zr,1}(t)$, $C_{\alpha r,1}$, $F_{zr,eff,1}$ and $\zeta_{r,1}$ of the rear axle of the towing car

The system characteristics at the rear axle of the towing car, incl. $F_{zr,1}(t)$, $C_{\alpha r,1}$, $F_{zr,eff.1}$ and $\zeta_{r,1}$, are shown in Figure 6-13 respectively. With the harmonic force generator, the abnormal harmonic phenomenon in the rear axle load is simulated very well with similar amplitude and phase. Therefore, the axle cornering stiffness $C_{\alpha r,1}$ and effective axle load $F_{zr,eff,1}$ match with those from the experimental data much better. But there is still one problem about the phase shift of the harmonic force. A complicated unclear nonlinear phenomenon exists in the experimental data and might change rapidly even within one yaw oscillation cycle. Such a case exists in the time window 54-56s. The harmonic phase shift still has obvious difference, which is also indicated by the different variation tendency in $F_{zr,eff,1}$. Such rapidly changed harmonic phase shift is hardly simulated without a physical understanding about the harmonic and a corresponding physical module.

Despite such a problem, the harmonic force in the 1st time window causes a reduction in the $F_{zr,eff,1}$ and $C_{\alpha r,1}$, and consequently makes the critical stable system become unstable. The harmonic force in the 2nd time window gives a positive effect and restores the system to the critical stable state again.

In general, through the simulation study, the validation of the simulation model is refined and time varying system characteristics can be simulated as well, which owes to the approach of a harmonic force generator and the sensitivity analysis on this basis.

6.5 Conclusions

Based on the theoretical analysis and effective axle load evaluation algorithm derived in Section 4.4.2, impact study of nonlinearity-induced harmonic dynamic axle load on the dynamic stability of a CTC is the focus in this chapter. It serves as a linkage between the horizontal dynamics and vertical dynamics for the purpose of understanding the dynamic coupling. This chapter covers some original contribution on this topic.

Considering the nonlinearity-induced harmonic dynamic axle load in vehicle systems, asymmetric characteristic of suspension component is a major source. The sources for the asymmetric characteristic of suspension component can be sorted into two categories, expected asymmetry and undesired asymmetry or failure. In order to explain the physical mechanism of the nonlinearity-induced harmonic in vehicle systems, harmonic dynamic axle load induced by damper nonlinear characteristics is summarized in Table 6-1 above. However, although impact study of harmonic dynamic axle load induced by undesired asymmetry or failure on the dynamic stability of a CTC is the objective of this chapter, interaction from harmonic dynamic axle load induced by original existing nonlinear property cannot be excluded because of many possible sources leading to expected asymmetry in the system.

In this chapter, a phenomenon of harmonic oscillation near the first harmonic of the dominant yaw oscillation frequency in the dynamic axle load of a CTC is found in the road tests, although the root cause for such effect has many possibilities. The discovered harmonic oscillation in dynamic axle load is time varying and changes rapidly over time. The TFA result shows that, it can indeed affect the effective axle load and axle cornering stiffness. However, through the experimental study, the influences of its amplitude and phase cannot be studied separately.

A simulation study based on a new design is another option to achieve this goal. A yaw-rate-based simulation method is designed for a harmonic force generator. On this basis, sensitivity analysis of the influence of the harmonic amplitude or phase on the dynamic stability is performed with the simulation model validated in Chapter 5. The result shows that, the relative phase shift of the harmonic force can induce a change of ca. 10 km/h in v_{crit} while the amplitude change of the harmonic force can induce a change of ca. 10 km/h in v_{crit} as well (amplitude of the harmonic force is within 0.2-1.2 kN). It follows that, on the one hand the simulation result is consistent with the analysis of the effective axle load described in Figure 4-5. On the other hand, the quantification of the effective

axle load described in Section 4.4.2 seems to be effective as well.

Based on the impact study of nonlinearity-induced harmonic dynamic axle load on the dynamic stability of a CTC above, the second-phase validation is performed for the simulation model validated in Chapter 5. A simulation study shows that, with appropriate modification for the amplitude and phase shift of the harmonic force in selected time windows, the time varying system characteristics in the experimental data can be simulated very well by a simulation model with this new harmonic force generator. Hence, the system simulation model in Chapter 5 has been refined further.

However, there is still one problem about the phase shift of the harmonic force. A complicated unclear nonlinear phenomenon exists in the experimental data and might change rapidly even within one yaw oscillation cycle. Such rapidly changed harmonic phase shift is hardly simulated without a physical understanding about the harmonic and a corresponding physical module.

Despite such a problem, through the simulation study, the validation of the simulation model is refined and time varying system characteristics can be simulated as well, which owes to the innovative harmonic force generator and the sensitivity analysis on this basis.

7 Summary and Outlook

7.1 Summary

The objective of this thesis is stability investigation of car-trailer combinations (CTCs) based on time-frequency analysis. A state-of-the-art survey shows that very few research activities were performed to study the coupling between the vertical dynamics and horizontal dynamics, particularly for the system stability analysis. Even for the normal passenger car, stability analysis is mainly focused in the horizontal plane. However, this dynamic coupling deserves more attention for CTCs due to their dynamically natural characteristics. On this basis, a time-frequency analysis based parameter identification method (TFA-based PIM) is proposed, in which a linear STM and MTWFFT method are integrated. And an impact study of nonlinearity-induced harmonic dynamic axle load on the system dynamic stability is conducted as an intermediate step to the ultimate intention, investigation of the influence from vertical dynamics on the system dynamic stability in horizontal plane (e.g. influence from damper characteristics in suspension).

The TFA-based PIM aims to study the time varying vehicle dynamics under harmonic conditions. Only common lateral and yaw measurements are necessary for the purpose of indispensible inputs. With this PIM, axle cornering stiffness can be estimated with an acceptable accuracy. Other vehicle dynamics parameters, like normalized axle cornering stiffness and instantaneous friction coefficient, are also available with the assistance of such a method. Besides, the coupling between the vertical dynamics and horizontal dynamics is also discussed with the derivation of an effective axle load, by which the influence of a harmonic dynamic axle load on the axle cornering stiffness can be described. This effective axle load evaluation algorithm is also integrated into the PIM. In principle, the TFA-based PIM proposed in this thesis is a combination of a linear STM, the MTWFFT and an effective axle load evaluation algorithm. It can be applied for any time varying vehicle system, if its linear STM is available. This adaptability is a prominent advantage.

Another constructive contribution is impact study of nonlinearity-induced harmonic dynamic axle load on the dynamic stability of CTCs. This original work introduces the analysis of nonlinear dynamics in this thesis. Although impact study of harmonic dynamic axle load induced by undesired nonlinearity or failure of some suspension component is the ultimate objective, interaction from harmonic dynamic axle load induced by original existing expected nonlinearity cannot be excluded because of many possible sources like the practical damper characteristics in the system. A theoretical analysis of

the system dynamic stability and the influence of harmonic dynamic axle load on the axle cornering stiffness lay a solid foundation for a study of the harmonic influence on the system dynamic stability. Based on the TFA-based PIM including the effective axle load evaluation algorithm, the time varying harmonic effect found in the experimental study is quantified. To simulate the influence of the harmonic wheel load oscillations, a synthetic force generator is applied, which is synchronized to the phase of the yaw rate with a defined phase shift. Hence, the sensitivity analysis of the influence of the harmonic amplitude or phase of this force on the system dynamic stability is performed with a simulation model validated in the horizontal plane. The relative phase shift of the harmonic force can induce a change of ca. 10 km/h in v_{crit} while the amplitude change of the harmonic force can induce a change of ca. 10 km/h in v_{crit} as well (amplitude of the harmonic force is within 0.2-1.2 kN).

The application scope of this novel TFA-based PIM is mainly identification of systems with time varying properties, which aims for the model identification to build up simulation models. An application case, parameter identification of a car-caravan combination under its dynamically critical stable state, is performed for the purpose of a complex simulation model validation within the range of linear lateral dynamics. The results show that the TFA-based PIM is effective and has great application potential in vehicle system dynamics. Moreover, based on the impact study of nonlinearity-induced harmonic dynamic axle load, the change of the system dynamic critical speed is actually determined and so is the reason why the temporal changes of the system dynamic stability can be explained by the fluctuations in the amplitude and/or the phase of the superimposed harmonic dynamic axle load. Therefore, the system simulation model can be refined further.

7.2 Outlook

Based on the contribution in this thesis, further research on this topic can be planned considering the following five aspects.

For the theoretical analysis, the linear single-track model can be extended when the vertical dynamics is considered and added step by step. Because the axle cornering stiffness can be expressed by a multiplication of the normalized axle cornering stiffness and the effective axle load, influence study and sensitivity analysis of the effective axle load to the system dynamic stability are feasible in analytical way within the range of linear lateral dynamics. Therefore, the system state-space representation can be extended as well.

For the TFA-based PIM, there is still some potential for refinement and extension. Firstly, as mentioned in Section 4.2, a consideration with possible amplitude and phase

corrections can further refine the analysis result of the MTWFFT method, besides the frequency correction. Secondly, although the MTWFFT method is adaptable for any time varying vehicle system, the use of a linear STM is still a drawback to represent accurately the vehicle behavior in various driving maneuvers. Hence, two possible extensions of the TFA-based PIM to nonlinear time varying vehicle dynamics can be considered further, incl. the integration of a nonlinear STM or double-track model (DTM), or direct acquisition of a time domain signal of the wheel side-slip angle with the assistance of optical sensors, like Correvit® or wheel vector sensor. Finally, the functional goal of the TFA-based PIM, aiming for the system model identification to build up simulation models, might be extended to the online model identification for vehicle dynamics control if unknown components are used by customer. For this purpose, how to select the moving time window from the historical signal will be the key point.

For the impact study of nonlinearity-induced harmonic dynamic axle load on the system dynamic stability, two problems still exist in the future work. One is about the theoretical analysis and derivation of the effective axle load. The difference between the case with a +90° phase shift condition and the case with a -90° phase shift condition cannot be distinguished with the current effective axle load evaluation algorithm in Section 4.4.2. The possible explanation is the difference of the transient axle load within the length of the moving time window (ca. two yaw oscillations) resulting from the asymmetric characteristic of suspension component cannot be clearly revealed due to the limitation, the mean effect in the MTWFFT. However, this difference is clearly found in the simulation study in Section 6.3. This problem has to be considered for the purpose of a refined effective axle load evaluation algorithm. The other problem is about the Magic Formula tire model applied in the simulation. Here whether the normal Magic Formula tire model can represent the real tire behavior under various harmonic conditions even within the tire linear range in the road test is still not confirmed.

For the simulation model validation, three points have to be considered. Firstly, there is still ca. 10 km/h deviation in the system dynamic critical speed v_{crit} between the experiment and simulation. But this deviation in v_{crit} disappears in a linear STM with the estimated axle cornering stiffnesses. It gives a strong indication that, such a deviation in v_{crit} might result from the coupling between the vertical dynamics and horizontal dynamics or an aerodynamic effect. This points out a further potential for the simulation model validation. Secondly, for the yaw moment of inertia of the trailer, the estimated amplitudes have a clear deviation of ca. 580 kgm^2 (ca. 5.5 %) between the experiment and simulation. This also points out a further potential for the simulation model validation. Finally, a complicated unclear nonlinear phenomenon seems to exist in the experimental data and might change rapidly even within one yaw oscillation cycle. A physical understanding about the harmonic and a corresponding physical module might be necessary if such rapidly changed harmonic has to be simulated.

For the study of the coupling between the vertical dynamics and horizontal dynamics, the influence of the characteristics of specific suspension component (e.g. a hydraulic damper or gas spring) on the system dynamic stability is of great concern. The research result can serve as a guideline for a robust suspension design considering the variations of its structural components.

A Appendices

A.1 System parameters in STM and CarMaker® simulation model

Table A: System parameters incl. the values used in the STM and CarMaker® simulation model

Parameter	Description	Value	Unit
m_1	Mass of towing car	1955	kg
m_2	Mass of trailer	1880	kg
$I_{z,1}$	Yaw moment of inertia of towing car	2690	kgm^2
$I_{z,2}$	Yaw moment of inertia of trailer	10350	kgm^2
$l_{f,1}$	Distance from front axle to COG of towing car	1.302	m
$l_{r,1}$	Distance from rear axle to COG of towing car	1.383	m
$l_{h,1}$	Distance from hitch point to COG of towing car	2.166	m
$l_{hr,1}$	Distance from hitch point to rear axle of towing car	0.783	m
l_1	Wheel base of towing car	2.685	m
$l_{f,2}$	Distance from front axle to COG of trailer	0.124	m
$l_{r,2}$	Distance from rear axle to COG of trailer	0.526	m
$l_{h,2}$	Distance from hitch point to COG of trailer	5.073	m
$l_{hf,2}$	Distance from hitch point to front axle of trailer	4.949	m
l_2	Wheel base of trailer	0.65	m
i_s	Steering ratio	15	-

Table B: System parameters incl. the values used in the STM

Parameter	Description	Value	Unit
$C_{\alpha f,1}$	Front axle cornering stiffness of the towing car	109.3	kN/rad
$C_{\alpha r,1}$	Rear axle cornering stiffness of the towing car	185.2	kN/rad
$C_{\alpha f,2}$	Front axle cornering stiffness of the trailer	131.2	kN/rad
$C_{\alpha r,2}$	Front axle cornering stiffness of the trailer	124.4	kN/rad

A.2 System matrices in STM

System matrices in Eq. (3.14):

$$\mathbf{M} = \begin{bmatrix} m_1 + m_2 & -m_2(l_{h,1} + l_{h,2}) & -m_2 l_{h,2} & 0 \\ m_1 l_{h,1} & I_{z,1} & 0 & 0 \\ -m_2 l_{h,2} & I_{z,2} + m_2 l_{h,2}(l_{h,1} + l_{h,2}) & I_{z,2} + m_2 l_{h,2}^2 & 0 \\ 0 & 0 & 0 & 1 \end{bmatrix}$$

$$\mathbf{D} = \begin{bmatrix} d_{11} & d_{12} & d_{13} & d_{14} \\ d_{21} & d_{22} & 0 & 0 \\ d_{31} & d_{32} & d_{33} & d_{34} \\ 0 & 0 & 1 & 0 \end{bmatrix}$$

$$d_{11} = -\frac{C_{\alpha f,1} + C_{\alpha r,1} + C_{\alpha f,2} + C_{\alpha r,2}}{v_x}$$

$$d_{21} = -\frac{C_{\alpha f,1}(l_{f,1} + l_{h,2}) + C_{\alpha r,1}(l_{h,1} - l_{r,1})}{v_x}$$

$$d_{31} = \frac{C_{\alpha f,2}(l_{h,2} - l_{f,2}) + C_{\alpha r,2}(l_{h,2} + l_{r,2})}{v_x}$$

$$d_{12} = \frac{-C_{\alpha f,1} l_{f,1} + C_{\alpha r,1} l_{r,1} + C_{\alpha f,2}(l_{h,1} + l_{h,2} - l_{f,2}) + C_{\alpha r,2}(l_{h,1} + l_{h,2} + l_{r,2}) - (m_1 + m_2) v_x^2}{v_x}$$

$$d_{22} = \frac{-C_{\alpha f,1} l_{f,1}(l_{f,1} + l_{h,1}) + C_{\alpha r,1} l_{r,1}(l_{h,1} - l_{r,1}) - m_1 l_{h,1} v_x^2}{v_x}$$

$$d_{32} = \frac{-C_{\alpha f,2}(l_{h,2} - l_{f,2})(l_{h,1} + l_{h,2} - l_{f,2}) - C_{\alpha r,2}(l_{h,2} + l_{r,2})(l_{h,1} + l_{h,2} + l_{r,2}) + m_2 l_{h,2} v_x^2}{v_x}$$

$$d_{13} = \frac{C_{\alpha f,2}(l_{h,2} - l_{f,2}) + C_{\alpha r,2}(l_{h,2} + l_{r,2})}{v_x}$$

$$d_{33} = -\frac{C_{\alpha f,2}(l_{h,2} - l_{f,2})^2 + C_{\alpha r,2}(l_{h,2} + l_{r,2})^2}{v_x}$$

$$d_{14} = C_{\alpha f,2} + C_{\alpha r,2}$$

$$d_{34} = -\left[C_{\alpha f,2}(l_{h,2} - l_{f,2}) + C_{\alpha r,2}(l_{h,2} + l_{r,2})\right]$$

$$\mathbf{E} = \begin{bmatrix} C_{\alpha f,1}/i_s \\ C_{\alpha f,1}(l_{f,1} + l_{h,1})/i_s \\ 0 \\ 0 \end{bmatrix}$$

A.3 Spectrum-line-interpolation algorithm

A triple-spectrum-line-interpolation algorithm proposed by Niu[103] *et al*. is introduced in this section. This correction algorithm is also integrated into the TFA-based PIM and the evaluation method to obtain the yaw moment of inertia for the purpose of a more accurate frequency, amplitude and phase result.

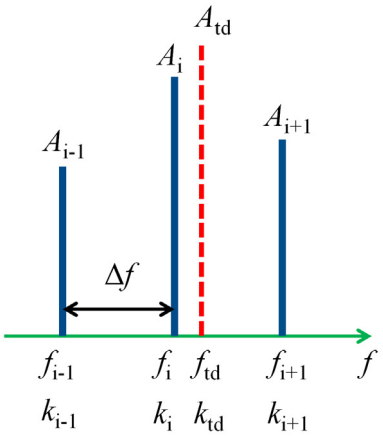

Figure A.3-1: Triple-spectrum-line-interpolation algorithm

Here f_i is the detected dominant frequency at the spectrum line k_i where the maximum amplitude, A_i, along with its corresponding phase φ_i exists in the spectrum, while A_{i-1} and A_{i+1} are the left and right adjacent amplitudes at the spectrum lines k_{i-1} and k_{i+1}. φ_{i-1} and φ_{i+1} are the left and right adjacent phases at the spectrum lines k_{i-1} and k_{i+1}. Hence, three spectrum lines are utilized in the correction. Δf is the frequency resolution. The ultimate goal of this interpolation algorithm is to evaluate the true instantaneous dominant frequency, f_{td}, the corresponding amplitude A_{td} and phase φ_{td} as accurately as possible. f_{td} locates at the spectrum line k_{td}, which is normally not an integer.

Obtaining an analytical expression of f_{td}, the corresponding amplitude A_{td} and phase φ_{td} is not easy or might even be impossible. Therefore, a polynomial approximation of the solution follows from

$$f_{td} = k_{td} \cdot \Delta f = (k_i + x) \cdot \Delta f = f_i + x \cdot \Delta f$$

$$A_{td} = \frac{1}{4}(A_{i-1} + 2A_i + A_{i+1}) \cdot p(x)$$

$$\approx \frac{1}{4}(A_{i-1} + 2A_i + A_{i+1}) \cdot (c_0 + c_2 \cdot x^2 + \cdots + c_{2n} \cdot x^{2n})$$

[103] Niu et al.: An Algorithm for … Triple-spectrum-line Interpolation FFT, 2012.

$$\varphi_{td} = \varphi_i + \frac{\pi}{2} - x \cdot \pi$$

Where

$$\begin{cases} r_A = \frac{A_{i+1} - A_{i-1}}{A_i} = g(x) \\ x = \frac{f_{td} - f_i}{\Delta f} = g^{-1}(r_A) \end{cases}$$

Here, again a polynomial approximation of the solution for x is given according to

$$x = g^{-1}(r_A) \approx c_1 \cdot r_A + c_3 \cdot r_A^3 + \cdots + c_{2n+1} \cdot r_A^{2n+1}$$

Therefore, the polynomial approximations for x and $p(x)$ are crucial in this triple-spectrum-line-interpolation algorithm and they depend on the selective weighting time window in the MTWFFT. Because the Hanning window is frequently utilized in the TFA-based PIM, the expressions of the polynomial approximations for x and $p(x)$ related to the Hanning window are given according to

$$x = 0.66666287 \cdot r_A - 0.07398320 \cdot r_A^3 + 0.01587358 \cdot r_A^5 - 0.00311639 \cdot r_A^7$$

$$p(x) = 1.33333327 + 0.52658791 \cdot x^2 + 0.11699742 \cdot x^4 + 0.02103885 \cdot x^6$$

References

Agilent Technologies: Spectrum Analysis Basics, Application Note 150, Agilent Technologies, USA, 2004

Alonso Fernandez, M. A.; Sharp, R. S.: Caravan active braking system - effective stabilisation of snaking of combination vehicles (No. 2001-01-3188), SAE Technical Paper, 2001

Anderson, R. J.; Kurtz, E. F.: Handling characteristics simulations of car-trailer systems, SAE paper 800545, 1980

Autoevolution – virtual: http://www.autoevolution.com/news/volvo-renegade-trailer-stability-assist-8293.html, last access: February 28th 2015

Baffet, G.; Charara, A.; Lechner, D.: Estimation of vehicle sideslip, tire force and wheel cornering stiffness, Control Engineering Practice, Volume 17, Issue 11, November 2009, p. 1255-1264, 2009

Bedük, M. D.; Çalışkan, K.; Henze, R.; Küçükay, F.: Effects of damper failure on vehicle stability, Proceedings of the Institution of Mechanical Engineers, Part D: Journal of automobile engineering, 2013, 227(7), p. 1024-1039, 2013

Bevan, B. G.; Smith, N. P.; Ashley, C.: Some factors influencing the stability of car/caravan combinations, In Proceedings of the IMechE Conference on Road vehicle handling, IMechE Conference Publication C123, Nuneaton, Warwickshire, UK, 24–26 May 1983, p. 221-228, 1983

Börner M.; Isermann R.: Adaptive one-track model for critical lateral driving situations, Proceedings of the 6th International Symposium on Advanced Vehicle Control (AVEC), Hiroshima, Japan, 2004

Caravan Buyers Guide – virtual: http://caravanbuyersguide.com.au/tow-vehicle-caravan-weight/, last access: February 28th 2015

Darling, J.; Akwe, S. O.: An experimental investigation into car & caravan stability, Bailey Caravans of Bristol, Department of Mechanical Engineering, University of Bath, UK, 2002

Darling, J.; Tilley, D.; Gao, B.: An experimental investigation of car-trailer high-speed stability, Proceedings of the Institution of Mechanical Engineers, Part D: Journal of Automobile Engineering, 2009, 223: p. 471-484, 2009

Deng, W; Kang, X.: Parametric study on vehicle-trailer dynamics for stability control, SAE paper 2003-01-1321, 2003

Deng, W.; Lee, Y. H.; Tian, M.: An integrated chassis control for vehicle-trailer stability and handling performance (No. 2004-01-2046), SAE Technical Paper, 2004

Dixon J. C.: Linear and non-linear steady state vehicle handling, Proceedings of the Institution of Mechanical Engineers, Part D: Journal of Automobile Engineering, 202.3: p. 173-186, 1988

Dixon, J. C.: The Shock Absorber Handbook, second edition, by SAE International Inc, 2007

Dixon J. C.: Tires, Suspension and Handling, second edition, Society of Automotive Engineers, Warrendale, 1996

Dorf, R. C.; Bishop, R. H.: Modern Control Systems, twelfth edition, Prentice Hall, 2011

Dugoff, H.; Murphy, R. W.: The Dynamic Performance of Articulated Highway Vehicles - A Review of the State-of-the-Art, SAE Trans., Vol. 80, p. 897, 1971

Eshleman, R. L.: Particular Handling Safety Problems of Trucks and Articulated Vehicles, Vehicle Safety Research Integration Symposium, Washington, D.C., 1973

Feldman, M.: Hilbert Transform Applications in Mechanical Vibration, John Wiley & Sons, UK, 2011

Florissen G.: Autonomes anhängerbasiertes elektronisches Bremskonzept zur Steigerung der Fahrsicherheit von Pkw-Gespannen, Doctoral dissertation (in German), RWTH Aachen University, 2007

Fischer, G.; Heyken, R.; Trächtler, A.: Aktive Gespannstabilisierung beim BMW X 5 - Eine Weiterentwicklung der Fahrdynamikregelung DSC (in German), p. 333, 2002

Fratila, D.: Lateral stability of passenger car/caravan combinations, Doctoral dissertation, Department of Mechanical Engineering, University of Bath, UK, 1994

Fratila, D.; Darling, J.: Simulation of coupled car and caravan handling behavior, Vehicle System Dynamics, 1996, 26, p. 397-429, 1996

Gao, R. X.; Yan, R.: Wavelets: Theory and applications for manufacturing, Springer Science & Business Media, 2010

Hac A.; Fulk D.; Chen H.: Stability and Control Considerations of Vehicle-Trailer Combination, SAE SP, 2188, 125, 2008

Heißing B.; Ersoy M.: Chassis Handbook, Vieweg and Teubner, 2011

Her H.; Suh J.; Yi K.: Integrated control of the differential braking, the suspension damping force and the active roll moment for improvement in the agility and the stability, Proceedings of the Institution of Mechanical Engineers, Part D: Journal of Automobile Engineering, 2014

Hewson, P.: Method for estimating tyre cornering stiffness from basic tyre information, Proceedings of the Institution of Mechanical Engineers, Part D: Journal of Automobile Engineering, December 1, 2005; vol. 219, 12: p. 1407-1412, 2005

Hoepke, E.; Breuer, S.; et al.: Nutzfahrzeugtechnik (in German), 6. Auflage,Vieweg, 2010

Hogan, J. A.; Lakey, J. D.: Time-Frequency and Time-Scale Methods, Springer-Verlag New York Inc, USA, 2004

IPG CarMaker: Reference Manual, Version 4.0.5, 2013

IPG CarMaker: User's Guide, Version 4.0.5, 2013

IPG CarMaker – virtual: www.ipg.de, last access: February 26th 2015

Isermann, R.; Münchhof, M.: Identification of Dynamic Systems - an introduction with applications, Springer Deutschland, 2011

ISO 9815: Road vehicles - Passenger-car and trailer combinations - Lateral stability test, International Organization for Standardization, 2003

Kageyama, I.; Nagai, R.: Stabilization of passenger car-caravan combination using four wheel steering control, Vehicle System Dynamics, 1995, 24(4-5), p. 313-327, 1995

Kang, D.; Ming, X.; Xiaofei, Z.: Phase difference correction method for phase and frequency in spectral analysis, Mechanical Systems and Signal Processing 14.5 (2000): 835-843, 2000

Kistler Automotive GmbH: User Manuals of Correvit S-350 Aqua Sensor and Wheel Vector Sensor RV-4, Kistler Automotive GmbH, Wetzlar, 2012

Kurtz, E. F.; Anderson, R. J.: Handling Characteristics of Car-Trailer Systems; A State-of-the-Art Survey, Vehicle System Dynamics: International Journal of Vehicle Mechanics and Mobility, 1977, 6:4, p. 217-243, 1977

Leontopoulos, C.; Robb, D. A.; Besant, C. B.: Vibration analysis for the design of a high-speed generator for a turbo-electric hybrid vehicle, Proceedings of the Institution of Mechanical Engineers, Part D: Journal of Automobile Engineering 212.4: p. 271-283, 1998

Lundquist, C.; Schön, T.: Recursive Identification of Cornering Stiffness Parameters for an Enhanced Single Track Model, Proceedings of the 15th IFAC Symposium on System Identification: Vol. 15, Part 1, 2009

Ming, X.; Kang, D.: Corrections for Frequency, Amplitude and Phase in A Fast Fourier Transform of A Harmonic Signal, Mechanical Systems and Signal Processing, Volume 10, Issue 2, March 1996, p. 211-221, 1996

Mitschke, M.; Sagan, E.: Fahrdynamik von Pkw-Wohnanhängerzügen (in German), Verlag TÜV Rheinland, 1988

Niu, S. S.; Liang, Z. R.; Zhang, J. H.; Su, H. F.; Sun, H. F.: An Algorithm for Electrical Harmonic Analysis Based on Triple-spectrum-line Interpolation FFT (in Chinese), Proceedings of the Chinese Society for Electrical Engineering, 2012, 32(16): 130-136, 2012

Obermüller, A.: Modellbasierte Fahrzustandsschätzung zur Ansteuerung einer aktiven Hinterachskinematik, Doctoral dissertation (in German), Technischen Universität München, 2012

Pacejka, H. B.: Tire and Vehicle Dynamics, third edition, Butterworth-Heinemann, UK, 2012

Payri, F.; Luján, J. M.; Guardiola, C.; Rizzoni, G.: Injection diagnosis through common-rail pressure measurement, Proceedings of the Institution of Mechanical Engineers, Part D: Journal of Automobile Engineering, 220.3: p. 347-357, 2006

Peschke, W.; Mankau, H.: Auftriebskräfte am Wohnanhänger beeinflussen die Stabilität von Wohnwagengespannen (in German), Automobil Revue, 18, 51–53, 1982

Quatieri, T. F.: Discrete-Time Speech Signal Processing: Principles and Practice, Prentice Hall, USA, 2001

Rajamani, R.: Vehicle dynamics and control, Springer Science & Business Media, 2011

Sagan, E.: Fahreigenschaften von PKW-Wohnanhängerzügen: Antrieb, Bremsen, Fahrstabilität und Schwingungen, Doctoral dissertation (in German), Technische Universität Carolo-Wilhelmina zu Braunschweig, 1983

Schütz, T.: Hucho-Aerodynamik des Automobils – Strömungsmechanik, Wärmetechnik, Fahrdynamik, Komfort (in German), 6. Auflage, Springer Vieweg, 2013

Sharp, R. S.; Alonso Fernandez, M. A.: Car-caravan snaking. Part 1: the influence of pintle pin friction, Proceedings of the Institution of Mechanical Engineers, Part C: Journal of Mechanical Engineering Science, 2002, 216, p. 707-722, 2002

Sharp, R. S.; Alonso Fernandez, M. A.: Car-caravan snaking. Part 2: Active caravan braking, Proceedings of the Institution of Mechanical Engineers, Part C: Journal of Mechanical Engineering Science, 2002, 216, p. 723-736, 2002

Sierra, C.; Tseng, E.; Jain, A.; Peng, H.: Cornering stiffness estimation based on vehicle lateral dynamics, Vehicle System Dynamics, Vol. 44, Iss. sup1, 2006

Standen, P.: Towed vehicle aerodynamics, Doctoral dissertation, University of Bath, UK, 1999

Stanković, L.; Böhme, J. F.: Time-frequency analysis of multiple resonances in combustion engine signals, Signal Processing, 79.1: p. 15-28, 1999

Vulli, S.; Dunne, J. F.; Potenza, R.; Richardson, D.; King, P.: Time-frequency analysis of single-point engine-block vibration measurements for multiple excitation-event identification, Journal of Sound and Vibration, 321.3: p. 1129-1143, 2009

Wagner, M.; Karlsson, E.; Konig, D.; Törk, C.: Time variant system identification for car engine signal analysis, Proceedings of the European Signal Processing Conference (EUSIPCO), Edinbourgh, Scotland, 1994

Wei, C. Y.: Study on Handling Stability of Caravan, Doctoral dissertation (in Chinese), Jiangsu University, Zhenjiang, China, 2008

Weir, D. H.; Klein, R. H.; Zellner, J. W.: Crosswind Response and Stability of Car Plus Utility Trailer Combinations, SAE 820137, 1982

Wesemeier, D.; Isermann, R.: Identification of vehicle parameters using stationary driving maneuvers, Control Engineering Practice, Volume 17, Issue 12, December 2009, p. 1426-1431, 2009

Wikipedia – virtual: http://en.wikipedia.org/wiki/Time-frequency_analysis, last access: February 23rd 2015

Wikipedia – virtual: http://en.wikipedia.org/wiki/Time-frequency_representation, last access: February 23rd 2015

Williams, D.: The mathematical theory of the snaking of two-wheeled trailers, with practical rules and devices for preventing snaking, Proceedings of the Institution of Mechanical Engineers: Automobile Division 5.1, p. 175-190, 1951

Winner, H.: Skriptum zur Vorlesung "Fahrdynamik und Fahrkomfort" (Ride and Handling), Fachgebiet Fahrzeugtechnik (FZD), Technische Universität Darmstadt, 2014

Winner, H.: Skriptum zur Vorlesung "Kraftfahrzeugtechnik" (in German), Fachgebiet Fahrzeugtechnik (FZD), Technische Universität Darmstadt, 2014

Wohnmobile Bürstner – virtual: http://www.kfz-kleinanzeigen.com/detailanzeige-39719420.html, last access: February 28th 2015

Wu, D. H.: A theoretical study of the yaw/roll motions of a multiple steering articulated vehicle, Proceedings of the Institution of Mechanical Engineers, Part D: J. Automobile Engineering, 2001, 215, p. 1257-1265, 2001

ZF Sachs AG: Suspension Technology, ZF Sachs AG, 2011

Zhang, N.; Claus, S.; Wang, Y.; Winner, H.: Analysis Methods for Time-Variant Harmonic Vehicle Dynamics Experiments, 14th Internationale VDI Tagung, Reifen-Fahrwerk-Fahrbahn, VDI Berichte 2211, p. 273-286, 2013

Zhu, J. J.; Khajepour, A.; Esmailzadeh, E.: Handling transient response of a vehicle with a planar suspension system, Proceedings of the Institution of Mechanical Engineers, Part D: Journal of Automobile Engineering, 2011

Zomotor, A.: Fahrwerktechnik: Fahrverhalten (in German), Vogel: Wurzburg, 1991

Zomotor, A.; Richter, K.-H.; Kuhn, W.: Untersuchungen über die Stabilität und das aerodynamische Störverhalten von Pkw-Wohnanhängerzügen (in German), Automobil-Industrie, 3, 331–340, 1982

Own Publications

Zhang, N.; Claus, S.; Wang, Y.; Winner, H.: Analysis Methods for Time-Variant Harmonic Vehicle Dynamics Experiments, 14. Internationale VDI-Tagung, Reifen-Fahrwerk-Fahrbahn (14. International VDI Conference, Tyres-Chassis-Road), Hannover, 22-23, Oktober, 2013, VDI Berichte 2211, p. 273-286, 2013

Zhang, N.; Xiao, H.; Winner, H.: A parameter identification method based on time-frequency analysis for time-varying vehicle dynamics, Proceedings of the Institution of Mechanical Engineers, Part D: Journal of Automobile Engineering, 2015 (in press)

Zhang, N.; Xiao, H.; Winner, H.: Nonlinearity-induced Time-varying Harmonic Dynamic Axle Load and Its Impact on Dynamic Stability of Car-trailer Combinations, Nonlinear Dynamics, 2015 (in review)

Zhang, N.; Xiao, H.; Shao, Z. J.; Winner, H.: Stability Investigation of Car-trailer combinations depending on Damper Properties, In Proceedings of 24th International Symposium on Dynamics of Vehicles on Roads and Tracks, IAVSD, 2015, August 17-21, Graz, Austria, 2015 (Abstract is accepted)

Advised Student Works

Gao, C.: Modellierung und Simulation von Aerodynamik des Gespannsystems (*Modeling and Simulation of Aerodynamics of Car-trailer Combination System*). Master-Thesis Nr. 534/13 am Fachgebiet Fahrzeugtechnik der Technischen Universität Darmstadt, 2013

Hofmann, T.: Identifikation und Ermittlung der dynamischen Stabilität eines Gespanns in Abhängigkeit von Dämpfercharakteristi-ken mit Hilfe der Fahrdynamiksimulation (*Identification and Investigation of Dynamic Stability of a Car-trailer Combination on the Dependence of Damper Characteristics by means of Driving Dynamics Simulation*). Bachelor-Thesis Nr. 1203/14 am Fachgebiet Fahrzeugtechnik der Technischen Universität Darmstadt, 2014

Li, H. G.: Modellierung und Validierung eines Gespannsystems (*Modeling and Validation of a Car-trailer Combination System*). Master-Thesis Nr. 519/13 am Fachgebiet Fahrzeugtechnik der Technischen Universität Darmstadt, 2013

Shao, Z. J.: Identifikation und Ermittlung der dynamischen Stabilität eines Gespanns in Abhängigkeit von Dämpfercharakteristiken durch die Änderung des Wankverhaltens des Systems (*Identification and Investigation of Dynamic Stability of a Car-trailer Combination on the Dependence of Damper Characteristics through the Change of System Roll Behavior*). Master-Thesis Nr. 571/15 am Fachgebiet Fahrzeugtechnik der Technischen Universität Darmstadt, 2015

Wu, Q. P.: Untersuchung der Radlastschwankungen vom Gespannsystem (*Analysis of Wheel Load Fluctuations of Car-trailer Combinations*). Master-Thesis Nr. 535/13 am Fachgebiet Fahrzeugtechnik der Technischen Universität Darmstadt, 2013

Zhang, X. L.: Identifikation, Quantifizierung und Simulation des dynamischen Verhaltens von Dämpfern (*Identification, Quantification and Simulation of Damper Dynamic Behavior*). Master-Thesis Nr. 533/13 am Fachgebiet Fahrzeugtechnik der Technischen Universität Darmstadt, 2013

Resume

Persönliche Daten

Name:	Ning Zhang
Geburtsdatum:	01. January 1985
Geburtsort:	Xuzhou, Jiangsu Province, P.R. China

Schulzeit

09/1997 – 07/2000	Junior Middle School in Suining town Xuzhou, Jiangsu Province, P.R. China
09/2000 – 06/2003	Senior Middle School in Suining town Xuzhou, Jiangsu Province, P.R. China Abschluss: Allgemeine Hochschulreife

Studium

08/2003 – 06/2007	Studium Allgemeiner Maschinenbau Southeast University, Nanjing, P.R. China Abschluss: Bachelor of Engineering
09/2007 – 06/2010	Vehicle Engineering Southeast University, Nanjing, P.R. China Abschluss: Master of Engineering

Berufstätigkeit

10/2010 – 05/2015	Wissenschaftlicher Mitarbeiter am Fachgebiet Fahrzeugtechnik der Technischen Universität Darmstadt